

LIGO Laboratory / LIGO Scientific Collaboration

LIGO-T080210-00-D

ADVANCED LIGO

8/27/08

**AOS: Stray Light Control (SLC)
Conceptual Design, Stable Recycling Cavity**

Michael Smith

Distribution of this document:
LIGO Science Collaboration

This is an internal working note
of the LIGO Project.

California Institute of Technology
LIGO Project – MS 18-34
1200 E. California Blvd.
Pasadena, CA 91125
Phone (626) 395-2129
Fax (626) 304-9834
E-mail: info@ligo.caltech.edu

Massachusetts Institute of Technology
LIGO Project – NW22-295
185 Albany St
Cambridge, MA 02139
Phone (617) 253-4824
Fax (617) 253-7014
E-mail: info@ligo.mit.edu

LIGO Hanford Observatory
P.O. Box 1970
Mail Stop S9-02
Richland, WA 99352
Phone 509-372-8106
Fax 509-372-8137

LIGO Livingston Observatory
P.O. Box 940
Livingston, LA 70754
Phone 225-686-3100
Fax 225-686-7189

<http://www.ligo.caltech.edu/>

Table of Contents

1	INTRODUCTION.....	12
1.1	PURPOSE.....	12
1.2	SCOPE.....	12
1.2.1	<i>Stray Light Control</i>	12
1.3	DEFINITIONS.....	14
1.4	ACRONYMS.....	14
1.5	APPLICABLE DOCUMENTS.....	15
1.5.1	<i>LIGO Documents</i>	15
1.5.2	<i>Non-LIGO Documents</i>	16
2	CATALOG OF SLC DESIGN REQUIREMENTS.....	17
3	STRAY LIGHT CONTROL CONCEPTUAL DESIGN CHARACTERISTICS.....	18
3.1	COC WEDGE ANGLE DETERMINATION.....	18
3.1.1	<i>Beam Profile in Recycling Cavity</i>	18
3.1.2	<i>Wedge Angles for Non-folded IFO</i>	18
3.1.2.1	BS Wedge Angle.....	18
3.1.2.2	ITM Wedge Angle.....	19
3.1.2.3	CP Wedge Angle.....	20
3.1.2.4	Stay Clear Diameter.....	20
3.1.2.5	PRM and SRM Wedge Angle.....	23
3.1.2.6	PR2 and SR2 Wedge Angle.....	24
3.1.2.7	PR3 and SR3 Wedge Angle.....	26
3.1.2.8	ETM Wedge Angle.....	27
3.1.2.9	ETM Reaction Mass Wedge Angle.....	27
3.1.2.10	COC Wedge Angle Summary, Non-folded IFO.....	27
3.1.3	<i>Wedge Angles for Folded IFO</i>	28
3.1.3.1	COC Wedge Angle Summary, Folded IFO.....	28
3.2	STRAY LIGHT CONTROL PERFORMANCE CHARACTERISTICS.....	29
3.2.1	<i>Scattered Light Sources</i>	29
3.2.2	<i>Summary of Scattered Light Displacement Noise</i>	31
3.2.3	<i>Output Faraday Isolator</i>	33
3.2.3.1	Faraday Isolator Forward Transmissivity.....	34
3.2.3.2	Faraday Isolator Reverse Transmissivity.....	34
3.2.3.3	BRDF of Faraday Surfaces.....	34
3.2.3.4	Faraday Isolator Suspension.....	34
3.2.3.5	Scattered Light Displacement Noise of Suspended Output Faraday Isolator.....	36
3.2.3.6	Stay Clear Diameter.....	36
3.2.4	<i>Arm Cavity Baffle</i>	37
3.2.4.1	Incident Power on Arm Cavity Baffle.....	37
3.2.4.2	Arm Cavity Baffle Motion.....	38
3.2.4.2.1	HEPI Displacement.....	38
3.2.4.2.2	Minimum Arm Cavity Baffle Motion Requirements.....	39
3.2.4.2.3	Arm Cavity Baffle Suspension Transfer Functions.....	39
3.2.4.3	Arm Cavity Baffle Surface BRDF.....	41
3.2.4.4	Arm Cavity Baffle Reflectivity.....	43
3.2.4.5	Seismic Motion of the Vacuum Manifold.....	43
3.2.4.6	Scattered Light Displacement Noise of Suspended Arm Cavity Baffle.....	44
3.2.4.7	Fringe Wrapping of Arm Cavity Baffle Displacement Noise.....	45
3.2.4.8	Stay Clear Diameter.....	45
3.2.5	<i>Cryopump Baffle</i>	46
3.2.5.1	Cryopump Baffle Suspension.....	47
3.2.5.2	Cryopump Blocking.....	47
3.2.5.3	Cryopump Baffle Motion Requirements.....	48
3.2.5.4	Cryopump Baffle Surface BRDF.....	49
3.2.5.5	Cryopump Baffle Reflectivity.....	49

3.2.5.6	Seismic Motion of the Cryopump Scattering Surfaces	50
3.2.5.7	Scattered Light Displacement Noise of Suspended Cryopump Baffle	50
3.2.5.8	Fringe-wrapping of Cryopump Baffle Displacement Noise	50
3.2.5.9	Stay Clear Zone	51
3.2.6	Elliptical Baffles	51
3.2.6.1	ITM Elliptical Baffle	51
3.2.6.1.1	ITM Elliptical Baffle Seismic Attenuation	51
3.2.6.1.2	ITM Elliptical Baffle Surface BRDF	53
3.2.6.1.3	ITM Elliptical Baffle Reflectivity	53
3.2.6.1.4	Seismic Motion of the Vacuum Chamber	53
3.2.6.1.5	Scattered Light Displacement Noise of Suspended ITM Elliptical Baffle	54
3.2.6.1.6	Stay Clear Diameter	55
3.2.6.2	PRM Elliptical Baffle	55
3.2.6.2.1	Motion of PRM Elliptical Baffle	55
3.2.6.2.2	Power Hitting the PRM Elliptical Baffle from IO Side	56
3.2.6.2.3	PRM Elliptical Baffle Surface BRDF	56
3.2.6.2.4	PRM Elliptical Baffle Reflectivity	56
3.2.6.2.5	Scattered Light Displacement Noise of PRM Elliptical Baffle	56
3.2.6.2.6	Stay Clear Diameter	57
3.2.7	Wide Angle Scatter from COC	57
3.2.7.1	Manifold Baffle	58
3.2.7.1.1	Seismic Motion of Manifold Baffle	58
3.2.7.2	Manifold Wall	58
3.2.7.2.1	Seismic Motion of Manifold Wall	58
3.2.7.3	Back of Arm Cavity Baffle and Cylinder	58
3.2.7.4	BSC Chamber Wall	58
3.2.7.4.1	Summary Scattered Light Displacement Noise of Wide-angle COC Scattering	58
3.2.8	Output Window	61
3.2.8.1	Output Window BRDF	63
3.2.8.2	Seismic Motion of the Output Windows	63
3.2.8.3	Scattered Light Displacement Noise of Output Window	63
3.2.8.4	Reflected Light from AS Output Window	64
3.2.8.5	Output Septum Windows Removal	65
3.2.8.5.1	Stay Clear Diameter	65
3.2.9	Hartmann Viewports	65
3.2.9.1	Hartmann Viewport BRDF	66
3.2.9.2	Reflected Light from Hartmann Viewport	67
3.2.9.2.1	Scattered Light Displacement Noise of Ghost Beams	67
3.2.10	ITM GBAR1, GBAR3, and GBAR4 Ghost Beams	67
3.2.10.1	PR2/SR2 Cavity Beam Dump BRDF	67
3.2.10.2	PR2/SR2 Cavity Beam Dump Reflectivity	67
3.2.10.3	Scattered Light Displacement Noise of Ghost Beams	67
3.2.11	ITM HR, BS AR, AND BS HR Ghost Beams	68
3.2.11.1	Beam Tube Baffle BRDF and Reflectivity	68
3.2.11.2	Scattered Light Displacement Noise of Ghost Beams	68
3.2.12	BS GBHR3P, BS GBHR	70
3.2.12.1	Scattered Light Displacement Noise of Ghost Beams	70
3.2.13	ITMX PO Beam (BS GBAR1)	71
3.2.14	PRM Ghost Beams	71
3.2.14.1	PRM GBAR1	71
3.2.14.2	PRM GBAR3	72
3.2.14.3	PRM GBHR3	72
3.2.14.4	PRM Plate Beam Dump Surface BRDF and Reflectivity	72
3.2.14.5	Scattered Light Displacement Noise of Ghost Beams	72
3.2.15	PR2 Ghost Beams	72
3.2.15.1	PR2 GBAR0t	72
3.2.15.2	PR2 GBAR0t Cavity Beam Dump Surface BRDF and Reflectivity	72
3.2.15.3	RC PO Beam (PR2 GBARt)	72
3.2.15.4	PR2 GBAR3	73
3.2.15.5	PR2 GBHR3	73
3.2.15.6	PR2 Plate Beam Dump Surface BRDF and Reflectivity	74

3.2.15.7	Scattered Light Displacement Noise of Ghost Beams	74
3.2.16	<i>PR3 Ghost Beams</i>	74
3.2.16.1	PR3 GBAR0t	74
3.2.16.2	PR3 GBAR3	74
3.2.16.3	PR3 GBHR3	74
3.2.16.4	PR3 Plate Beam Dump Surface BRDF and Reflectivity	74
3.2.16.5	Scattered Light Displacement Noise of PR3 Ghost Beams	75
3.2.17	<i>SRM Ghost Beams</i>	75
3.2.17.1	SRM GBAR3	75
3.2.17.2	SRM GBHR3	75
3.2.17.3	SRM Plate Beam Dump Surface BRDF and Reflectivity	75
3.2.17.4	Scattered Light Displacement Noise of Ghost Beams	75
3.2.18	<i>SR2 Ghost Beams</i>	75
3.2.18.1	SR2 GBAR0t	75
3.2.18.2	SR2 GBAR3	76
3.2.18.3	SR2 GBHR3	76
3.2.18.4	SR2 Plate Beam Dump Surface BRDF and Reflectivity	77
3.2.18.5	Scattered Light Displacement Noise of Ghost Beams	77
3.2.19	<i>SR3 Ghost Beams</i>	77
3.2.19.1	SR3 GBAR0t	77
3.2.19.2	SR3 GBAR3	77
3.2.19.3	SR3 GBHR3	77
3.2.19.4	SR3 Plate Beam Dump Surface BRDF and Reflectivity	77
3.2.19.5	Scattered Light Displacement Noise of SR3 Ghost Beams	78
3.2.20	<i>ETM Telescope Baffle</i>	78
3.2.20.1	ETM Telescope Baffle Motion Requirements	79
3.2.20.2	ETM Telescope Baffle Surface BRDF	79
3.2.20.3	ETM Telescope Baffle Reflectivity	79
3.2.20.4	Seismic Motion of the ETM Telescope Baffle Scattering Surfaces	80
3.2.20.5	Scattered Light Displacement Noise of Suspended ETM Telescope Baffle	80
3.3	STRAY LIGHT CONTROL PHYSICAL CHARACTERISTICS	80
3.3.1	<i>Faraday Isolator</i>	80
3.3.2	<i>Arm Cavity Baffle</i>	81
3.3.3	<i>Arm Cavity Baffle Cylinder</i>	82
3.3.4	<i>Elliptical Baffle</i>	83
3.3.4.1	ITM Elliptical Baffle	83
3.3.4.2	PRM Elliptical Baffle	83
3.3.5	<i>Manifold Baffle</i>	83
3.3.6	<i>Septum Window</i>	84
3.3.7	<i>PR2/SR2 Cavity Beam Dump</i>	84
3.3.8	<i>Cryopump Baffle</i>	85
3.3.9	<i>ETM Telescope Baffle</i>	85
3.4	STRAY LIGHT CONTROL INTERFACE DEFINITIONS	86
3.4.1	<i>Interfaces to other LIGO detector subsystems</i>	86
3.4.1.1	Mechanical Interfaces	86
3.4.1.2	Electrical Interfaces	86
3.4.1.2.1	Suspended Baffles and Beam Dumps	86
3.4.1.2.2	Faraday Isolator	86
3.4.1.3	Optical Interfaces	86
3.4.1.4	Stay Clear Zone	86
3.4.1.4.1	Arm Cavity Baffle	86
3.4.1.4.2	ITMX, ITMY, and BS Beam Dump	87
3.4.1.4.3	Cryopump Baffle	87
3.4.1.4.4	ETM Telescope Baffle	87
3.4.1.4.5	Elliptical Baffle	87
3.4.2	<i>Interfaces external to LIGO detector subsystems</i>	87
3.5	STRAY LIGHT CONTROL RELIABILITY	87
3.6	STRAY LIGHT CONTROL MAINTAINABILITY	87
3.7	STRAY LIGHT CONTROL ENVIRONMENTAL CONDITIONS	87
3.7.1.1.1.1	Natural Environment	87

3.7.1.1.1.2	Induced Environment.....	88
3.8	STRAY LIGHT CONTROL TRANSPORTABILITY.....	88
4	STRAY LIGHT CONTROL DESIGN AND CONSTRUCTION.....	89
4.1.1.1	Materials and Processes.....	89
4.1.1.1.1	Materials.....	89
4.1.1.1.2	Processes.....	89
4.1.1.1.2.1	Cleaning.....	89
4.1.1.1.3	Component Naming.....	89
4.1.1.2	Stray Light Control Workmanship.....	89
4.1.1.3	Stray Light Control Interchangeability.....	89
4.1.1.4	Stray Light Control Safety.....	90
4.1.1.5	Stray Light Control Human Engineering.....	90
4.1.2	<i>Stray Light Control Assembly and Maintenance</i>	90
4.1.3	<i>Stray Light Control Documentation</i>	90
4.1.3.1	Stray Light Control Specifications.....	90
4.1.3.2	Stray Light Control Design Documents.....	90
4.1.3.3	Stray Light Control Engineering Drawings and Associated Lists.....	90
4.1.3.4	Stray Light Control Technical Manuals and Procedures.....	91
4.1.3.4.1	Procedures.....	91
4.1.3.5	Stray Light Control Documentation Numbering.....	91
4.1.3.6	Stray Light Control Test Plans and Procedures.....	91
4.1.4	<i>Stray Light Control Logistics</i>	91
4.1.5	<i>Stray Light Control Precedence</i>	91
4.1.6	<i>Stray Light Control Qualification</i>	91
5	QUALITY ASSURANCE PROVISIONS.....	92
5.1	GENERAL.....	92
5.1.1	<i>Responsibility for Tests</i>	92
5.1.2	<i>Special Tests</i>	92
5.1.2.1	Engineering Tests.....	92
5.1.2.1.1	Witness Sample Scattering Tests of Baffle and Beam Dump Material.....	92
5.1.2.1.2	ETM Telescope Performance Test.....	92
5.1.2.1.3	ETM Telescope Suspension Damping Test.....	92
5.1.2.1.4	Faraday Isolator Performance Test.....	92
5.1.2.1.5	Faraday Isolator Suspension Damping Test.....	92
5.1.2.1.6	TBD.....	92
5.1.2.2	Reliability Testing.....	92
5.1.3	<i>Configuration Management</i>	92
5.2	QUALITY CONFORMANCE INSPECTIONS.....	92
5.2.1	<i>Inspections</i>	92
5.2.2	<i>Demonstration</i>	93
5.2.3	<i>Test</i>	93
6	PREPARATION FOR DELIVERY.....	94
6.1	PREPARATION.....	94
6.2	PACKAGING.....	94
6.3	MARKING.....	94
7	APPENDIX A—SCATTERED LIGHT NOISE THEORY.....	95
7.1	SCATTERED LIGHT REQUIREMENT.....	95
7.2	SCATTERED POWER INTO THE IFO.....	96
7.2.1	<i>Output Faraday Isolator Scatter</i>	97
7.2.2	<i>Arm Cavity Baffle Surface Scatter</i>	97
7.2.3	<i>Arm Cavity Baffle Reflected Light</i>	98
7.2.4	<i>ITM Elliptical Baffle Surface Scatter</i>	99
7.2.5	<i>ITM Elliptical Baffle Reflected Light</i>	101
7.2.6	<i>PRM Elliptical Baffle</i>	101

7.2.7	<i>ITM (ETM) Wide-Angle Scatter</i>	103
7.2.7.1	Scattering from the Back of Arm Cavity Baffle	104
7.2.7.2	Scattering from the Cylindrical Baffle	104
7.2.7.3	Total Scattered Light Displacement Noise from Arm Cavity Baffle and Cylindrical Baffle	105
7.2.7.4	Scattering from the Manifold Baffle	105
7.2.7.5	Scatter from ITM Manifold Wall	106
7.2.7.6	Scattering from BSC Chamber Walls	106
7.2.7.7	Total Wide-Angle Scattered Light Displacement Noise from BSC Chamber, Manifold Walls, and Manifold Baffle	107
7.2.8	<i>Septum Window Scatter</i>	107
7.2.8.1	AS Output Window	107
7.2.8.2	AS Output Window Reflection	108
7.2.8.3	ITMX PO Septum Window	108
7.2.8.4	ITMX PO Septum Window Reflection	109
7.2.8.5	RC PO Septum Window	109
7.2.8.6	RC PO Septum Window Reflection	109
7.2.9	<i>ITMY Hartmann Viewport</i>	110
7.2.10	<i>ITMX Hartmann Viewport</i>	110
7.2.11	<i>Ghost Beams</i>	111
7.2.11.1	Ghost Beam Naming Convention	111
7.2.11.2	ITMAR1	112
7.2.11.3	ITMAR1 REFL	113
7.2.11.4	ITMAR3	113
7.2.11.5	ITMAR3 REFL	113
7.2.11.6	ITMHR3	114
7.2.11.7	BSAR3	114
7.2.11.8	BHR3	115
7.2.11.9	BSAR3P	115
7.2.11.10	BSAR3P REFL	115
7.2.11.11	BHR3P	116
7.2.11.12	BHR3P REFL	116
7.2.12	<i>PRM</i>	117
7.2.12.1	PRMAR1	117
7.2.12.2	PRMAR3	117
7.2.12.3	PRMHR3	117
7.2.12.4	Total Displacement Noise from PRM	117
7.2.13	<i>PRM2</i>	118
7.2.13.1	PR2AR0t	118
7.2.13.2	PR2AR3	118
7.2.13.3	PR2HR3	118
7.2.13.4	Total Displacement Noise from PR2	119
7.2.14	<i>PRM3</i>	119
7.2.14.1	PR3AR0t	119
7.2.14.2	PR3AR3	119
7.2.14.3	PR3HR3	119
7.2.14.4	Total Displacement Noise from PR3	120
7.2.15	<i>SRM</i>	120
7.2.15.1	SRMAR3	120
7.2.15.2	SRMHR3	120
7.2.15.3	Total Displacement Noise from SRM	120
7.2.16	<i>SRM2</i>	121
7.2.16.1	SR2AR0t	121
7.2.16.2	SR2AR3	121
7.2.16.3	SR2HR3	121
7.2.16.4	Total Displacement Noise from SR2	121
7.2.17	<i>SRM3</i>	122
7.2.17.1	SR3AR0t	122
7.2.17.2	SR3AR3	122
7.2.17.3	SR3HR3	122
7.2.17.4	Total Displacement Noise from SR3AR	122
7.2.18	<i>Cryopump Baffle Scatter</i>	123

7.2.19	Cryopump Baffle Reflected Scatter	123
7.2.20	ETM Telescope Baffle Scatter	124
7.2.21	ETM Telescope Baffle Reflection Scatter	124
7.2.22	Fringe-Wrapping.....	125
7.2.22.1.1.1	Damped Pendulum Example.....	127
7.3	SCATTERED LIGHT PARAMETERS	128

Table of Tables

Table 1:	COC Wedge Angles, Non-folded IFO	27
Table 2:	COC Wedge Angles, Folded IFO	28
Table 3:	Scattered Light Source, Incident Power and Scattered Power	29
Table 4:	Faraday Isolator Characteristics	81
Table 5 :	Faraday Isolator Suspension Characteristics	81
Table 6:	Arm Cavity Baffle Characteristics	81
Table 7:	Arm Cavity Baffle Suspension	82
Table 8:	Arm Cavity Baffle Cylinder Characteristics	82
Table 9:	Arm Cavity Baffle Suspension	82
Table 10:	ITM Elliptical Baffle Characteristics	83
Table 11:	PRM Elliptical Baffle Characteristics.....	83
Table 12:	Manifold Baffle.....	84
Table 13:	Septum Window Characteristics	84
Table 14:	Cavity Beam Dump Characteristics	84
Table 15:	Cryopump Baffle Characteristics	85
Table 16:	ETM Telescope Baffle Characteristics.....	85
Table 17:	Environmental Performance Characteristics	88
Table 18:	IFO parameter values used for scattered light calculation	128

Table of Figures

Figure 1:	AOS System Block Diagram	13
Figure 2:	Output beam and ITMX PO beam hitting SR3 mirror.....	18
Figure 3:	ITMX PO Beam from AR surface of BS, with scraper beam dump in front of SR2.....	19
Figure 4:	Scraper beam dump in front of PR2	20
Figure 5:	PR2 Cavity Beam Dump, Beam Clearance	21
Figure 6:	SR2 Cavity Beam Dump, Beam Clearance.....	22
Figure 7:	PRM beam dumps, elevation view.....	23
Figure 8:	SRM beam dumps, elevation view	24
Figure 9:	PR2 Plate Beam Dumps, elevation view	25
Figure 10:	SR2 Plate Beam Dumps, elevation view.....	25
Figure 11:	PR3 AR beam dump.....	26
Figure 12:	SR3 AR beam dump	27
Figure 13:	Scattered Light Displacement Noise, Septum Windows in Place	32
Figure 14:	Scattered Light Displacement Noise, Septum Windows Removed	33
Figure 15:	Initial LIGO Output Faraday Isolator Parts Suspended in a Modified LOS	35
Figure 16:	HAM optics table Seismic Motion Requirement.....	36
Figure 17:	Output Faraday Isolator SUS Amplitude Response	37
Figure 18:	Scattered Light Displacement Noise from Suspended Faraday Isolator	38

Figure 19: Suspended Arm Cavity Baffle	39
Figure 20: BSC HEPI Motion Spectrum	40
Figure 21: Arm Cavity Baffle Attenuation, Minimum Requirement	41
Figure 22: Transverse Transfer Function, ACB SUS	42
Figure 23: Yaw Transfer Function, ACB SUS	42
Figure 24: Vertical Transfer Function, Arm Cavity Baffle SUS	43
Figure 25: Seismic motion of vacuum manifold	44
Figure 26: Arm Cavity Baffle and Cryopump Baffle Scattered Light Displacement Noise	45
Figure 27: Arm Cavity Baffle Scattered Light Displacement Noise Caused by Fringe-wrapping ..	46
Figure 28: Conceptual Model of Suspended Cryopump Baffle	48
Figure 29: Cryopump Suspension Amplitude Response	49
Figure 30: Cryopump Baffle Scattered Light Displacement Noise Caused by Fringe-wrapping....	50
Figure 31: Suspended Elliptical Baffle	52
Figure 32: Elliptical Baffle SUS Amplitude Response	53
Figure 33: Seismic motion of BSC chamber	54
Figure 34: PRM Elliptical Baffle on HAM3	55
Figure 35: Elliptical Baffle Scattered Light Displacement Noise	57
Figure 36: Manifold Baffle	59
Figure 37: Arm Cavity Baffle with Cylindrical Baffle	60
Figure 38: Total wide-Angle COC Scattered Light Displacement Noise	61
Figure 39: Output Septum Plate	62
Figure 40: Output Septum Windows	63
Figure 41: Displacement Spectrum of HAM 6 Flange	64
Figure 42: Output Window Scattered Light Displacement noise	65
Figure 43: Hartmann Viewports	66
Figure 44: ITM GBAR1, GBAR3, and GBAR4 Beam Dump Scattered Light Displacement Noise .	68
Figure 45: ITM GBHR Beam Dump Scattered Light Displacement Noise	69
Figure 46: BS GBARX and GBHRX Scattered Light Displacement Noise	70
Figure 47: BS GBAR3P and BS GBHR3P Beam Dump Scattered Light Displacement Noise	71
Figure 48: PR2 GBAR0t beam dump	73
Figure 49: SR2 AR0t beam dump	76
Figure 50: PRM, PR2, PR3, SRM, SR2, SR3, Scattered Light Displacement Noise	78
Figure 51: ETM Telescope Baffle	79
Figure 52: Scattered Light Displacement Noise of ETM Telescope Baffle	80
Figure 53: Scattered Light Noise Transfer Functions	96
Figure 54: ARM CAVITY BAFFLE SCATTER	97
Figure 55: ITM ELLIPTICAL BAFFLE SCATTER AND REFLECTION	99
Figure 56: Wide-angle Scatter from ITM (ETM)	103
Figure 57: PRM, SRM, ITM, and ETM ghost beam naming convention	111
Figure 58: BS ghost beam naming convention	112
Figure 59: Noise Waveform at the Onset of Fringe-Wrapping, $\lambda/8$	126
Figure 60: Displacement Noise waveform with Fringe-wrapping, $\lambda/4$	126
Figure 61: Scattered Light Displacement Noise Caused by Fringe-wrapping	128

Abstract

This document will present the conceptual design for the AOS Stray Light Control subsystem for ADLIGO.

1 Introduction

1.1 Purpose

The purpose of this document is to present a conceptual design that meets the SLC Design requirements. Primary requirements are derived (“flowed-down”) from the LIGO principal science requirements. Secondary requirements, which govern Detector performance through interactions between AOS and other Detector subsystems, have been allocated by Detector Systems Engineering.

1.2 Scope

This document will present conceptual designs for the Stray Light Control (SLC) subsystem of AOS under the following assumptions: 1) the recycling cavity is assumed to be stable; 2) the wedge angles for the ITM, CP, and BS are horizontal.

1.2.1 Stray Light Control

A block diagram showing the principal scattering sources of the AOS System is shown in Figure 1.

AOS is responsible for controlling and reducing to acceptable levels the displacement noise due to scattered light injected into the IFO mode.

AOS is not responsible for scattering that occurs in the IO section, which is defined as everything prior to PRM on HAM2 and HAM8; and everything in the ISC section on HAM6, HAM1, HAM12, and HAM7.

The Stray Light Control subsystem will corroborate with the Systems group on the choice of COC wedge angles for producing PO beams.

The Stray Light Control subsystem will provide an ETM telescope baffle to block the excess light transmitted through the ETM that exceeds the clear aperture of the ETM telescope.

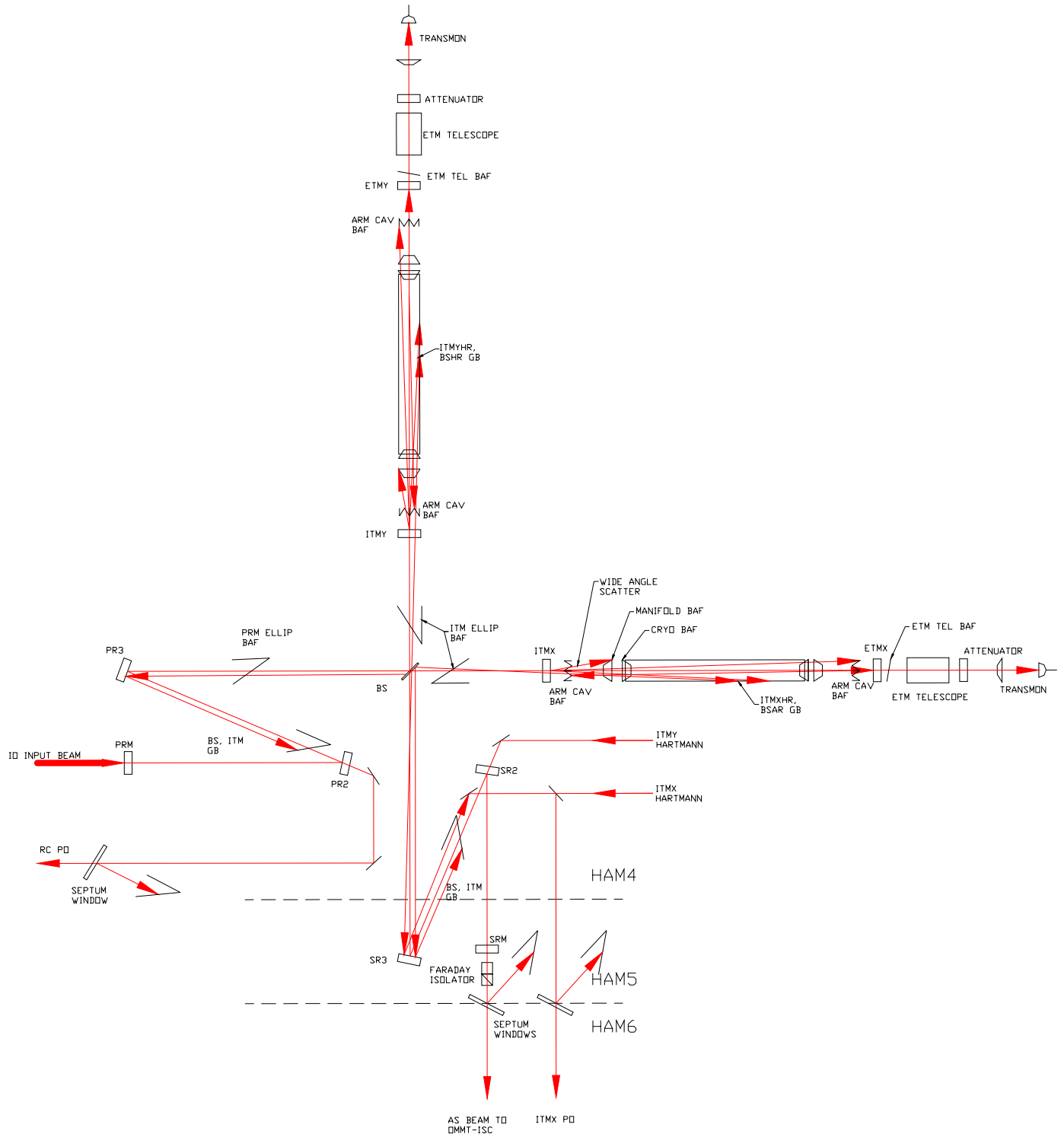


Figure 1: AOS System Block Diagram

1.3 Definitions

1.4 Acronyms

AOS - Auxiliary Optics Support

AR - Antireflection mirror coating

AS - anti-symmetric port signal

ASC - Alignment Sensing and Control

BS - Beam Splitter

BSC - Beam Splitter Chamber

CDS – Computer Data Systems

CP – Compensation plate

ETM_x, ETM_y - End Test Mass in the interferometer ‘X’ or ‘Y’ arm

HAM - Horizontal Access Module

HR – Hi-reflectance mirror coating

IFO - LIGO interferometer

IO - Input Optics

ISC- Interferometer Sensing and Control

ITM_x, ITM_y - Input Test Mass in the interferometer ‘X’ or ‘Y’ arm

LIGO - Laser Interferometer Gravity Wave Observatory

LSC - Length Sensing and Control

LVEA-vacuum equipment area

mm – millimeter

MMT – mode matching telescope

mrad – milliradian

MTBF – mean time before failure

NA – not applicable

nm – nanometer

OSEM – sensor/actuator head

PO - Pick-off

p-p, peak to peak

ppm - parts per million

PRM – Power Recycling Mirror

p-v, peak to valley

Q – quality factor
QPD – quadrant photo diode
RH – relative humidity
ReM – Reaction mass
rms - root-mean-square
rtHz – square root Hertz
SLC – Stray Light Control
SOS – Small Optic Suspension
SRD - Science Requirements Document
SRM – Signal Recycling Mirror
SW – Solid Works
TBD - To Be Determined
W - Watt
WFS – wave front sensor

1.5 Applicable Documents

1.5.1 LIGO Documents

1. E950111-A LIGO Naming Convention
2. E960022-B LIGO Vacuum Compatibility, Cleaning Methods and Qualification Procedures
3. L970061-00-D Guidance for Seismic Component Cleaning, Baking, and Shipping Preparation
4. M950046-F LIGO Project System Safety Management Plan
5. T040126-A Baffle Furnace Bake Procedure
6. G070657 LSC-Virgo meeting, 10/24/07, Hiro Yamamoto
7. MIL-C-104B
8. M060056-06 Advanced LIGO Reference Design
9. E990303-03 Seismic Isolation Subsystem Design Requirements Document
10. LIGO-T960065-03 Seismic Isolation Design Requirements Document
11. T060013-02, Inputs to Beam Tube Scattering and Optical Surface Roughness Requirement Analysis for Advanced LIGO (table2)
12. T060360-02 PO Mirror Assembly & Telescope, and OMMT Conceptual Design Requirements
13. T960151-02 Large and Small Optics Suspension Electronics Design Requirements

14. T070089-02 Wide-angle Scatter from LIGO Arm Cavities
15. T010076-01 Optical Layout for Advanced LIGO
16. M060062-00 HAM Single-stage Isolation Baseline Option Review Report
17. T060073-00 Transfer Functions of Injected Noise
18. T920004-00 Estimation of Special Optical Properties of a Triangular Ring Cavity
19. T980104-00 COS Final Design
20. T070003-00 Backscattering from the AS Port: A Comparison of P. Fritschel's Estimate and
21. T070061-00 AOS: Stray Light Control (SLC) Design Requirements
22. T080064-00 Controlling Light Scatter in Advanced LIGO
23. Robert Schofield (11/17/06 LHO ILOG)
24. T980027-00, Baffling Requirements for the 4K and 2K IFO
25. E980131-A, Component Specification, Faraday Isolator, 20 mm

1.5.2 Non-LIGO Documents

2 Catalog of SLC Design Requirements

The requirements for the SLC subsystem are derived in T070061-00 AOS: Stray Light Control (SLC) Design Requirements and are referenced below by paragraph number.

1. 4.2 Noise Requirements
2. 4.2.1 Direct Requirements
3. 4.2.2 Implied Requirement for Scattering Surfaces
4. 4.3 Faraday Isolator Requirements
5. 4.4 IO Baffle Requirement
6. 4.5 Cryopump Baffle Requirement
7. 4.6 BSC Chamber Components
8. 4.7 Clear Aperture Requirements
9. 4.8 Generic Requirements
10. 4.8.1 Mechanical Characteristics & Standards
11. 4.8.2 Electrical Characteristics & Standards
12. 4.8.3 Vacuum Compatibility Requirements
13. 4.8.4 Acoustic Requirements
14. 4.8.5 Earthquake Requirements
15. 4.8.6 Operating Environment
16. 4.8.7 Quality Assurance
17. 4.8.8 Reliability
18. 4.8.9 Maintainability
19. 4.8.10 Documentation
20. 4.8.11 Transportability
21. 4.8.11 Safety

3 Stray Light Control Conceptual Design Characteristics

3.1 COC Wedge Angle Determination

The COC wedge angles determine the separation between the main beam in the recycling cavity and the ghost beams that will either be intercepted with a pick-off mirror, or dumped on a beam dump.

3.1.1 Beam Profile in Recycling Cavity

The Beam cross section within the recycling cavity is non-Gaussian, and is determined in the vertical direction by the clear aperture of PR3, 245 mm, and in the horizontal direction by the clear aperture of the BS, 370 mm diameter by 60 mm thick, tilted at 45 degrees. The beam profile is approximately an ellipse with the horizontal semi-diameter of 107 mm and the vertical semi-diameter of 125 mm (see G070657 LSC-Virgo meeting, 10/24/07, Hiro Yamamoto , RC beam size calculation).

3.1.2 Wedge Angles for Non-folded IFO

3.1.2.1 BS Wedge Angle

The BS wedge angle of 0.04 deg was chosen to cause the prompt reflection from the AR surface of the beam splitter, BS GBAR1 (ITMX PO beam) to hit the center of the signal recycling telescope mirror SR3. See Figure 2.

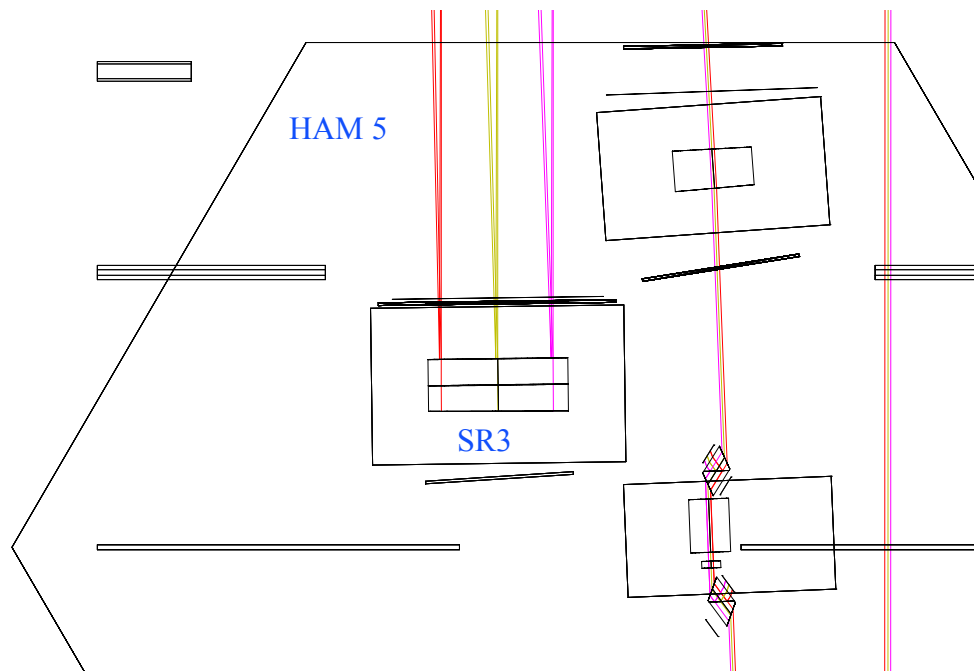


Figure 2: Output beam and ITMX PO beam hitting SR3 mirror

With this BS wedge angle, the ITMX PO beam separates from the main beam and passes through a hole in the scraper beam dump in front of SR2 mirror and is picked off with a small diameter mirror, as illustrated in the ZEMAX layout in Figure 3. The main, output beam also passes through a hole in the scraper beam dump and is reflected from SR2 back to SRM on HAM6.

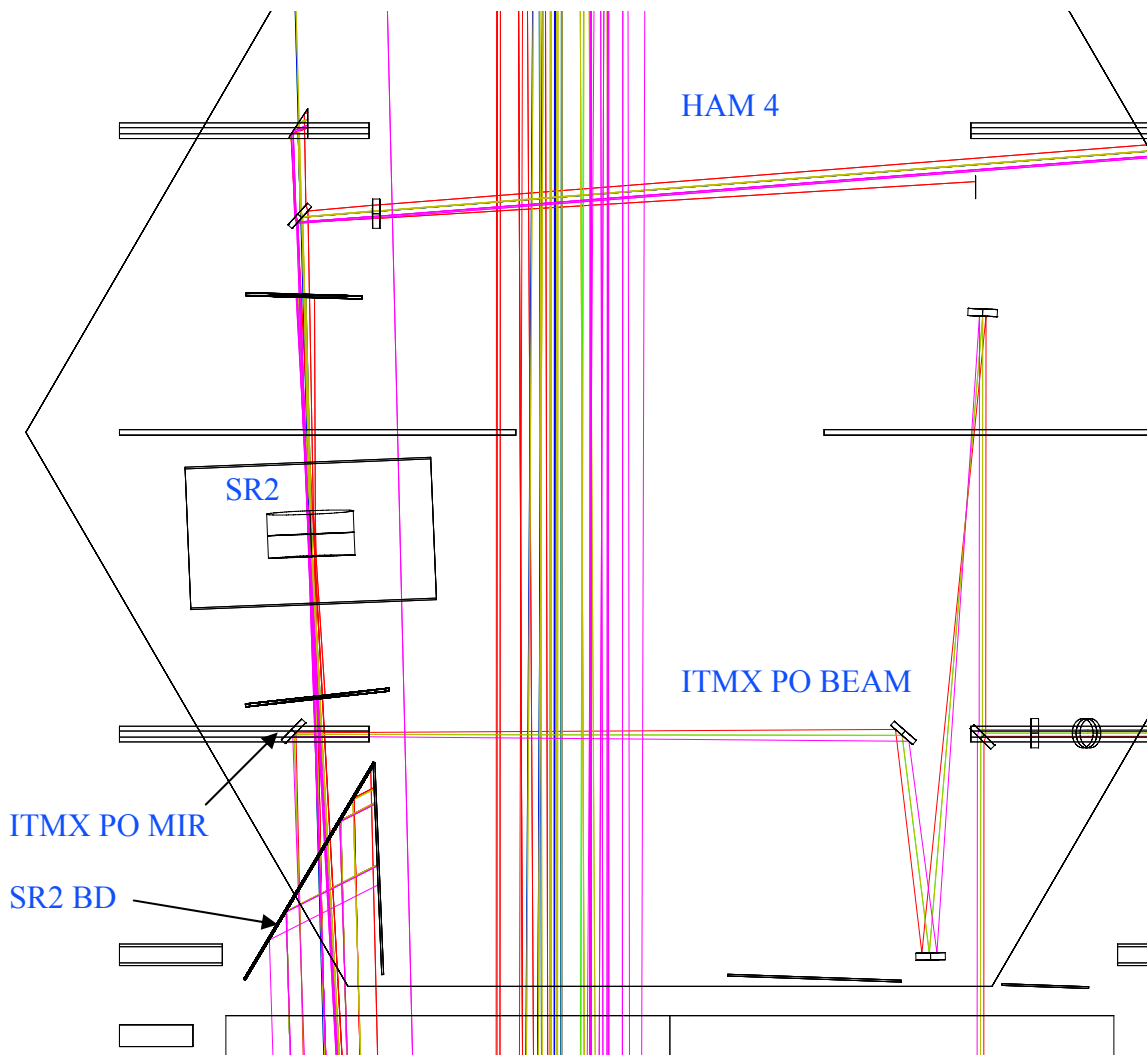


Figure 3: ITMX PO Beam from AR surface of BS, with scraper beam dump in front of SR2

3.1.2.2 ITM Wedge Angle

A minimum wedge angle of 0.08 deg was chosen for the ITM, commensurate with metrology of the AR and HR surfaces. With this small wedge angle, the ghost beams from the ITM enter the power recycling and the signal recycling telescopes and are caught by the “scraper” beam dumps in front of the PR2 and SR2 mirrors, as shown in Figure 3, and Figure 4.

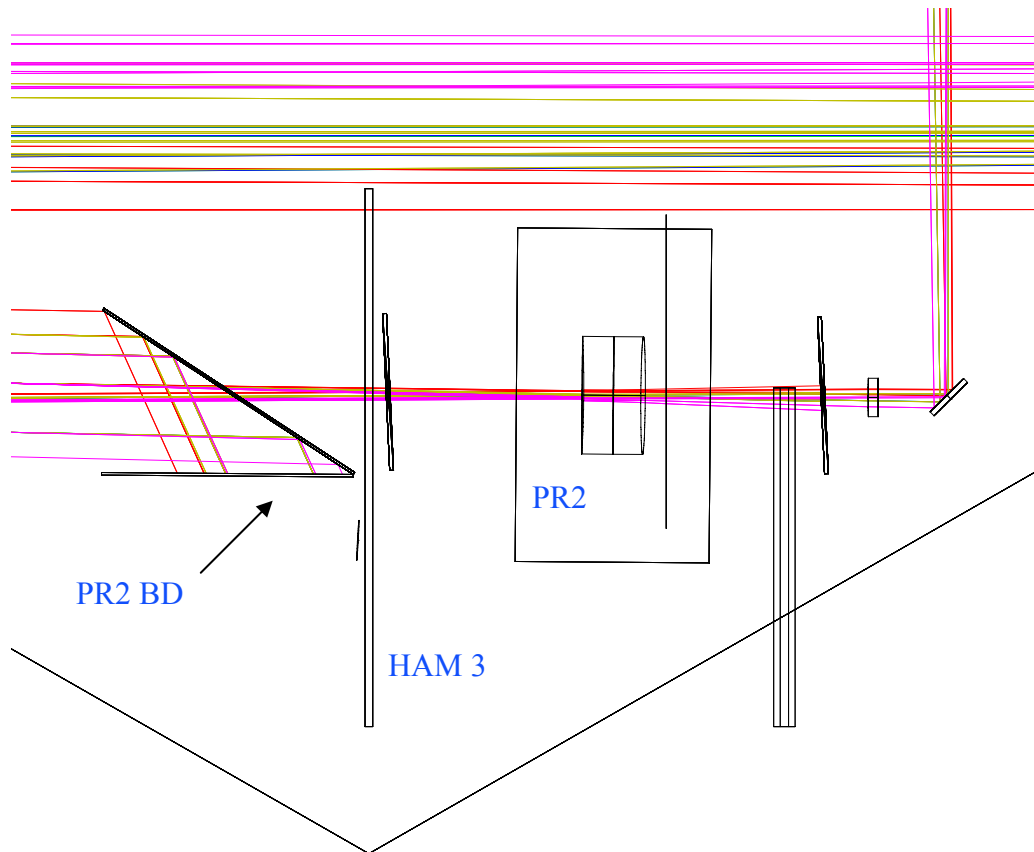


Figure 4: Scraper beam dump in front of PR2

3.1.2.3 CP Wedge Angle

The CP wedge angle was chosen to be 0.04 deg, the same as the BS wedge angle, in order to minimize the tooling requirements. The ghost beams from the internal reflections of the CP also will fall within the PR and SR telescopes and will be caught by the scraper beam dumps in front of the PR2 and SR2 mirrors.

3.1.2.4 Stay Clear Diameter

The clearance between the main beam and the ITM and BS ghost beams that land on the PR2 scraper cavity beam dump is shown in Figure 5. The minimum spacing between the main beam and the closest ghost beam is approximately 40 mm. The Gaussian beam diameters are less than 4 mm.

The clearance between the main beam and the ITM and BS ghost beams that land on the SR2 scraper cavity beam dump is shown in Figure 6. The minimum spacing between the main beam and the closest ghost beam is approximately 25 mm.

The beams are in the vicinity of the telescope's beam waists and the diameters of the beams will be < 2 mm.

This meets the requirement 4.7 Clear Aperture Requirements

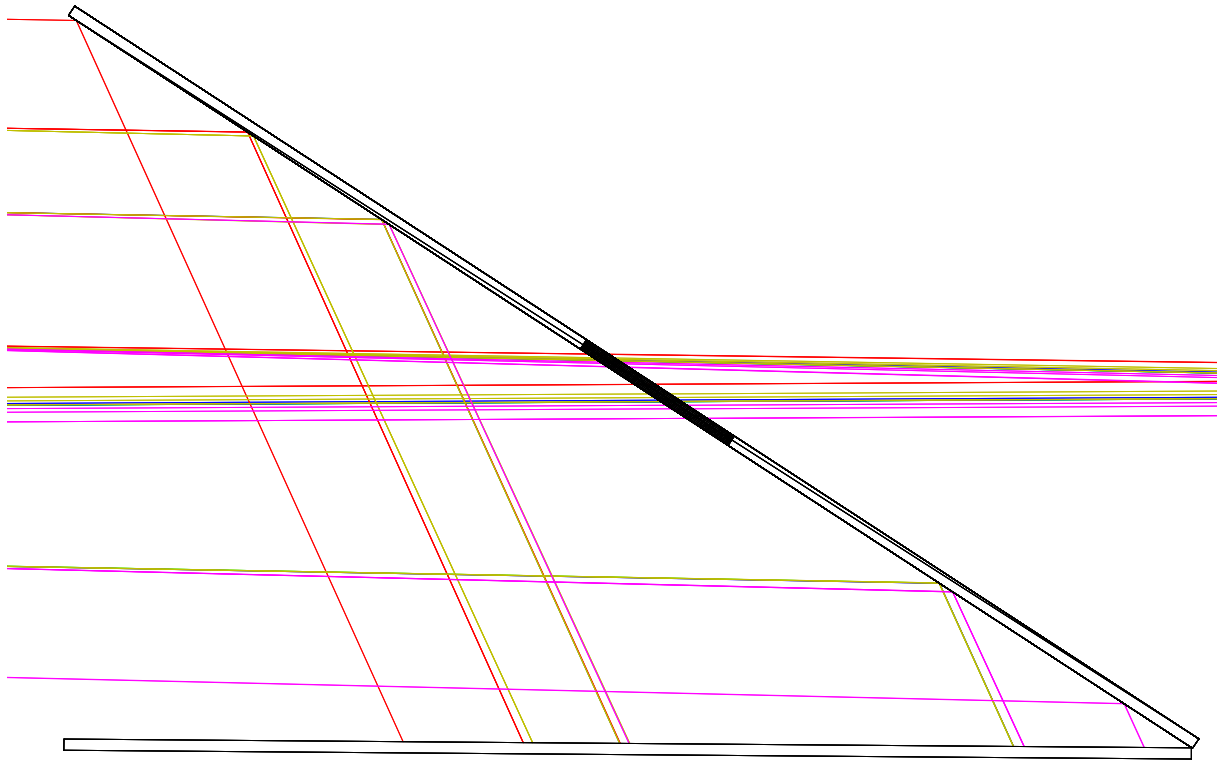


Figure 5: PR2 Cavity Beam Dump, Beam Clearance

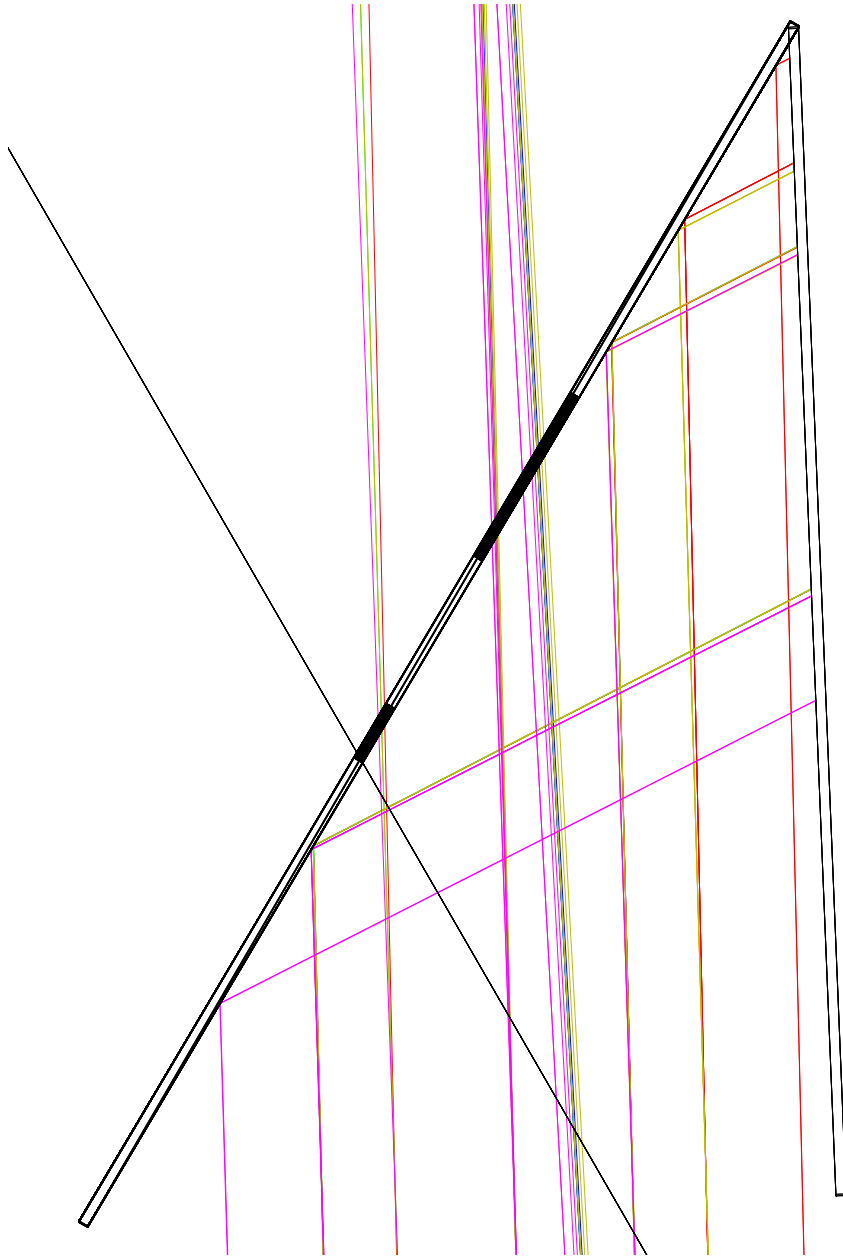


Figure 6: SR2 Cavity Beam Dump, Beam Clearance

3.1.2.5 PRM and SRM Wedge Angle

The PRM and SRM wedge angles will be 2 deg in the vertical direction. This ensures that the ghost beams separate far enough from the main beam to be caught in nearby beam dumps, as shown in Figure 7, and Figure 8.

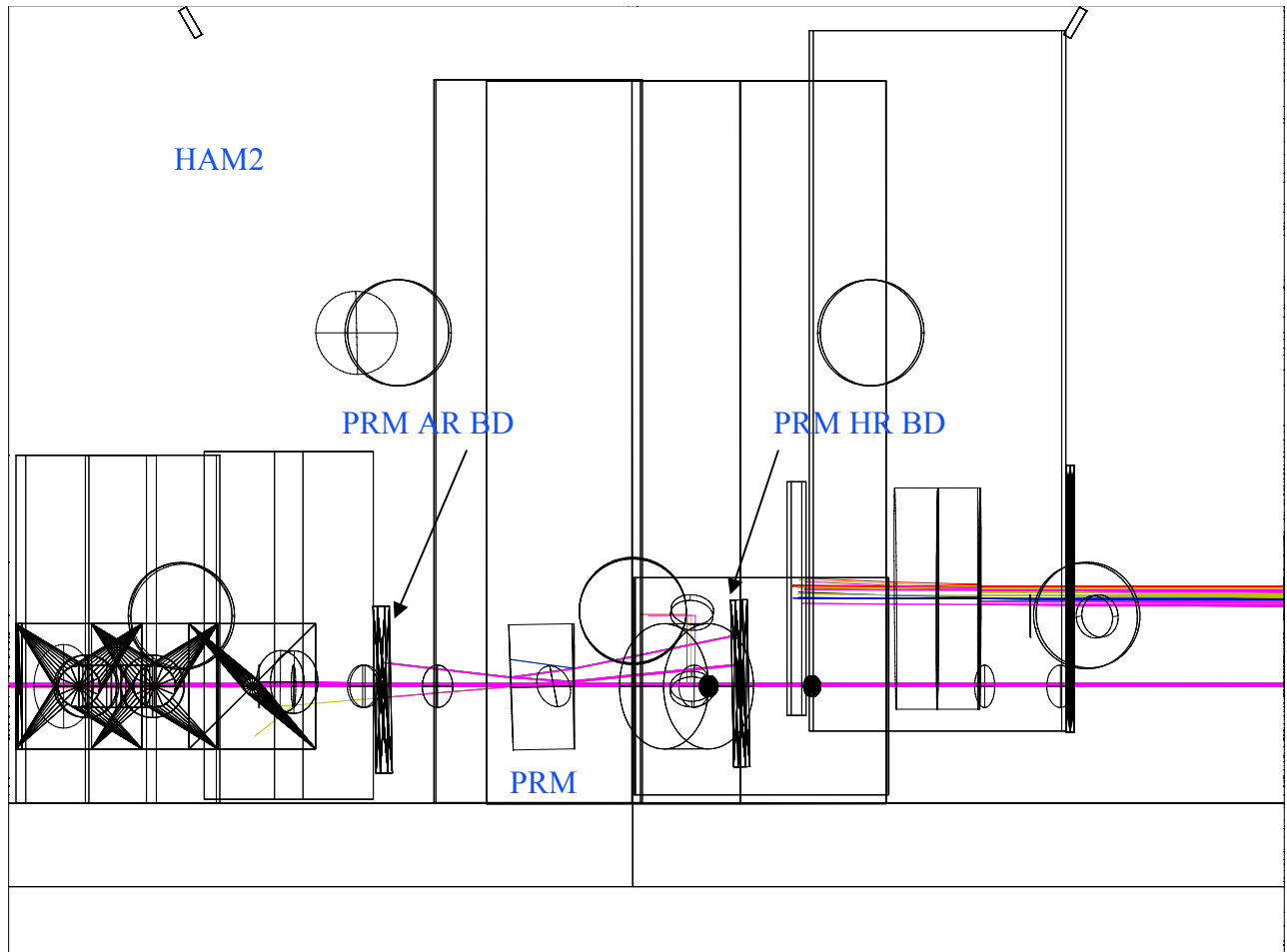


Figure 7: PRM beam dumps, elevation view

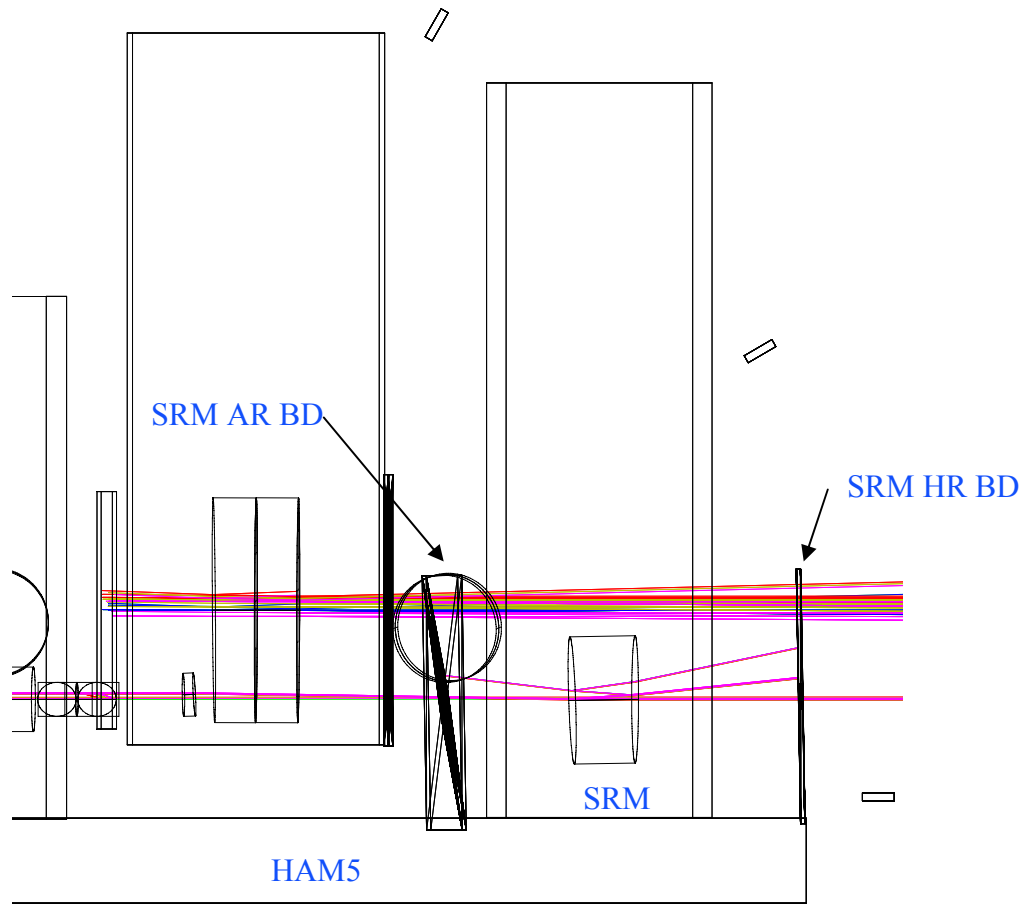


Figure 8: SRM beam dumps, elevation view

3.1.2.6 PR2 and SR2 Wedge Angle

The PR2 and SR2 wedge angles will be 2 deg. This ensures that the ghost beams will separate far enough from the main beam to be caught in nearby beam dumps, as shown in Figure 9 and Figure 10.

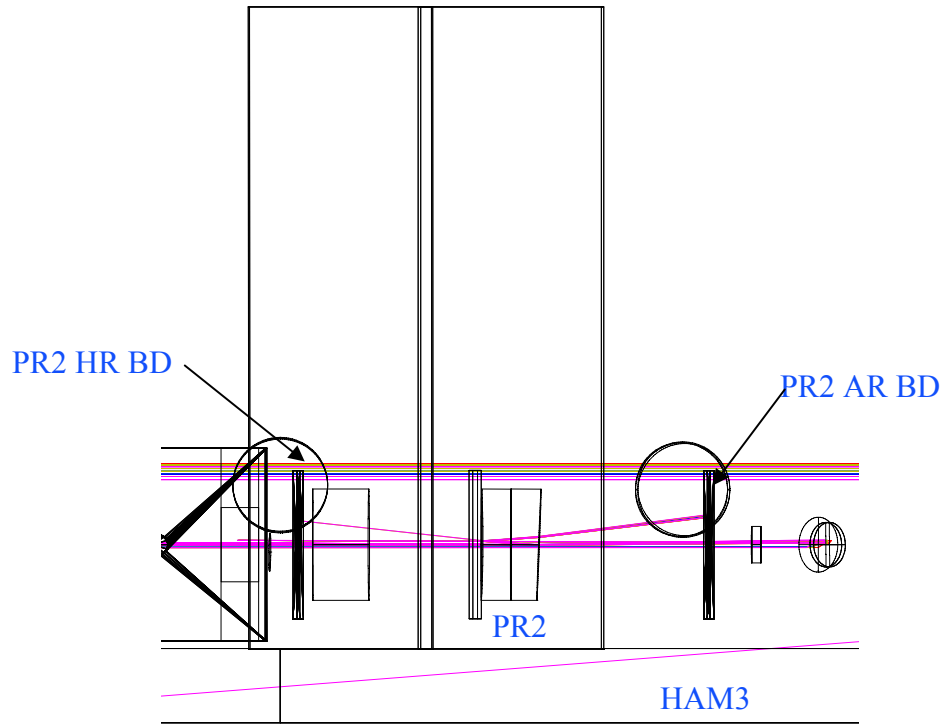


Figure 9: PR2 Plate Beam Dumps, elevation view

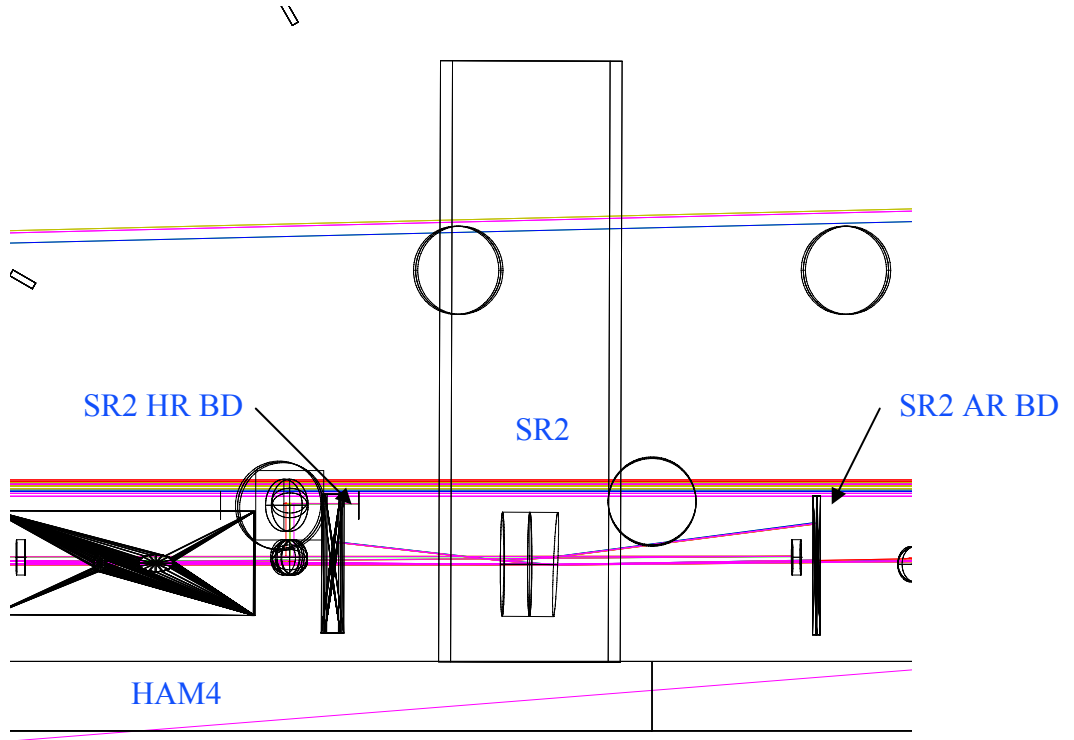


Figure 10: SR2 Plate Beam Dumps, elevation view

3.1.2.7 PR3 and SR3 Wedge Angle

The PR3 and SR3 wedge angles will be 0.6 deg. The ghost beams from the AR side will be caught in the beam dump adjacent to the AR surface, as shown in Figure 11, and Figure 12.

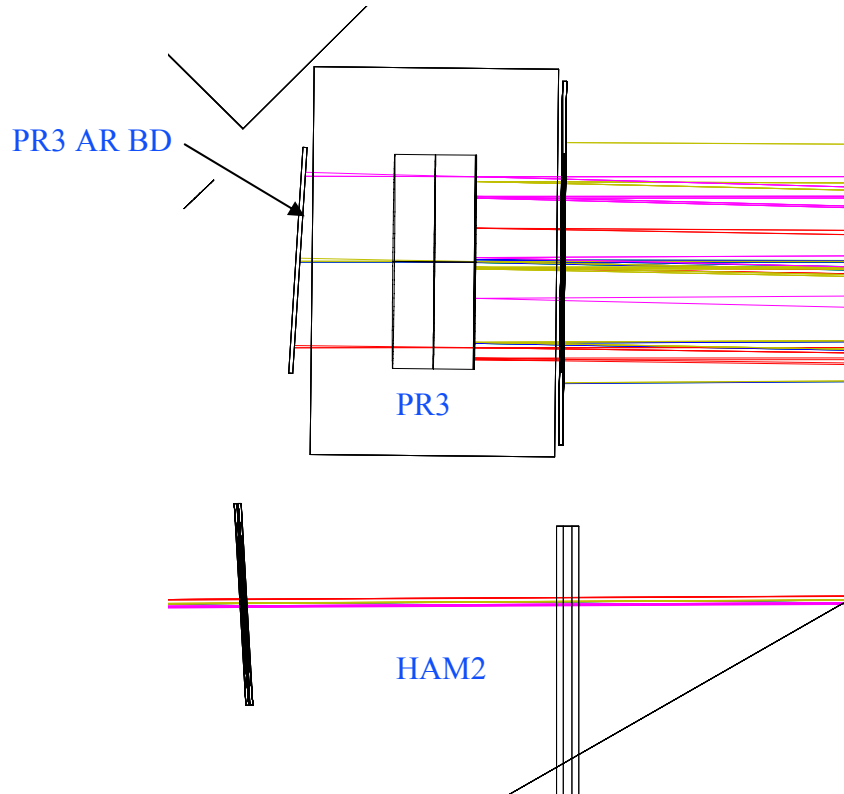


Figure 11: PR3 AR beam dump

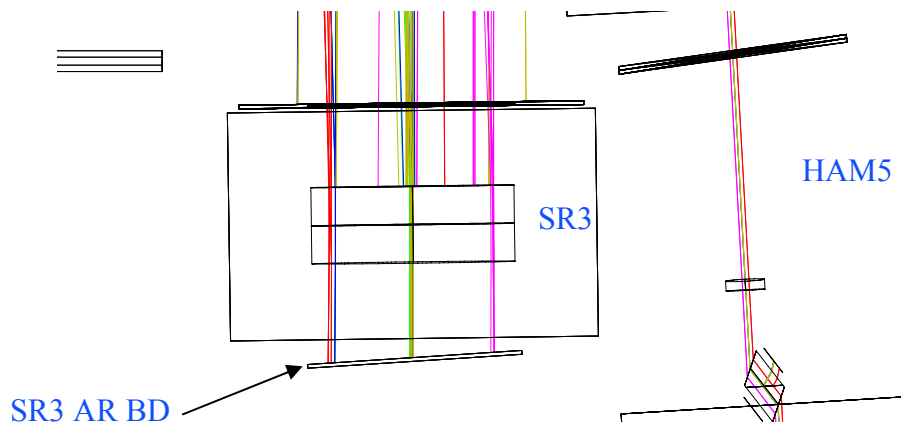


Figure 12: SR3 AR beam dump

The ghost beams from the HR surfaces of PR3 and SR3 will be allowed to hit the IO and OUT tube walls

3.1.2.8 ETM Wedge Angle

The ETM wedge will be 0.08 deg, the same as the ITM wedge, to minimize tooling requirements.

3.1.2.9 ETM Reaction Mass Wedge Angle

The ETM reaction mass wedge will be 0.04 deg, the same as the CP wedge, to minimize tooling requirements.

3.1.2.10 COC Wedge Angle Summary, Non-folded IFO**Table 1: COC Wedge Angles, Non-folded IFO**

Mirror	Wedge Angle, deg	Orientation	Direction	Symmetry
PRM	2	vertical	thick side up	symmetric
PR2	2	vertical	thick side up	symmetric
PR3	0.6	vertical	thick side up	symmetric
SRM	2	vertical	thick side up	symmetric
SR2	2	vertical	thick side up	symmetric
SR3	0.6	vertical	thick side up	symmetric
BS	0.04	horizontal	thin side -Y	symmetric
CPX	0.04	horizontal	thin side +Y	symmetric
CPY	0.04	horizontal	thin side +X	symmetric
ITMX	0.08	horizontal	thin side +Y	AR face perpendicular to substrate cylindrical axis
ITMY	0.08	horizontal	thin side +X	AR face perpendicular to substrate cylindrical axis
ETMX	0.08	horizontal	thin side -Y	AR face perpendicular to substrate cylindrical axis
ETMY	0.08	horizontal	thin side +X	AR face perpendicular to substrate cylindrical axis
ReMX	0.04	horizontal	thin side +Y	symmetric
ReMY	0.04	horizontal	thin side -X	symmetric

3.1.3 Wedge Angles for Folded IFO

The wedge angles for the folded IFO are exactly the same as the non-folded IFO.

In addition, the FM wedge angles will be 0.04 deg, the same as the BS, to minimize tooling requirements.

3.1.3.1 COC Wedge Angle Summary, Folded IFO

Table 2: COC Wedge Angles, Folded IFO

Mirror	Wedge Angle, deg	Orientation	Direction	Symmetry
PRM	2	vertical	thick side up	symmetric
PR2	2	vertical	thick side up	symmetric
PR3	0.6	vertical	thick side up	symmetric
SRM	2	vertical	thick side up	symmetric
SR2	2	vertical	thick side up	symmetric
SR3	0.6	vertical	thick side up	symmetric
BS	0.04	horizontal	thin side +Y	symmetric
CPX	0.04	horizontal	thin side -Y	symmetric
CPY	0.04	horizontal	thin side -X	symmetric
ITMX	0.08	horizontal	thin side -Y	AR face perpendicular to substrate cylindrical axis
ITMY	0.08	horizontal	thin side -X	AR face perpendicular to substrate cylindrical axis
ETMX	0.08	horizontal	thin side -Y	AR face perpendicular to substrate cylindrical axis
ETMY	0.08	horizontal	thin side +X	AR face perpendicular to substrate cylindrical axis
ReMX	0.04	horizontal	thin side +Y	symmetric
ReMY	0.04	horizontal	thin side -X	symmetric
FMX	0.04	horizontal	thin side -Y	symmetric
FMY	0.04	horizontal	thin side -Y	symmetric

3.2 Stray Light Control Performance Characteristics

3.2.1 Scattered Light Sources

The AOS scattered light sources that contribute to the total scattered light displacement noise are listed in Table 1, together with the incident power and the scattered power. The AOS scattered light displacement noise requirement was taken to be $< 1/14$ of the ADLIGO Science Requirement, which is one half of the total scattered light power budget.

Table 3: Scattered Light Source, Incident Power and Scattered Power

SCATTERING SOURCE	INCIDENT POWER, W	SCATTERED POWER, W
Faraday	1.35E-01	2.71E-11
AC_Baffle	7.33E+00	7.07E-18
AC_Baffle_Refl	1.76E-04	8.14E-26
AS_Window	1.35E-01	2.20E-17
AS_Window_Refl	3.38E-04	6.88E-19
ITMX_PO_Window	5.27E-02	4.30E-19
RC_PO_Window	1.35E-05	2.20E-22
Cryo_Baffle	2.77E+00	2.67E-18
Cryo_Baffle_Refl	6.64E-05	3.07E-26
ITM_GBAR1_BD	5.27E-02	1.52E-15
ITM_GBAR1_BD_Refl	1.26E-06	1.75E-23
ITM_GBAR3_BD	5.21E-02	1.49E-15
ITM_GBAR3_BD_Refl	1.25E-06	1.71E-23
ITM_GBAR4_BD	2.59E-06	3.68E-24
ITM_GBHR3_BEAM_TUBE_BAF	2.62E-04	1.25E-21
ITM_GBHR4_BEAM_TUBE_BAF	1.30E-08	3.10E-30
BS_GBAR3X_BEAM_TUBE_BAF	1.32E-04	1.12E-22
BS_GBAR4X_BEAM_TUBE_BAF	3.29E-09	6.99E-32
BS_GBHR3X_BEAM_TUBE_BAF	1.32E-04	1.12E-22
BS_GBHR4X_BEAM_TUBE_BAF	3.29E-09	6.99E-32
BS_GBAR3P_BD	2.63E-02	2.68E-16
BS_GBAR3P_Refl	6.32E-07	3.09E-24
BS_GBHR3P_BD	2.63E-02	2.68E-16
BS_GBHR3P_Refl	6.32E-07	3.09E-24
ITM_Ellip_Baffle	3.70E-01	1.26E-21

SCATTERING SOURCE	INCIDENT POWER, W	SCATTERED POWER, W
ITM_Ellip_Baffle	8.88E-06	1.45E-29
BSC_wide_angle	4.25E-04	0.00E+00
manifold_wide_angle	8.93E-01	0.00E+00
Total_BSC_Manifold_Wide_Angle		8.03E-20
AC_Baffle_wide_angle	4.67E+00	
AC_Baf_cyl_wide_angle	2.84E+00	
Total_AC_Baf_cyl_Wide_Angle		9.66E-18
PRM_Ellip_Baffle	2.50E-03	1.19E-17
PRM_Ellip_Baffle_Refl	6.00E-08	5.02E-29
ETM_Tel_Baffle	4.88E-02	3.32E-19
ETM_Tel_Baffle_Refl	3.42E-03	3.26E-21
manifold_wide_angle	8.93E-01	8.03E-20
AS_Window_Refl	3.38E-04	6.88E-19
ITMX_PO_Window_Refl	1.32E-04	1.34E-20
RC_PO_Window_Refl	3.37E-08	6.88E-24
ITMY_HARTMANN_BS_TRANS	1.35E-05	5.51E-19
ITMY_HARTMANN_VIEWPORT	3.37E-08	1.38E-27
ITMX_HARTMANN_VIEWPORT	2.63E-04	2.15E-19
ITMX_HARTMANN_VIEWPORT_REFL	3.29E-07	1.32E-23
PRM_GBAR1	6.25E-03	2.70E-19
PRM_GBAR3	1.76E-02	5.97E-16
PRM_GBHR3	4.71E-03	4.30E-17
PRM_Total		1.28E-15
PR2_GB0t	2.11E-01	8.59E-15
PR2_GBAR3	1.05E-05	2.15E-22
PR2_GBHR3	1.05E-09	2.15E-30
PR2_Total		1.72E-14
PR3_GB0t	2.11E-01	2.86E-15
PR3_GBAR3	1.05E-05	7.16E-24
PR3_GBHR3	1.05E-09	1.43E-31
PR3_GBAR_Total		5.73E-15
PR3_GBHR_Total		2.86E-31
SRM_GBAR3	2.59E-07	2.03E-21
SRM_GBHR3	1.08E-08	3.52E-24

SCATTERING SOURCE	INCIDENT POWER, W	SCATTERED POWER, W
SRM_Total		4.07E-21
SR2_GB0t	1.35E-05	5.51E-19
SR2_GBAR3	6.75E-10	1.38E-26
SR2_GBHR3	6.75E-14	1.38E-34
SR2_GBHR3	6.75E-14	1.38E-34
SR2_Total		1.10E-18
SR3_GB0t	1.35E-05	1.84E-19
SR3_GBAR3	6.75E-10	4.59E-28
SR3_GBHR3	6.75E-14	9.18E-36
SR3_GBAR_Total		3.67E-19
SR3_GBHR_Total		1.84E-35

3.2.2 Summary of Scattered Light Displacement Noise

A summary of the scattered light displacement noise with all the AOS noise sources mitigated, and with the Septum Windows in place is shown in Figure 13. The Scattered Light Noise exceeds the SRD requirement at approximately 26 Hz.

Removing the Septum Window meets the Scattered Light Noise Requirement, 4.2.1 Direct Requirements, at all frequencies, as shown in Figure 14.

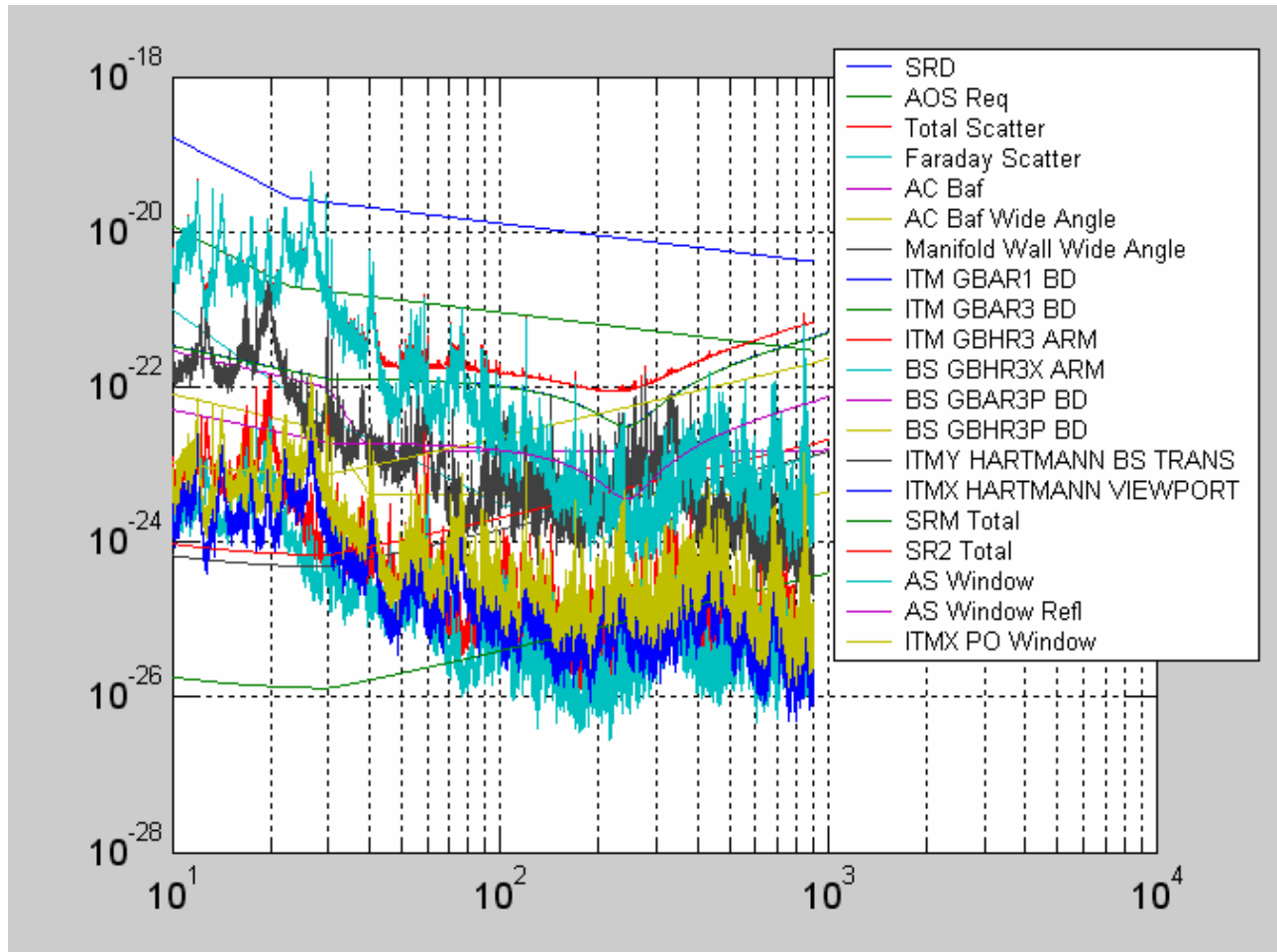


Figure 13: Scattered Light Displacement Noise, Septum Windows in Place

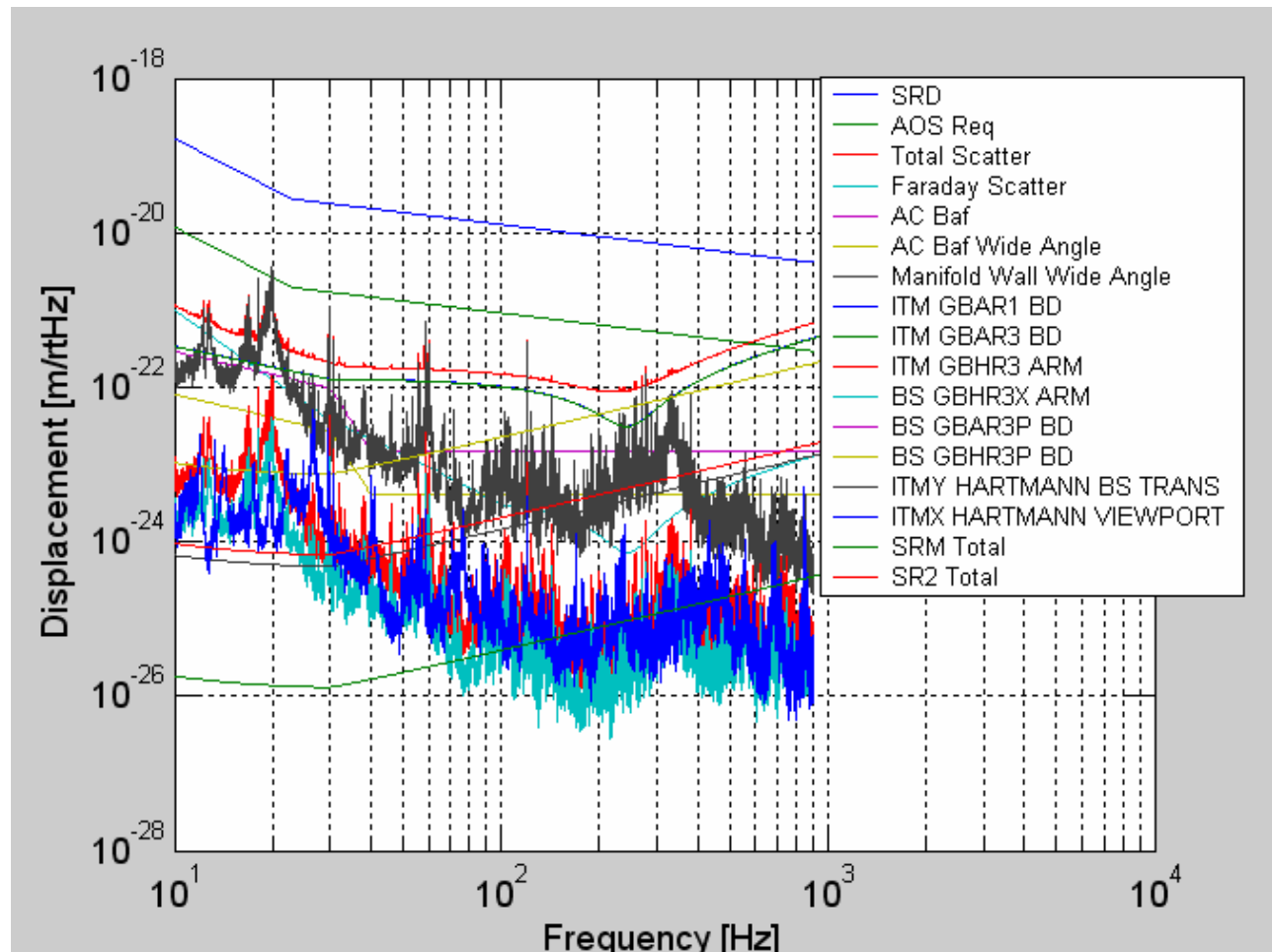


Figure 14: Scattered Light Displacement Noise, Septum Windows Removed

3.2.3 Output Faraday Isolator

The Initial LIGO Faraday Isolators will be re-used for ADLIGO with a modification to preserve the in-line beam direction and to allow the provision for injecting an external beam into the AS port of the IFO.

The scattered light model indicates that the Output Faraday Isolator must be suspended in order to reduce the scattered light noise from the optical surfaces. The optical surfaces are all in a vertical plane; therefore no motion isolation is required in the vertical direction.

A conceptual drawing of the Faraday Isolator suspended with a modified LOS structure is shown in Figure 15.

The pitch and yaw pointing angles of the Output Faraday Isolator will be pre-set during initial alignment. A remotely controlled Picomotor will provide a small amount of pitch motion to avoid a possible glint from the optical surfaces of the Faraday Isolator into the AS port of the IFO.

3.2.3.1 Faraday Isolator Forward Transmissivity

The measured transmissivity of the Initial LIGO Output Faraday Isolator is 98%.

This meets the requirement 4.3 Faraday Isolator Requirements.

3.2.3.2 Faraday Isolator Reverse Transmissivity

The measured reverse power transmission of the Initial LIGO Output Faraday Isolator is < 0.0001 .

This meets the requirement 4.3 Faraday Isolator Requirements.

3.2.3.3 BRDF of Faraday Surfaces

The Output Faraday Isolator has four calcite prism surfaces and one TGG crystal surface on the entrance side. These surfaces will scatter light back toward the antisymmetric port of the IFO. The light scattered by the additional surfaces beyond the Faraday rotator magnet will be attenuated by the reverse transmissivity of the Faraday Isolator and will be ignored.

The BRDF of the TGG surface was estimated using the fractal back-scattering model proposed by R. Weiss; see T920004-00 Estimation of Special Optical Properties of a Triangular Ring Cavity, for incidence angles between $1E-4$ and $1E-1$ radians.

$$\text{BRDF}(\theta) := \frac{\alpha}{\theta^2}$$

where

$$\alpha := 1.5 \cdot 10^{-3} \cdot S$$

and S is the total integrated scattering loss of the surface.

Assuming an incidence angle on the Faraday Isolator surfaces of $1.7E-2$ rad (1 deg) and a total scattering loss per surface of 100 ppm, the estimated BRDF is $5E-4 \text{ sr}^{-1}$.

It was assumed that the calcite prisms have a similar BRDF, and that the scattered light noise injected into the IFO will add in phase.

3.2.3.4 Faraday Isolator Suspension

The Output Faraday Isolator will be suspended by a modified LOS as shown in Figure 15. The length of the pendulum is estimated to be 0.4 m. Damping elements will provide damping to reduce the $Q < 1000$.

The suspension frame will be mounted to the HAM optical table, with the motion requirement shown in Figure 16.

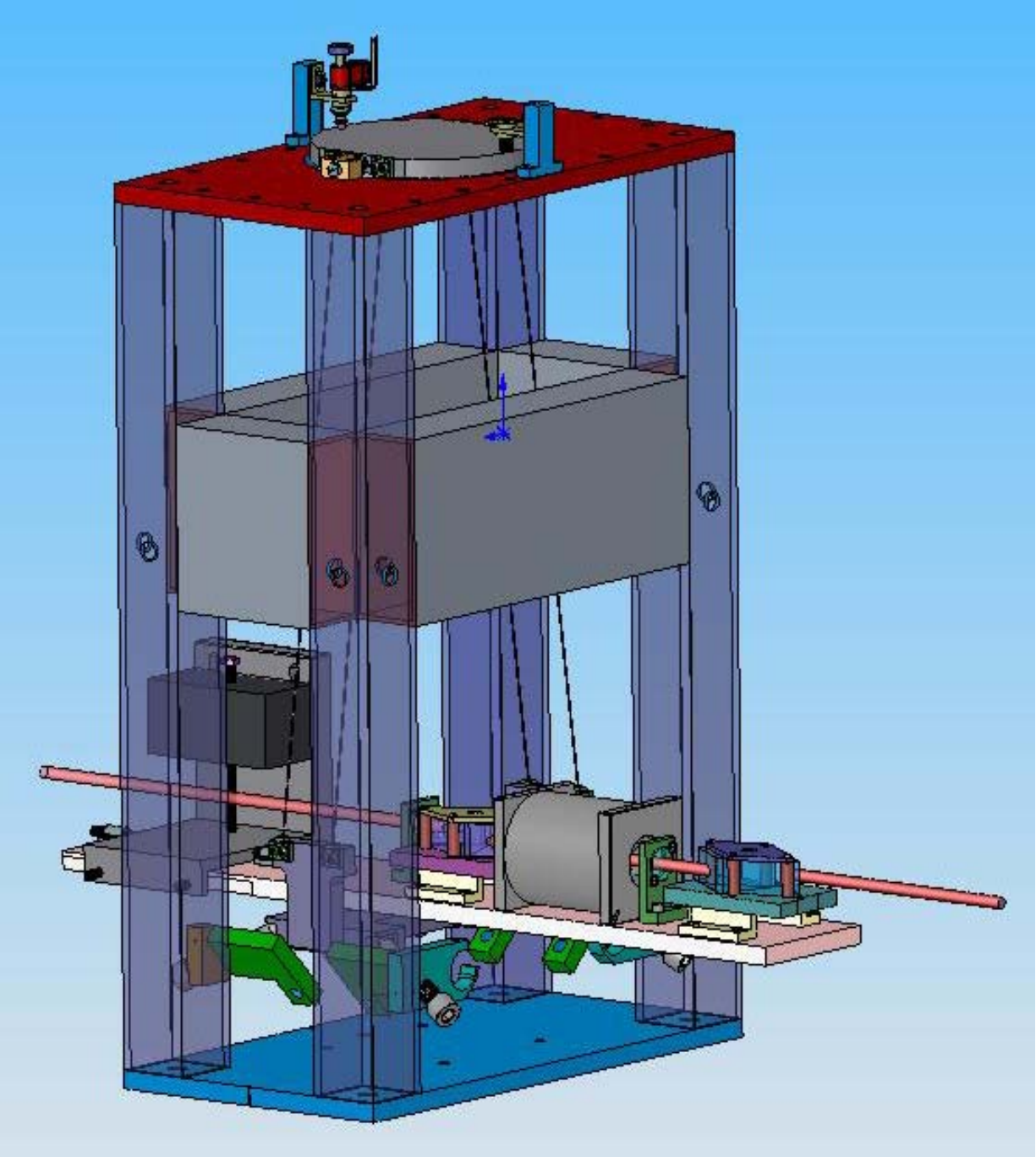


Figure 15: Initial LIGO Output Faraday Isolator Parts Suspended in a Modified LOS

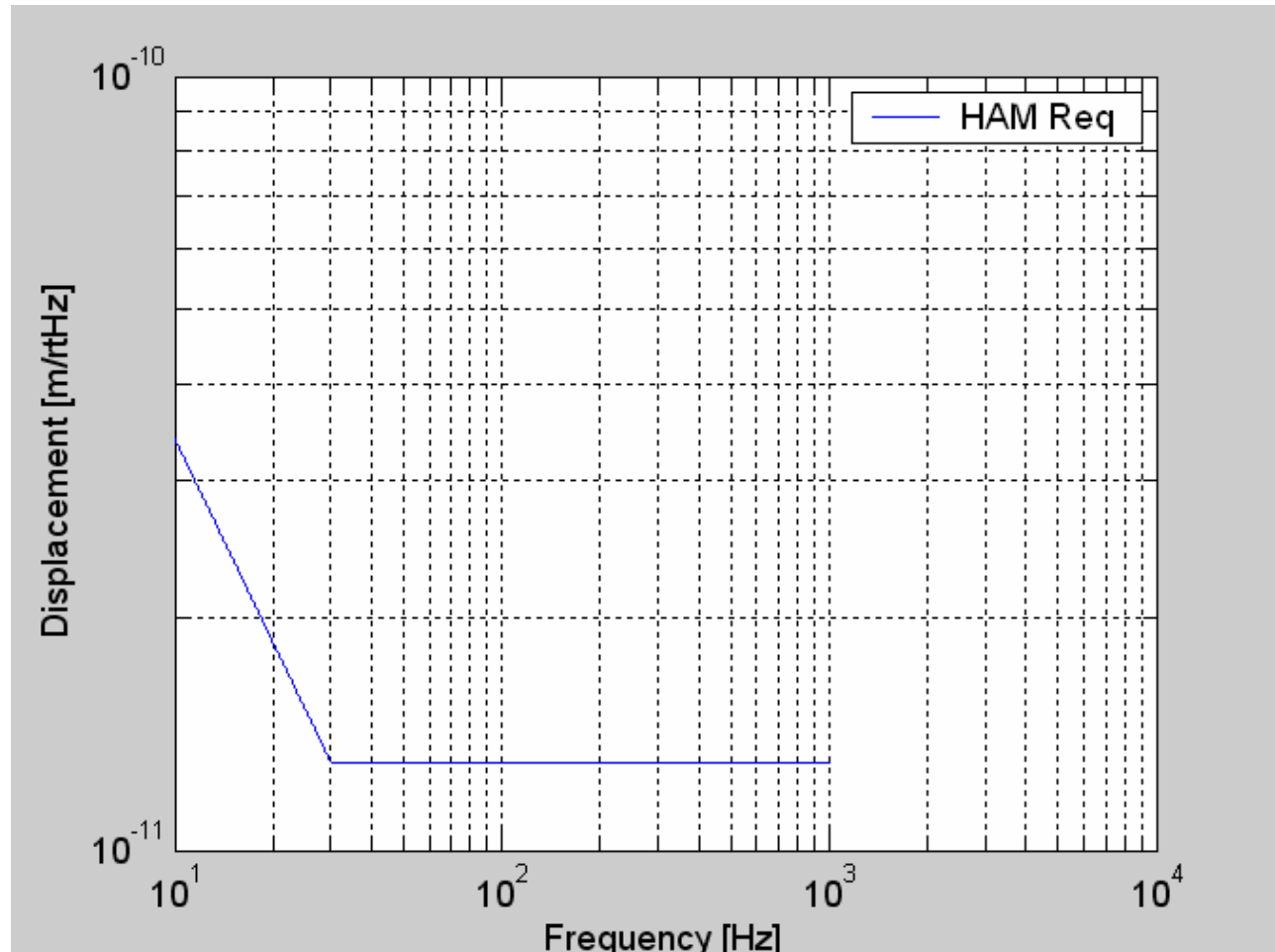


Figure 16: HAM optics table Seismic Motion Requirement

The minimum Output Faraday Isolator motion attenuation requirements were determined using the scattered light model, assuming five surfaces with BRDF of $5E-4 \text{ sr}^{-1}$, and are shown in the blue curve of Figure 17, together with a calculated simple pendulum transfer function, the green curve.

3.2.3.5 Scattered Light Displacement Noise of Suspended Output Faraday Isolator

The scattered light displacement noise caused by the suspended Output Faraday Isolator is shown in Figure 18.

3.2.3.6 Stay Clear Diameter

The clear aperture of the Faraday Isolator is 20 mm diameter. The AS Gaussian beam diameter at the output of the SRM is approximately 4 mm. The clear aperture of the Faraday Isolator will be pre-aligned within 2 mm of the beam centerline by referencing its position to the center of the ITM.

This meets the requirement 4.7 Clear Aperture Requirements

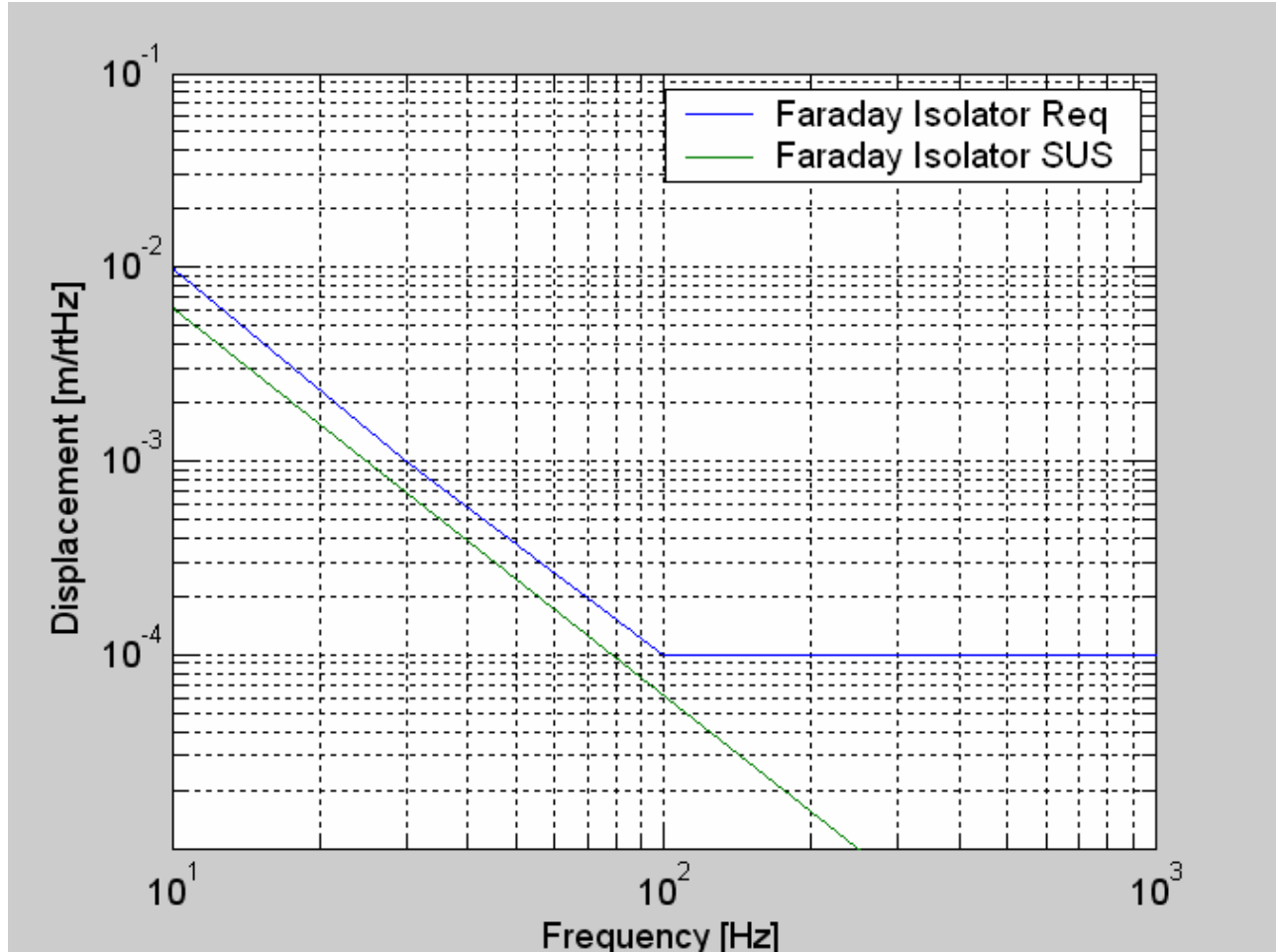


Figure 17: Output Faraday Isolator SUS Amplitude Response

3.2.4 Arm Cavity Baffle

3.2.4.1 Incident Power on Arm Cavity Baffle

The power scattered from the far COC mirror, at the opposite end of the arm cavity, into the annular region bounded by the outer radius of the near COC and the inside radius of the Cryopump Baffle will be incident on the Arm Cavity Baffle. It is given by

$$P_{acb} := P_a \cdot \int_{\theta_{itm}}^{\theta_{cp}} 2 \cdot \pi \cdot \theta \cdot BRDF_1(\theta) d\theta$$

The Initial LIGO pathfinder COC CSIRO, surface 2, S/N 2 was used to estimate the BRDF.

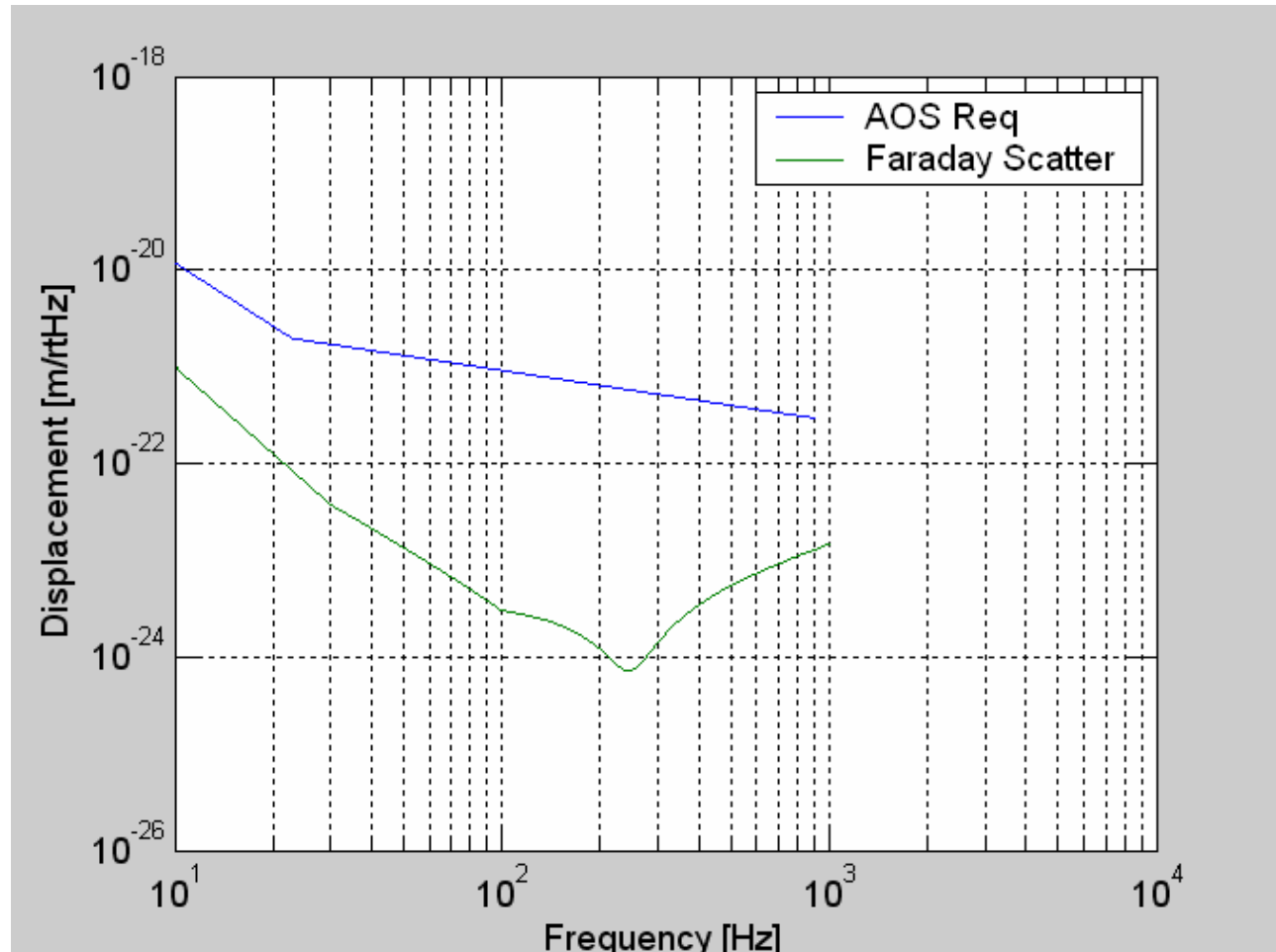


Figure 18: Scattered Light Displacement Noise from Suspended Faraday Isolator

$$\text{BRDF}_1(\theta) := \frac{2755.12}{\left(1 + 8.50787 \cdot 10^8 \cdot \theta^2\right)^{1.23597}}$$

Where θ_{itm} is 4.25 E-5 rad

θ_{cp} is 9.612 E-5 rad

and, P_a is the arm power 8.339 E5 W

$$P_{\text{acb}} = 7.3 \text{ W}$$

3.2.4.2 Arm Cavity Baffle Motion

3.2.4.2.1 HEPI Displacement

The Arm Cavity Baffle shown in Figure 19 will be suspended with a single pendulum from Stage “0” HEPI support ring of the BSC optical table adjacent to the HR side of the ITM and ETM. Earthquake stops will be mounted to the BSC vacuum enclosure.

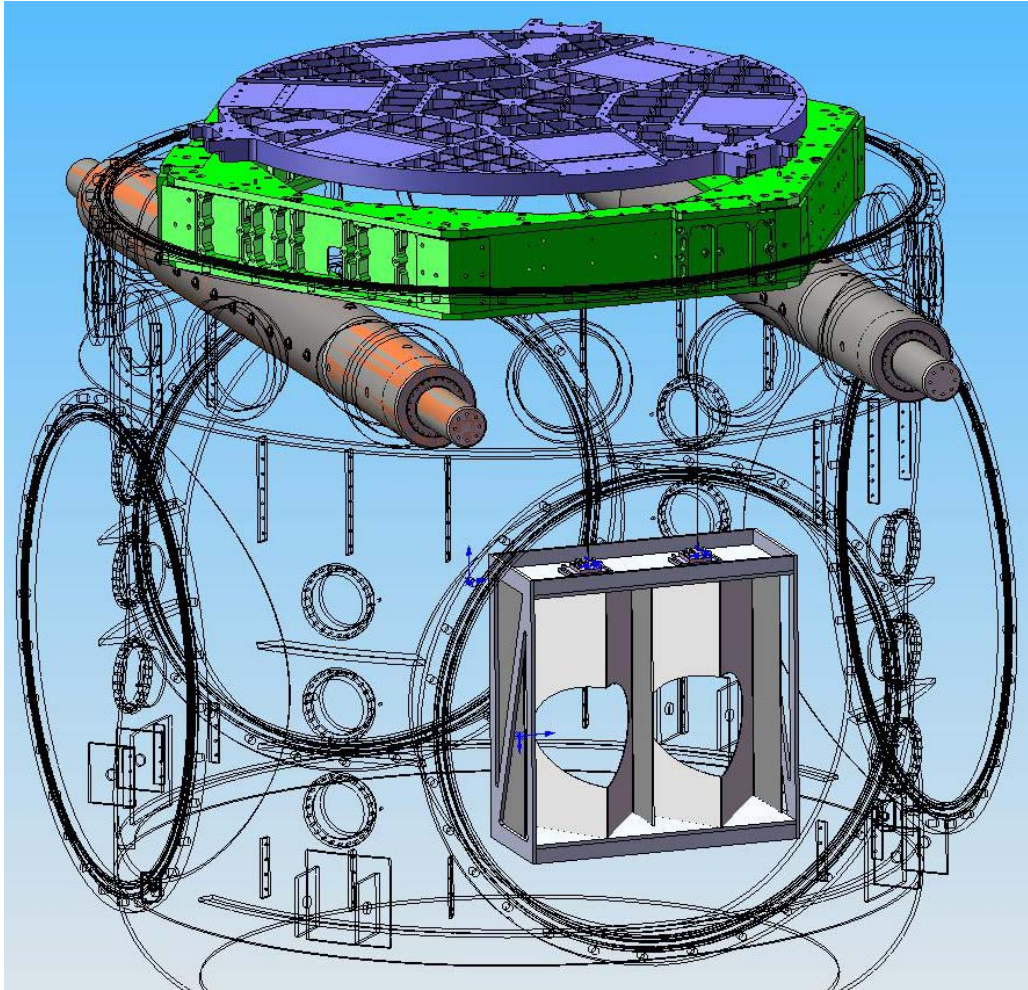


Figure 19: Suspended Arm Cavity Baffle

We will assume that the x-displacement spectrum of the BSC HEPI isolation system is described by Brian Lantz in the SEI elog entry ID: 596, 3/14/06, as shown in Figure 20.

3.2.4.2.2 Minimum Arm Cavity Baffle Motion Requirements

With an assumed BRDF of 0.05 sr^{-1} , the scattered light model indicates that the Arm Cavity Baffle requires 0.05 motion attenuation at frequencies $> 10 \text{ Hz}$, as shown in Figure 21.

3.2.4.2.3 Arm Cavity Baffle Suspension Transfer Functions

The pitch, roll, and yaw resonances of the two-wire Arm Cavity Baffle suspension were estimated using a Matlab model developed by the SUS group, and are all around 1 Hz , as shown in Figure 22, Figure 23, and Figure 24. With these transfer functions, the relative motion will be attenuated by a factor > 10 for frequencies $> 10 \text{ Hz}$, and will exceed the requirement.

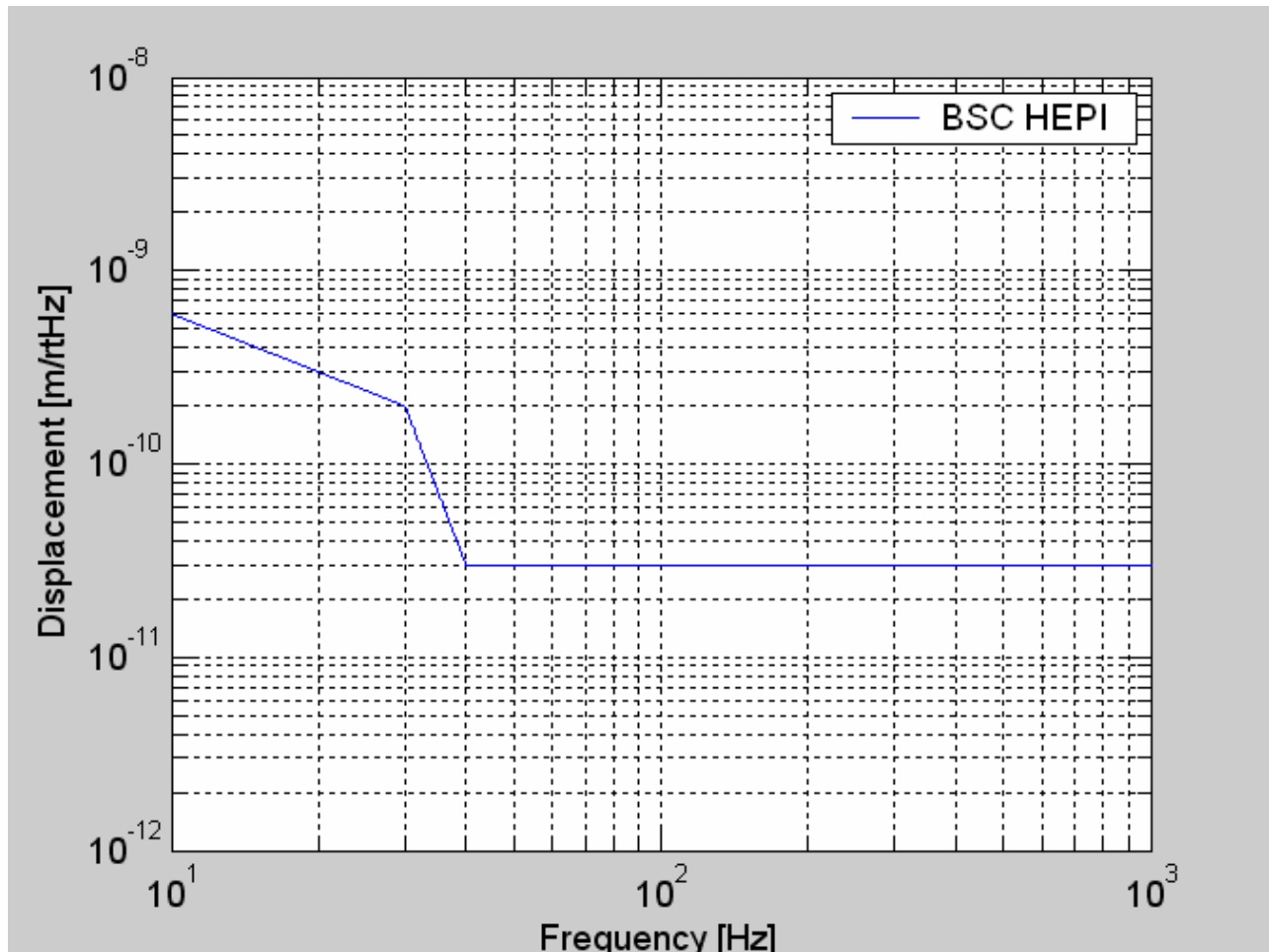


Figure 20: BSC HEPI Motion Spectrum

The hole in the Arm Cavity Baffle for the IFO beam extends in the longitudinal direction because of the tilt angle of the vertical baffle surfaces. The scattering surfaces of the exposed, rough edges of the baffle hole will exhibit a longitudinal motion due to coupling from the vertical motion. The average vertical-to-horizontal coupling factor is estimated to be 0.6.

Vertical springs will attach to the suspension wires to provide a vertical resonance around 1 Hz, shown by the green curves in the figures, which will reduce the vertical motion by a factor >10 and the coupled-longitudinal motion by a factor >17 @ frequencies > 10Hz.

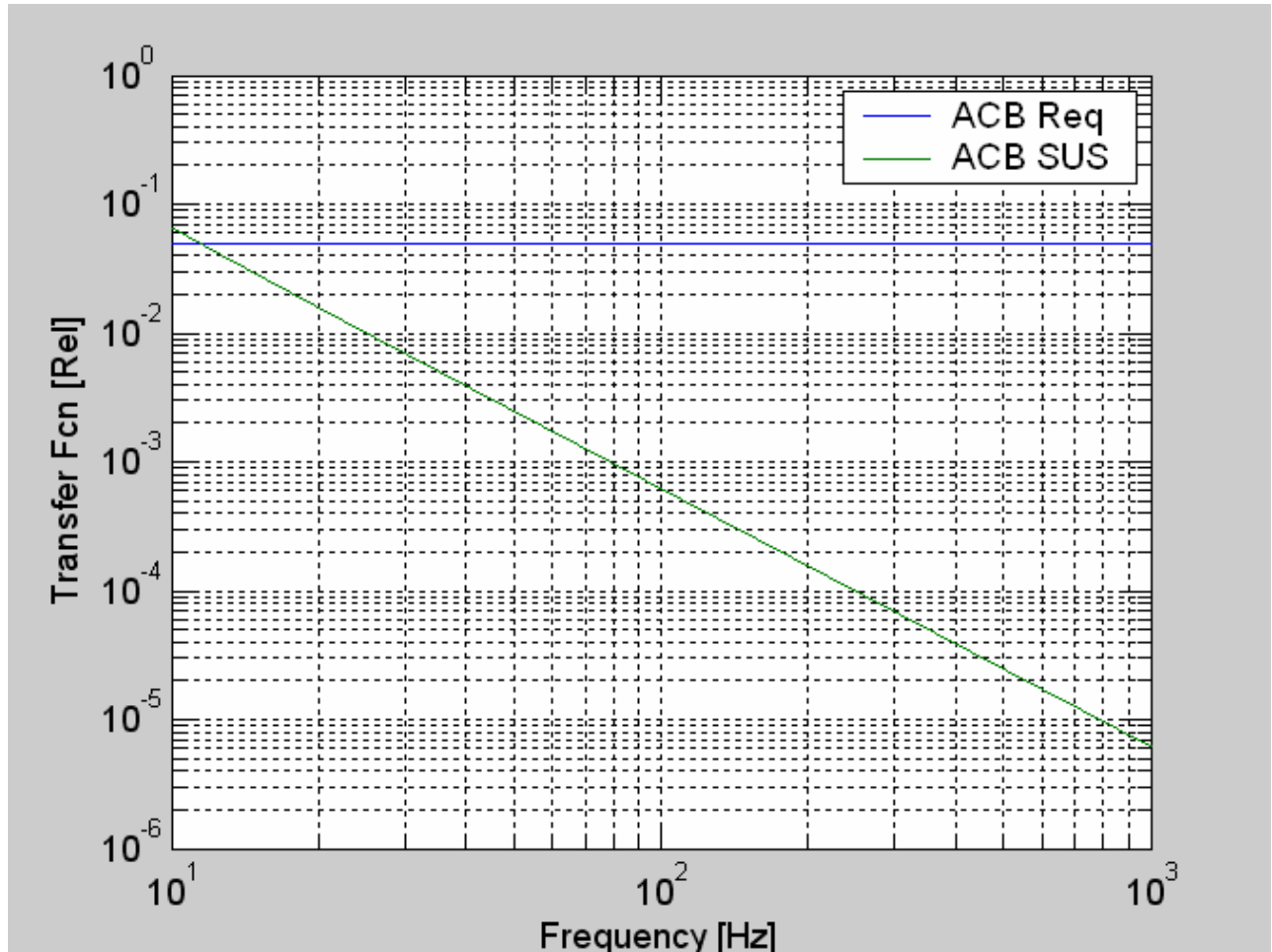


Figure 21: Arm Cavity Baffle Attenuation, Minimum Requirement

3.2.4.3 Arm Cavity Baffle Surface BRDF

The Arm Cavity Baffle will be constructed of oxidized polished stainless steel with the first surface inclined at an incidence angle 56 deg and is estimated to have a BRDF $< 0.05 \text{ sr}^{-1}$. See T980027-00, Baffling Requirements for the 4K and 2K IFO.

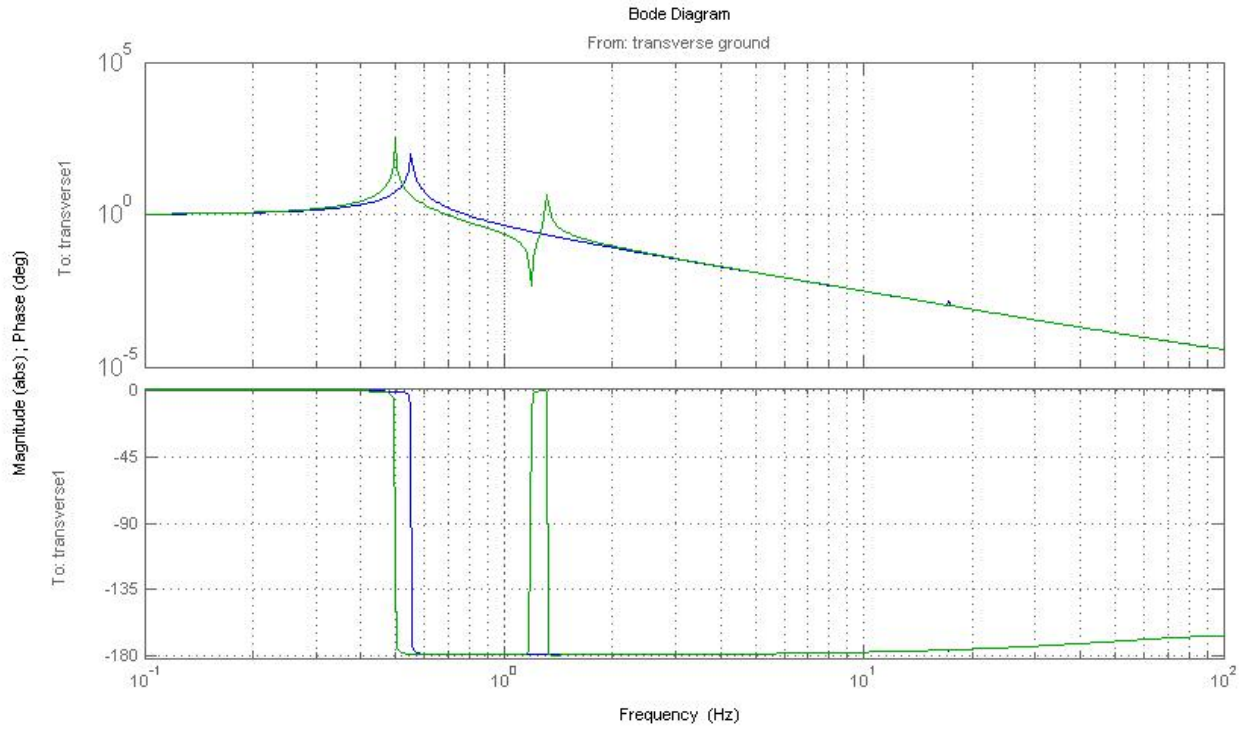


Figure 22: Transverse Transfer Function, ACB SUS

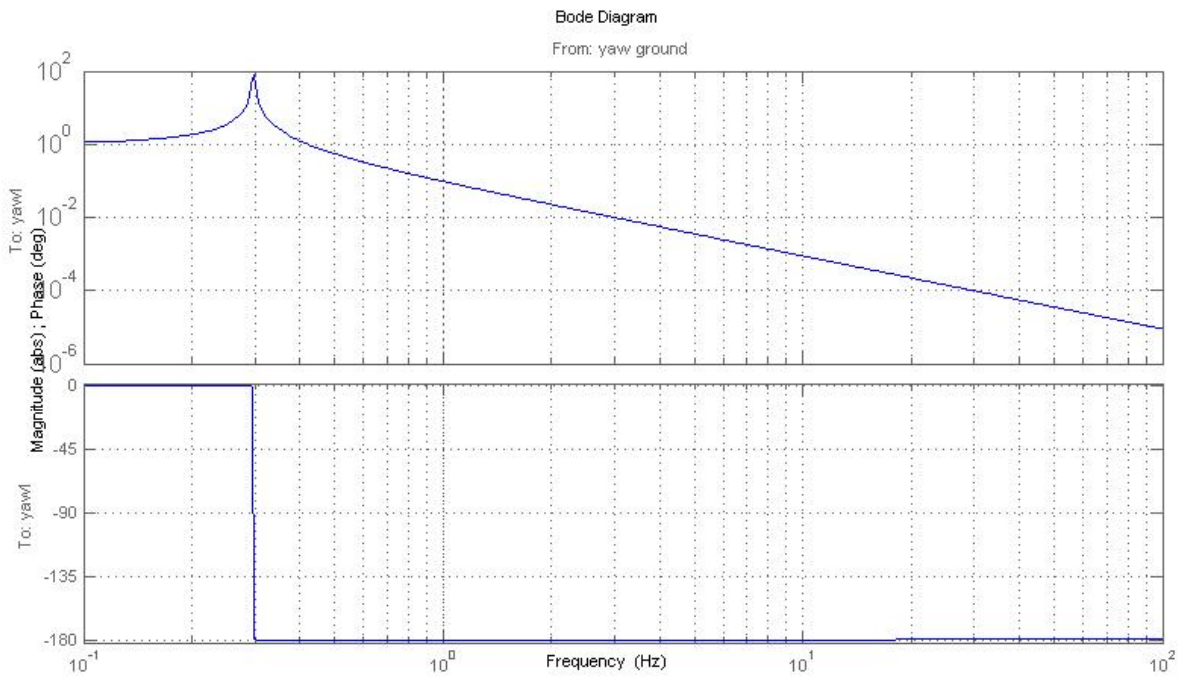


Figure 23: Yaw Transfer Function, ACB SUS

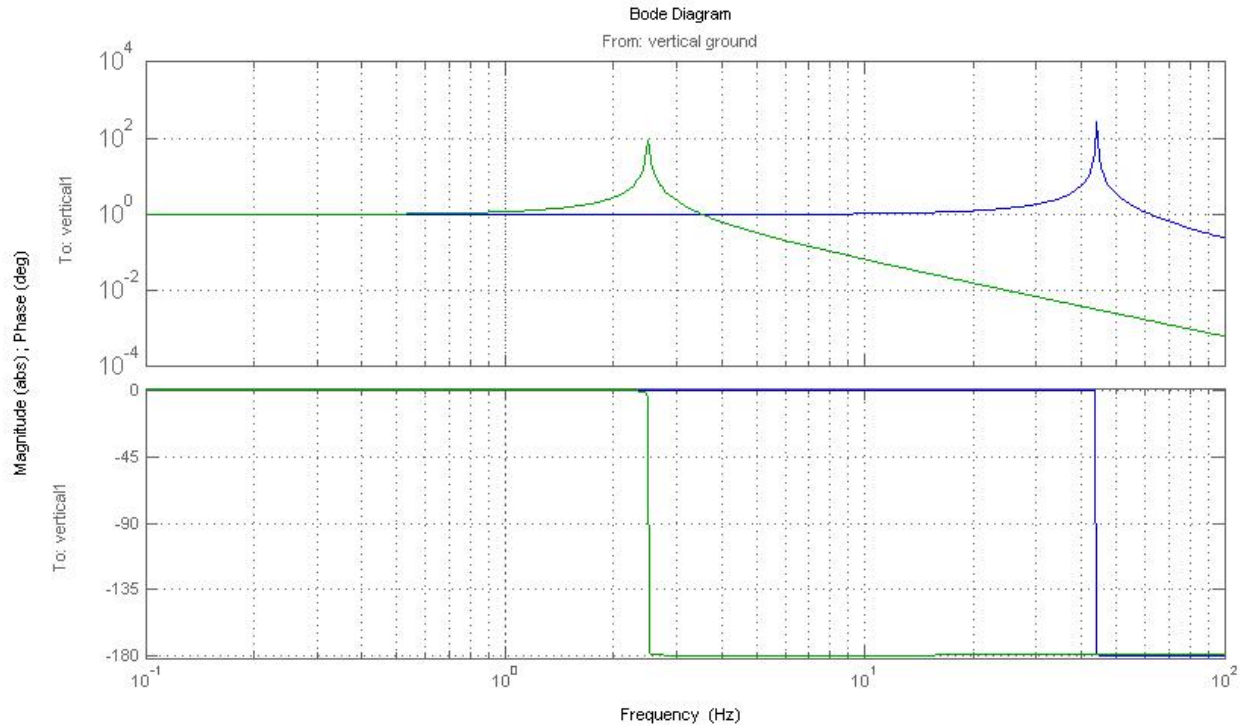


Figure 24: Vertical Transfer Function, Arm Cavity Baffle SUS

3.2.4.4 Arm Cavity Baffle Reflectivity

The light that is not absorbed by the Arm Cavity Baffle will reflect from the baffle surface onto the inside walls of the vacuum manifold, where it will scatter from the manifold, reflect again from the Arm Cavity Baffle, and enter the IFO mode at the far COC.

The scattered light model was used to calculate the requirement for the reflectivity of the Arm Cavity Baffle. Assuming a BRDF of the vacuum manifold wall of 0.1 sr^{-1} at an incidence angle of 40 deg, the reflectivity of the Arm Cavity Baffle must be $< 0.25\%$.

The reflectivity of the Arm Cavity Baffle with four internal bounces is estimated to be $2.4 \text{ E-}5$.

3.2.4.5 Seismic Motion of the Vacuum Manifold

The light that reflects from the Arm Cavity Baffle will scatter from the vacuum manifold, which has the seismic motion shown in Figure 25. See Robert Schofield (11/17/06 LHO ILOG).

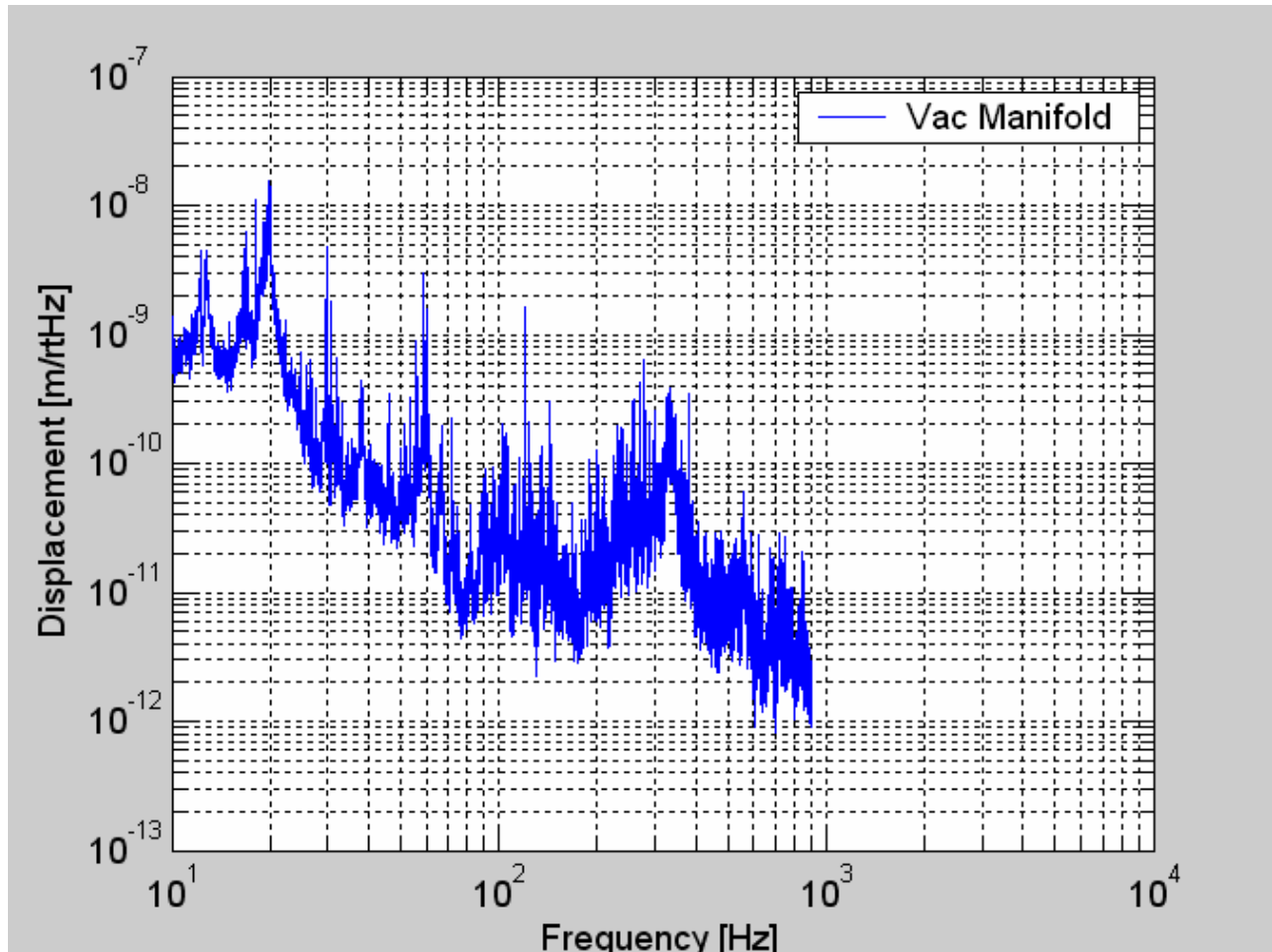


Figure 25: Seismic motion of vacuum manifold

3.2.4.6 Scattered Light Displacement Noise of Suspended Arm Cavity Baffle

The light that scatters directly from the surface of the suspended Arm Cavity Baffle has a phase noise caused by the seismic motion of the HEPI support structure attenuated by the transfer function of the Arm Cavity Baffle suspension.

The light that reflects from the baffle and subsequently scatters from the vacuum manifold walls will have a phase noise caused by the seismic motion of the walls. The vacuum manifold is assumed to have a BRDF = 0.1 sr^{-1}

The scattered light noise was calculated using the scattered light model and is shown in Figure 26.

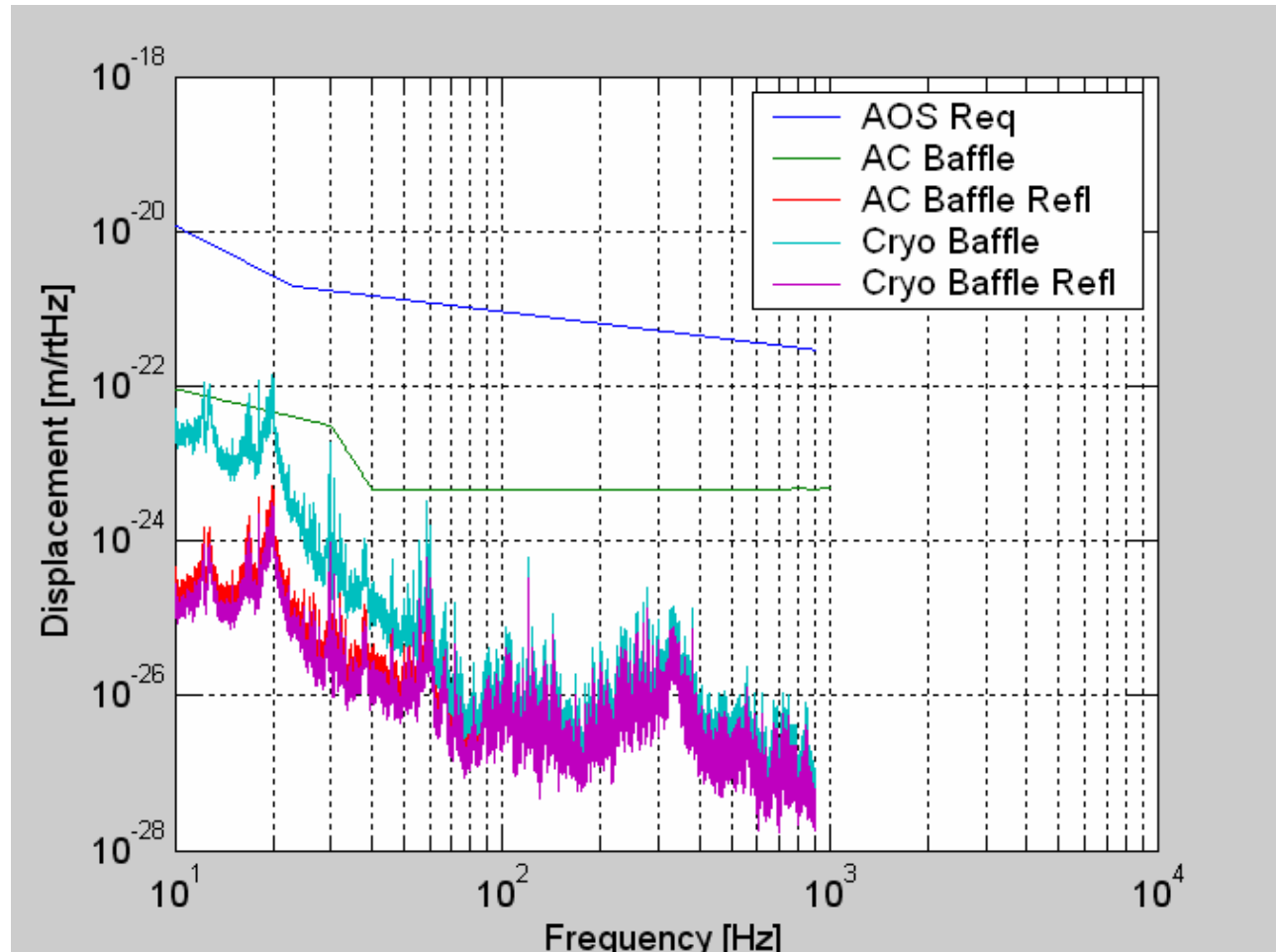


Figure 26: Arm Cavity Baffle and Cryopump Baffle Scattered Light Displacement Noise

3.2.4.7 Fringe Wrapping of Arm Cavity Baffle Displacement Noise

The Arm Cavity Baffle has a vertical bounce resonance at approximately 2.3 Hz. The displacement noise at the odd harmonics of the motion due to fringe wrapping was calculated using the fringe wrap model, see Fringe-Wrapping in Appendix A—Scattered Light Noise Theory, assuming a simple pendulum function with a $Q = 1000$ at the resonant frequency. The fringe wrapping does not cause excessive noise above 10 Hz, as shown in Figure 27.

3.2.4.8 Stay Clear Diameter

The clear aperture of the Arm Cavity Baffle is 346 mm diameter, which is larger than the diameter of the ITM and ETM COC. The clear aperture will be pre-aligned by referencing its position to the center of the HR surface of the COC in the quad suspension frame within 4 mm.

This meets the requirement 4.7 Clear Aperture Requirements.

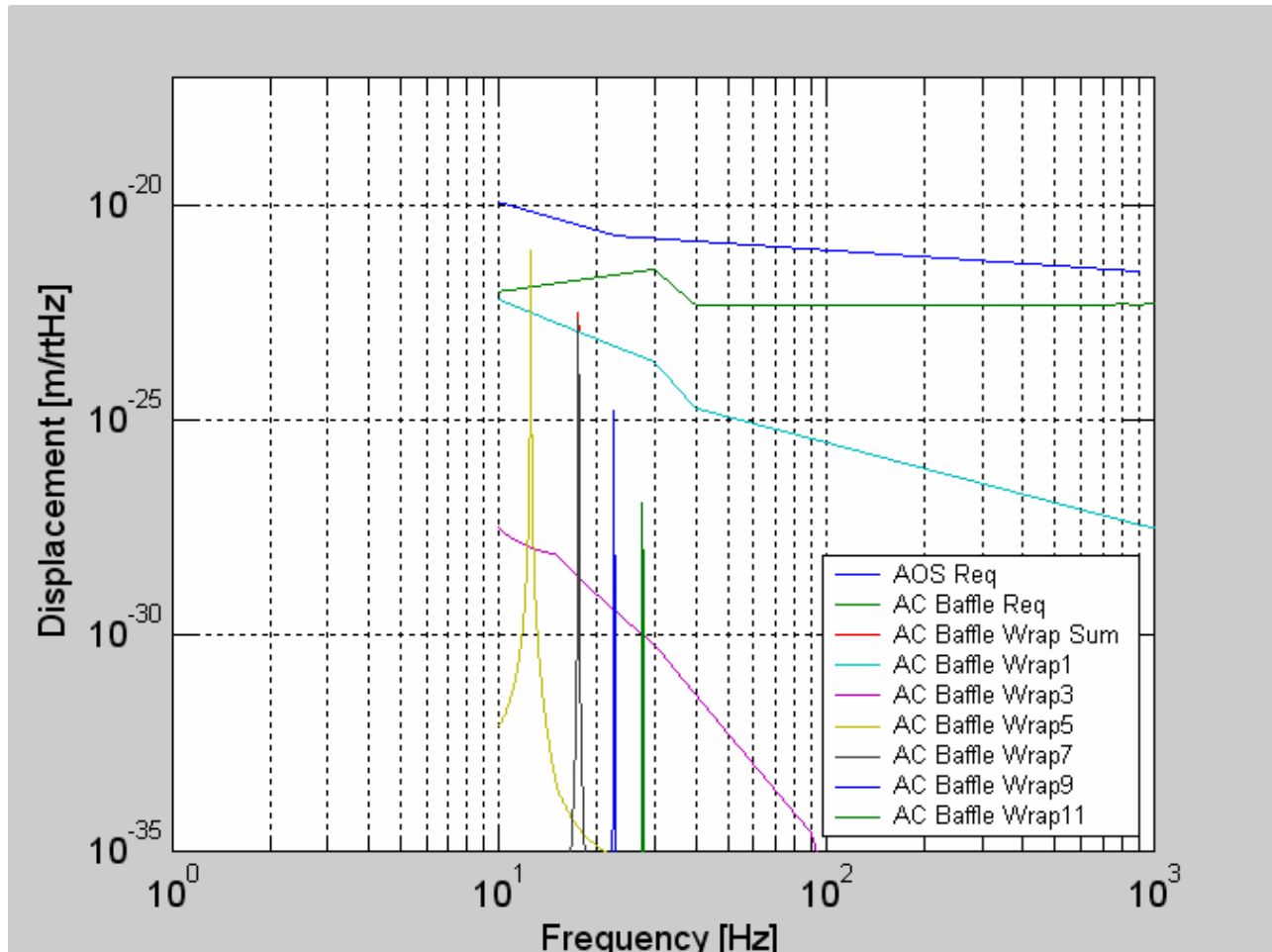


Figure 27: Arm Cavity Baffle Scattered Light Displacement Noise Caused by Fringe-wrapping

3.2.5 Cryopump Baffle

A concept for the suspended Cryopump Baffle is shown in Figure 28. The narrow angle scattered light from the far COC at the opposite end of the beam tube floods into the clear annular region between the shark's-tooth beam tube baffles and the cryopump baffle cylinder, from the right side in this picture. This light gets trapped by multiple reflections between the cylinder the cone and the annular plate with the viewport holes.

The power scattered from the far COC at the opposite end of the arm cavity into the annular region bounded by the inner radius of the Cryopump Baffle and the beam tube radius is incident on the Cryopump Baffle. The incident power is given by

$$P_{cp} := P_a \int_{\theta_{cp}}^{\theta_{bt}} 2 \cdot \pi \cdot \theta \cdot BRDF_1(\theta) d\theta$$

The Initial LIGO pathfinder COC CSIRO, surface 2, S/N 2 was used to estimate the BRDF.

$$\text{BRDF}_1(\theta) := \frac{2755.12}{\left(1 + 8.50787 \cdot 10^8 \cdot \theta^2\right)^{1.23597}}$$

Where θ_{cp} is 9.612 E-5 rad
 θ_{bt} is 1.327 E-4 rad
 and, P_a is the arm power 8.339 E5 W
 $P_{cp} = 2.8$ W

3.2.5.1 Cryopump Baffle Suspension

The Cryopump Baffle consists of a cylinder, a cone, and an annular baffle plate, which are suspended by springs from the circular, spool piece support ring. Eddy-current or elastomeric damping will be used to damp the pitch, yaw, and vertical motion.

3.2.5.2 Cryopump Blocking

The Cryopump Baffle will be placed inside the spool pieces closest to the cryopumps on the ITM side of the arms and the ETM side of the arms. It obscures the interior surfaces of the cryopump from the line of sight as viewed from the ITM and ETM HR surfaces and avoids backscattered light from the surfaces of the cryopump impinging on the ITM and ETM HR surfaces.

This meets the requirements: 4.5 Cryopump Baffle Requirement, and 4.7 Clear Aperture Requirements.

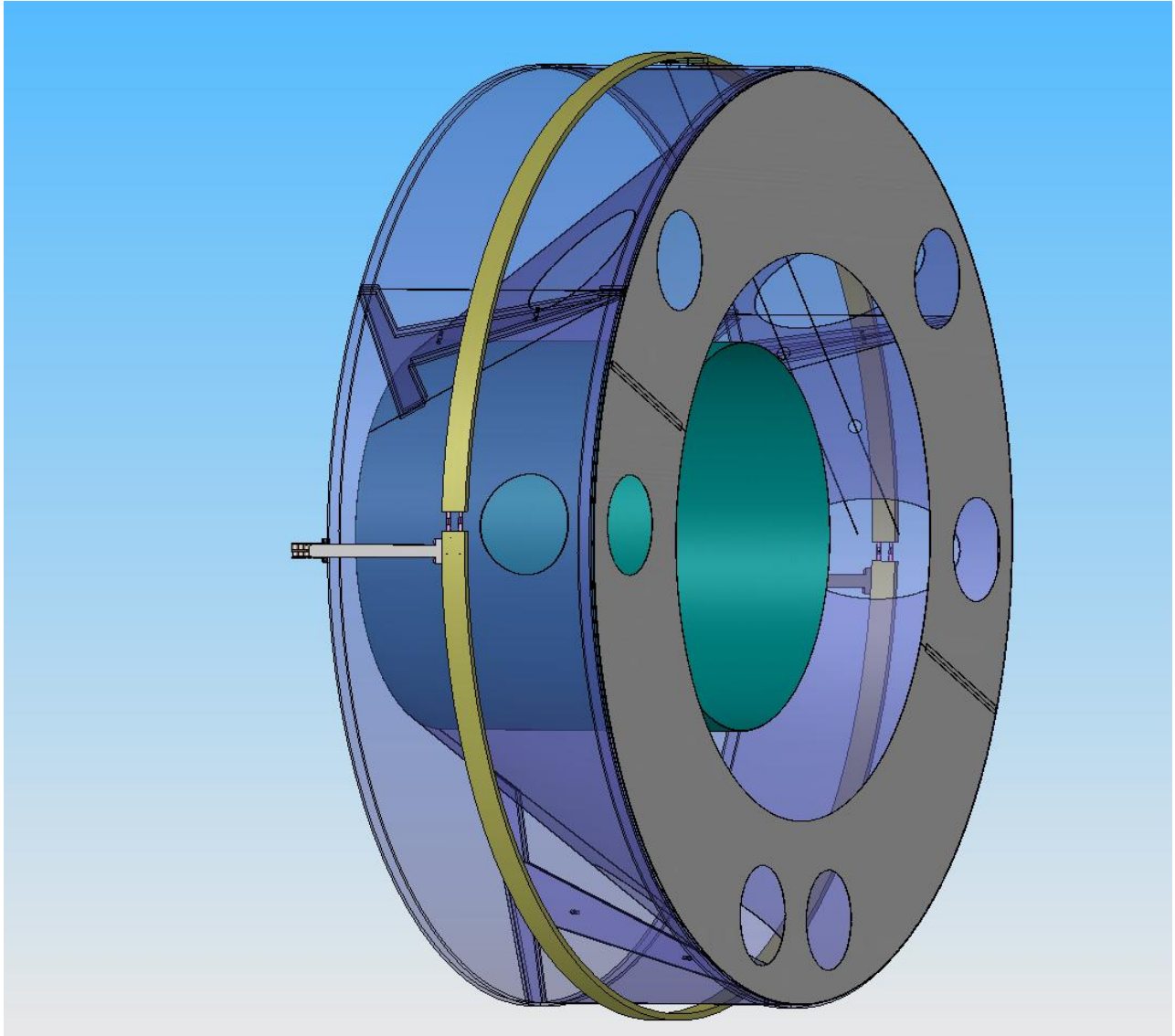


Figure 28: Conceptual Model of Suspended Cryopump Baffle

3.2.5.3 Cryopump Baffle Motion Requirements

Assuming a BRDF of 0.05 sr^{-1} , the minimum Cryopump Baffle motion attenuation requirements were determined using the scattered light model, and are shown in Figure 29. The actual pendulum response function will exceed the requirements.

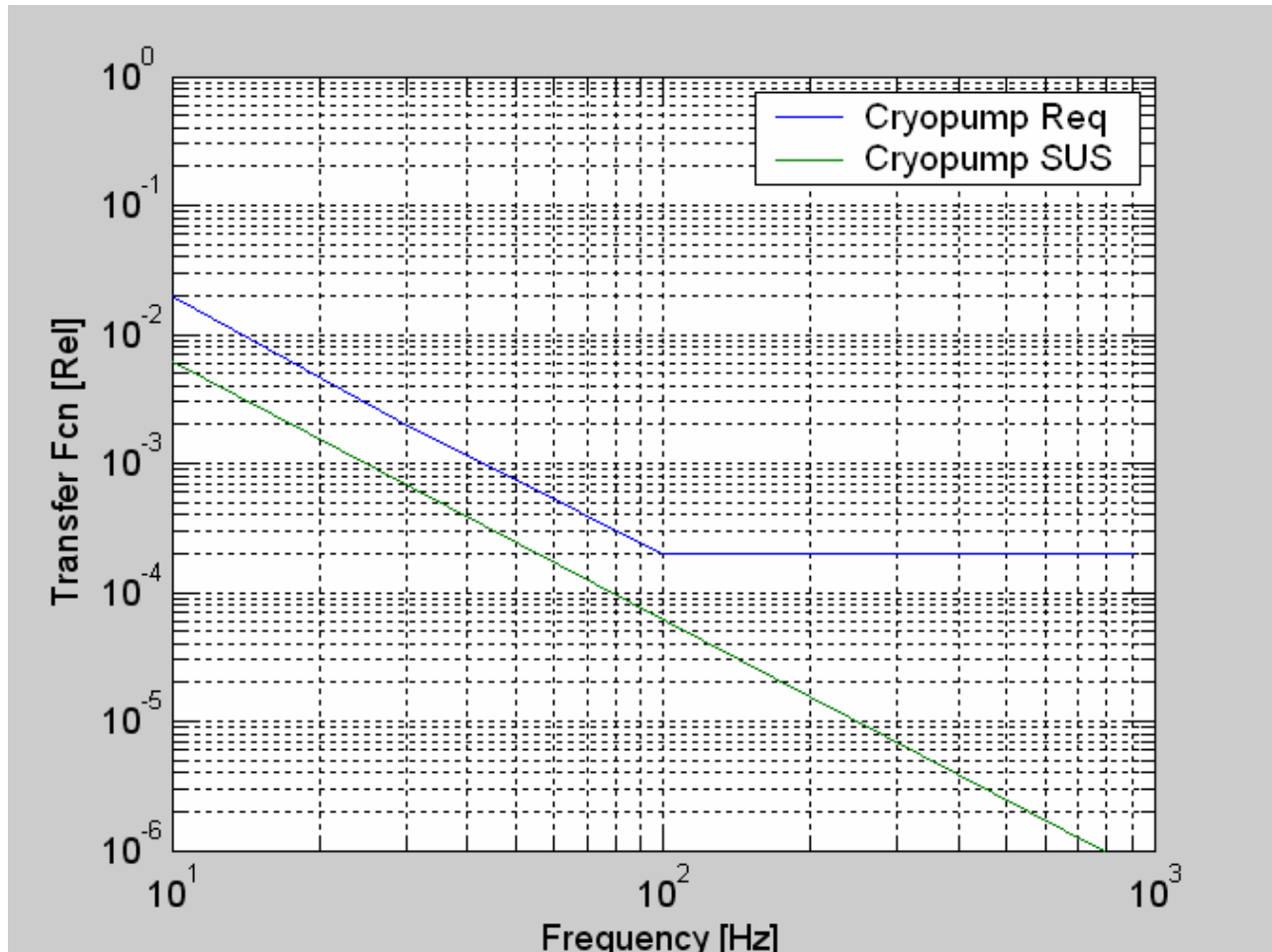


Figure 29: Cryopump Suspension Amplitude Response

3.2.5.4 Cryopump Baffle Surface BRDF

The Cryopump Baffle will be constructed of oxidized polished stainless steel with the first surface inclined at an incidence angle 56 deg and is estimated to have a BRDF $< 0.05 \text{ sr}^{-1}$. See T980027-00, Baffling Requirements for the 4K and 2K IFO.

3.2.5.5 Cryopump Baffle Reflectivity

The light that is not absorbed by the Cryopump Baffle will reflect from the baffle surface onto the insides of the spool piece. There, it will scatter, reflect again from the Cryopump Baffle, and enter the IFO mode at the far COC.

The scattered light model was used to calculate the requirement for the reflectivity of the Cryopump Baffle. Assuming a BRDF of the spool piece wall of 0.1, the reflectivity of the Cryopump Baffle must be < 0.01 .

The reflectivity of the Cryopump Baffle is estimated to be $2.4\text{E-}5$.

3.2.5.6 Seismic Motion of the Cryopump Scattering Surfaces

The surface of the suspended Cryopump Baffle has the seismic motion of the spool piece attenuated by the transfer function of the Cryopump Baffle suspension.

The light that reflects from the Cryopump Baffle will scatter from the spool piece wall, which has the seismic motion shown in Figure 25.

3.2.5.7 Scattered Light Displacement Noise of Suspended Cryopump Baffle

The scattered light displacement noise from the Cryopump Baffle is shown in Figure 26.

3.2.5.8 Fringe-wrapping of Cryopump Baffle Displacement Noise

The Cryopump Baffle has a pendulum resonance at approximately 0.8 Hz. The displacement noise at the odd harmonics of the motion due to fringe wrapping was calculated using the fringe wrap model, assuming a simple pendulum function with a $Q = 1000$ at the resonant frequency. The fringe wrapping does not cause excessive noise above 10 Hz, as shown in Figure 30.

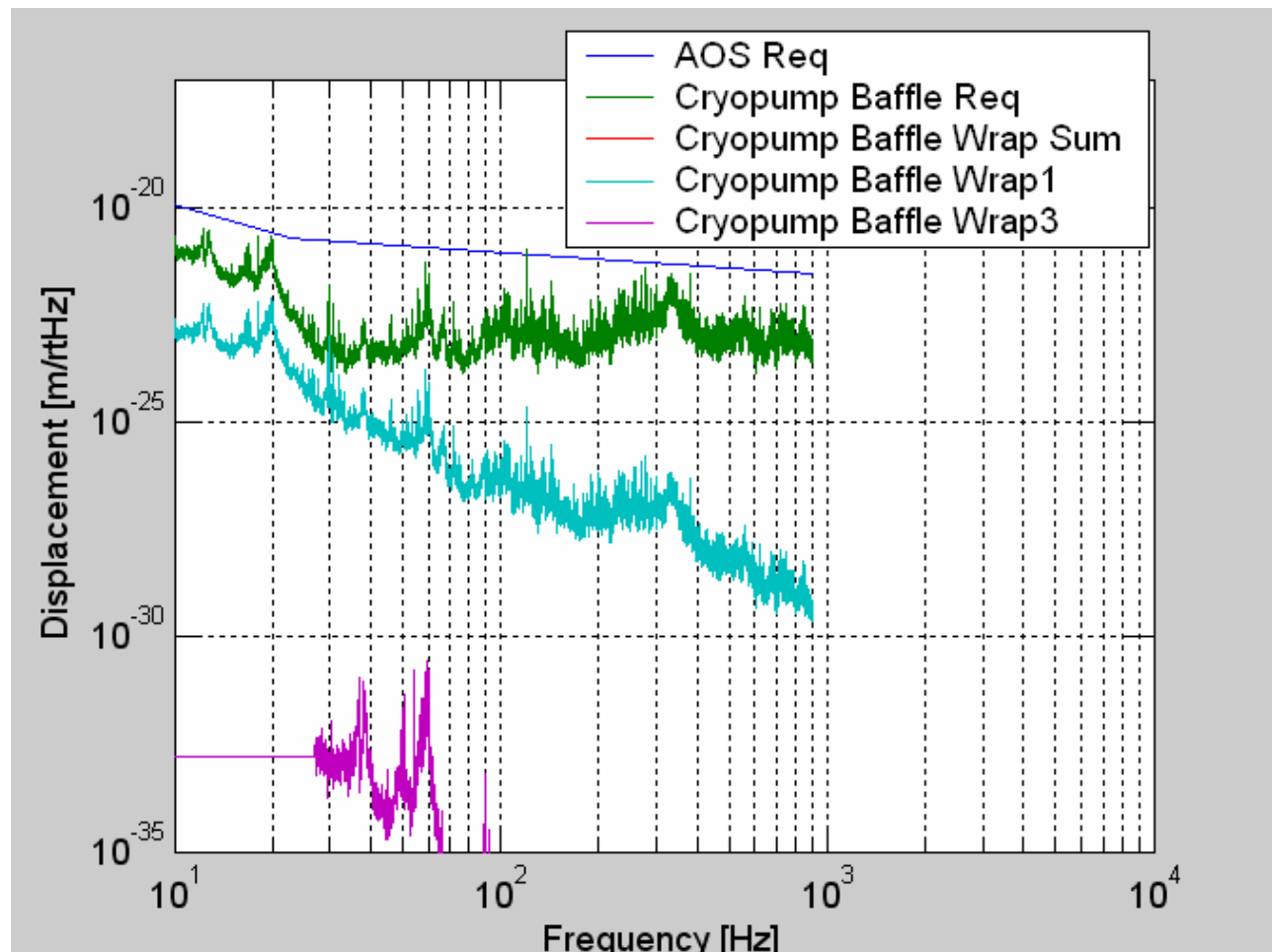


Figure 30: Cryopump Baffle Scattered Light Displacement Noise Caused by Fringe-wrapping

3.2.5.9 Stay Clear Zone

The clear aperture diameter of the Cryopump Baffle, 769 mm, is large enough to allow the folded and non-folded IFO beams of 315.4 mm diameter at the 1 ppm diameter to pass through without vignetting. The fractional geometric power loss of the IFO beam with a $w = 60$ mm passing once through the Cryopump Baffle is $1.4E-8$. With a 4 mm decentering of the baffle, the loss increases to $4E-8$. This is negligible compared to the transmission loss through the ETM mirror.

This meets the requirement 4.7 Clear Aperture Requirements.

3.2.6 Elliptical Baffles

The PRM Elliptical baffle will be placed inside the power recycling cavity between PR3 and the BS. Its purpose is to catch the overfilling of the Gaussian shaped beam entering the recycling cavity from PRM and reflecting from the PR3 mirror by vignetting the beam shape to match the vertical clear aperture of the PR3 mirror and the horizontal clear aperture of the tilted BS, which is approximately an elliptical beam profile.

The ITM Elliptical baffles will be placed on the X and Y arm sides of the BS. The purpose of these baffles is to catch the overfilling of the Gaussian shaped beams entering the recycling cavity from the arms and to vignette the beam shape to the elliptical beam profile described above.

3.2.6.1 ITM Elliptical Baffle

A conceptual drawing of the suspended ITM Elliptical Baffle is shown in Figure 31.

The baffle will be constructed of oxidized polished stainless steel with the first surface inclined at an incidence angle 56 deg and is estimated to have a BRDF < 0.05 sr⁻¹. See T980027-00, Baffling Requirements for the 4K and 2K IFO.

3.2.6.1.1 ITM Elliptical Baffle Seismic Attenuation

The ITM elliptical baffle will be suspended with a single pendulum from the HEPI support ring in the BS chamber. Earthquake stops will be mounted to the chamber walls.

The required motion attenuation of the ITM Elliptical Baffle is shown in Figure 32.

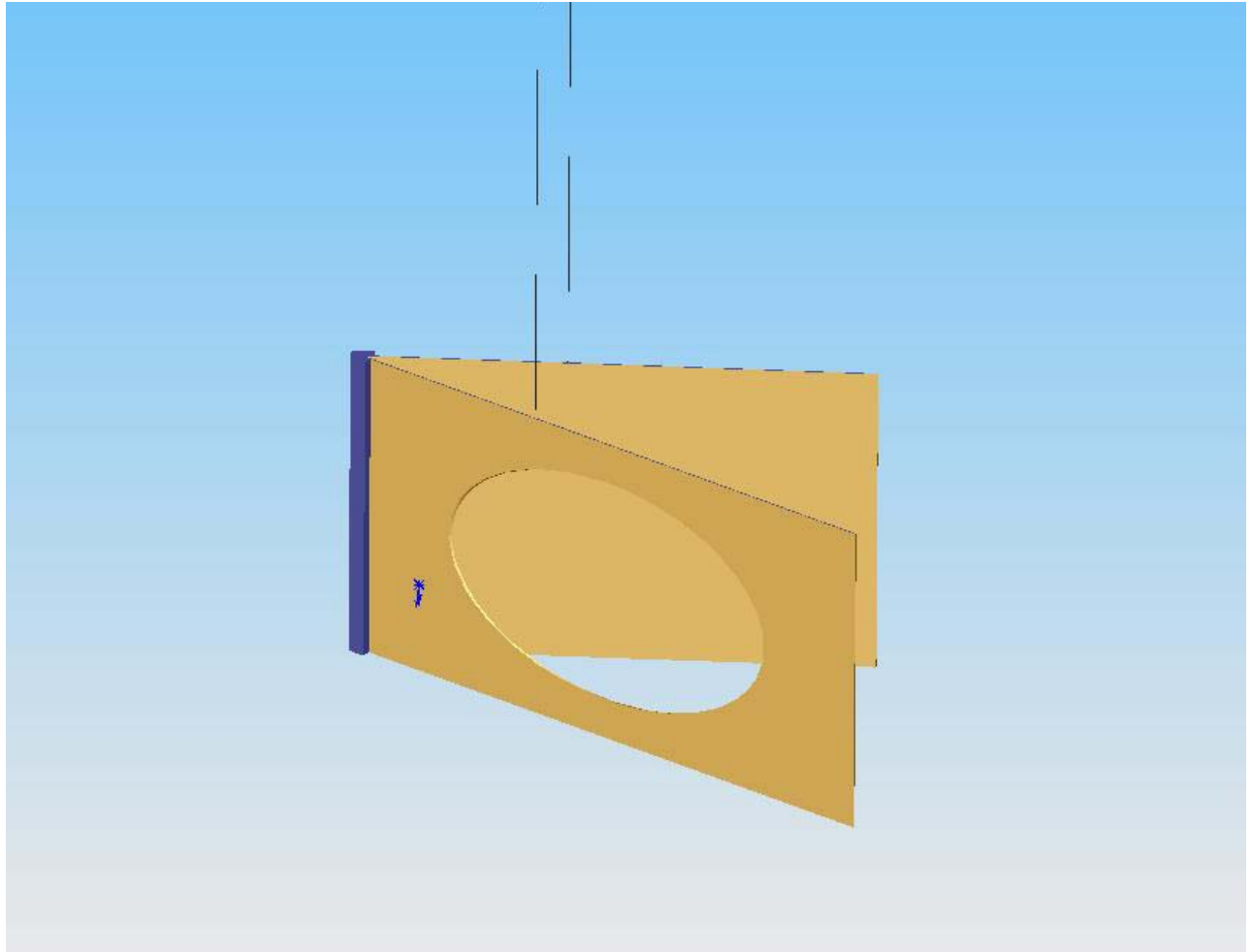


Figure 31: Suspended Elliptical Baffle

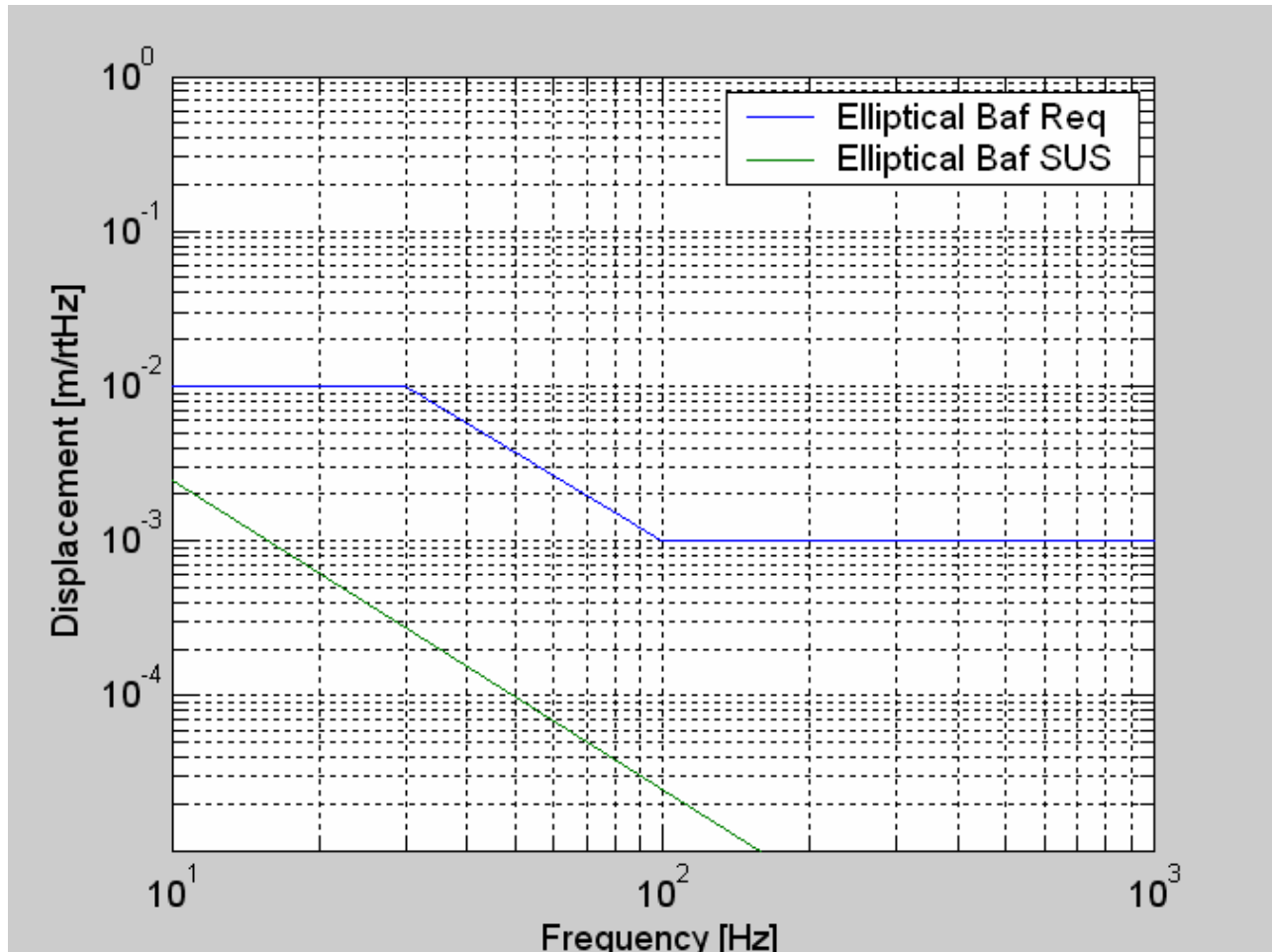


Figure 32: Elliptical Baffle SUS Amplitude Response

3.2.6.1.2 ITM Elliptical Baffle Surface BRDF

The ITM Elliptical Baffle will be constructed of oxidized polished stainless steel with the first surface inclined at an incidence angle 56 deg and is estimated to have a BRDF $< 0.05 \text{ sr}^{-1}$. See T980027-00, Baffling Requirements for the 4K and 2K IFO.

3.2.6.1.3 ITM Elliptical Baffle Reflectivity

The light that is not absorbed by the ITM Elliptical Baffle will reflect from the baffle surface onto the insides of the vacuum chamber. There, it will scatter from the wall, reflect again from the ITM Elliptical Baffle, and enter the IFO mode at the far COC.

The scattered light model determined that the reflectivity of the ITM Elliptical Baffle must be < 0.001 .

The multi-bounce reflectivity of the ITM Elliptical Baffle is estimated to be $2.4\text{E-}5$.

3.2.6.1.4 Seismic Motion of the Vacuum Chamber

The seismic motion of the vacuum chamber is shown in Figure 33. See Robert Schofield (11/17/06 LHO ILOG).

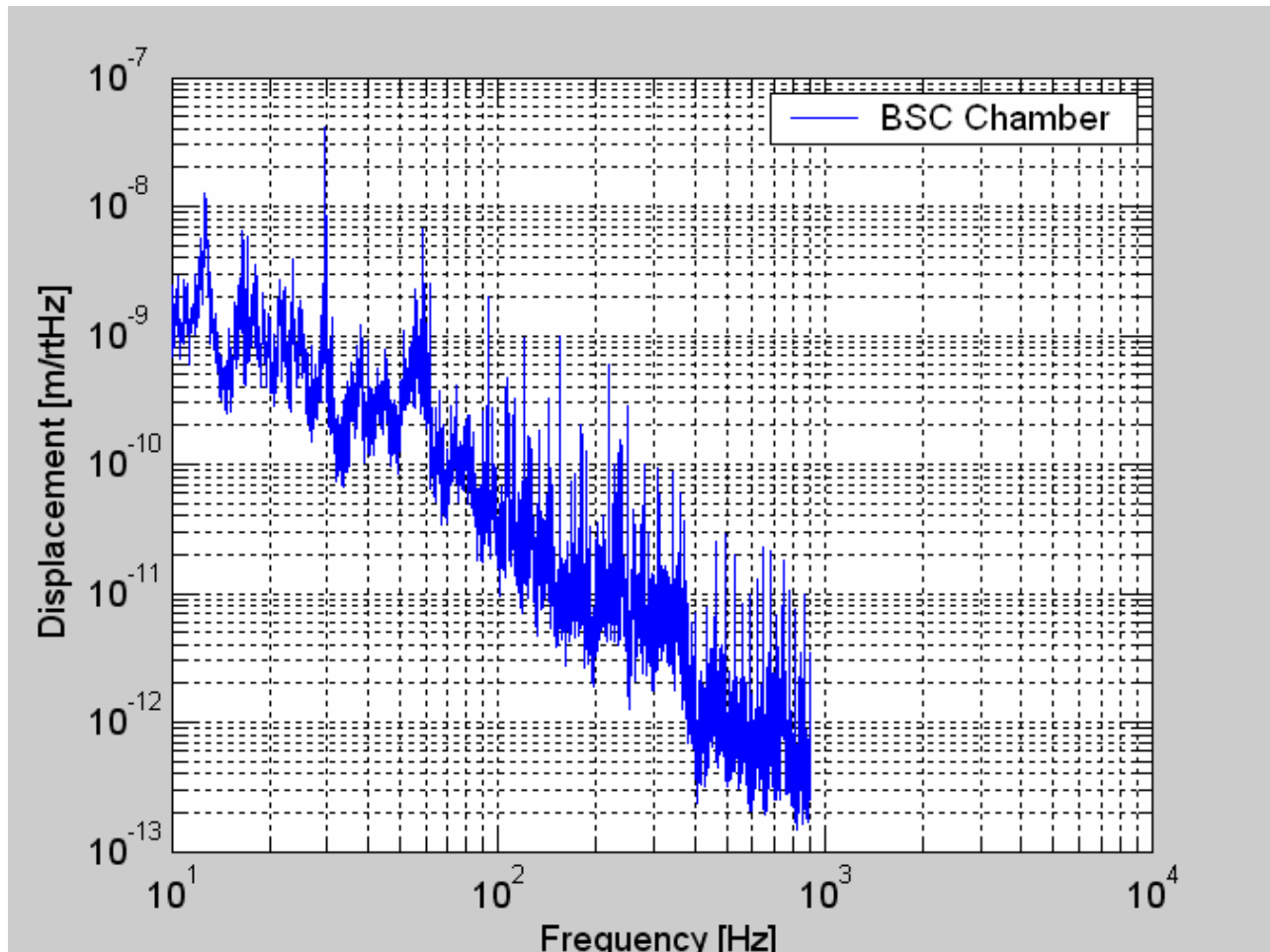


Figure 33: Seismic motion of BSC chamber

3.2.6.1.5 Scattered Light Displacement Noise of Suspended ITM Elliptical Baffle

The light that scatters directly from the surface of the suspended ITM Elliptical Baffle has a phase noise caused by the seismic motion of the HEPI support ring attenuated by the transfer function of the Elliptical Baffle suspension, which is shown in Figure 32.

The light that reflects from the baffle and subsequently scatters will have a phase noise caused by the seismic motion of the chamber walls.

The vacuum chamber walls are assumed to have a BRDF = 0.1 sr^{-1} . The Elliptical Baffle surface BRDF < 0.005 sr^{-1} .

The scattered light displacement noise from these two sources is shown in Figure 35.

3.2.6.1.6 Stay Clear Diameter

The clear aperture of the ITM Elliptical Baffle is 224 mm horizontal diameter and 259 mm vertical diameter. This is approximately the optimum beam profile in the recycling cavity as defined by Hiro. See G070657 LSC-Virgo meeting, 10/24/07, Hiro Yamamoto.

The PRM Elliptical Baffle will be aligned within 4 mm of the beam center.

This meets the requirement 4.7 Clear Aperture Requirements.

3.2.6.2 PRM Elliptical Baffle

The PRM Elliptical Baffle will be identical to the ITM Elliptical baffle shown in Figure 31.

The PRM Elliptical Baffle will mount directly to HAM3, and HAM9 optical tables, as shown in the Zemax layout, Figure 34.

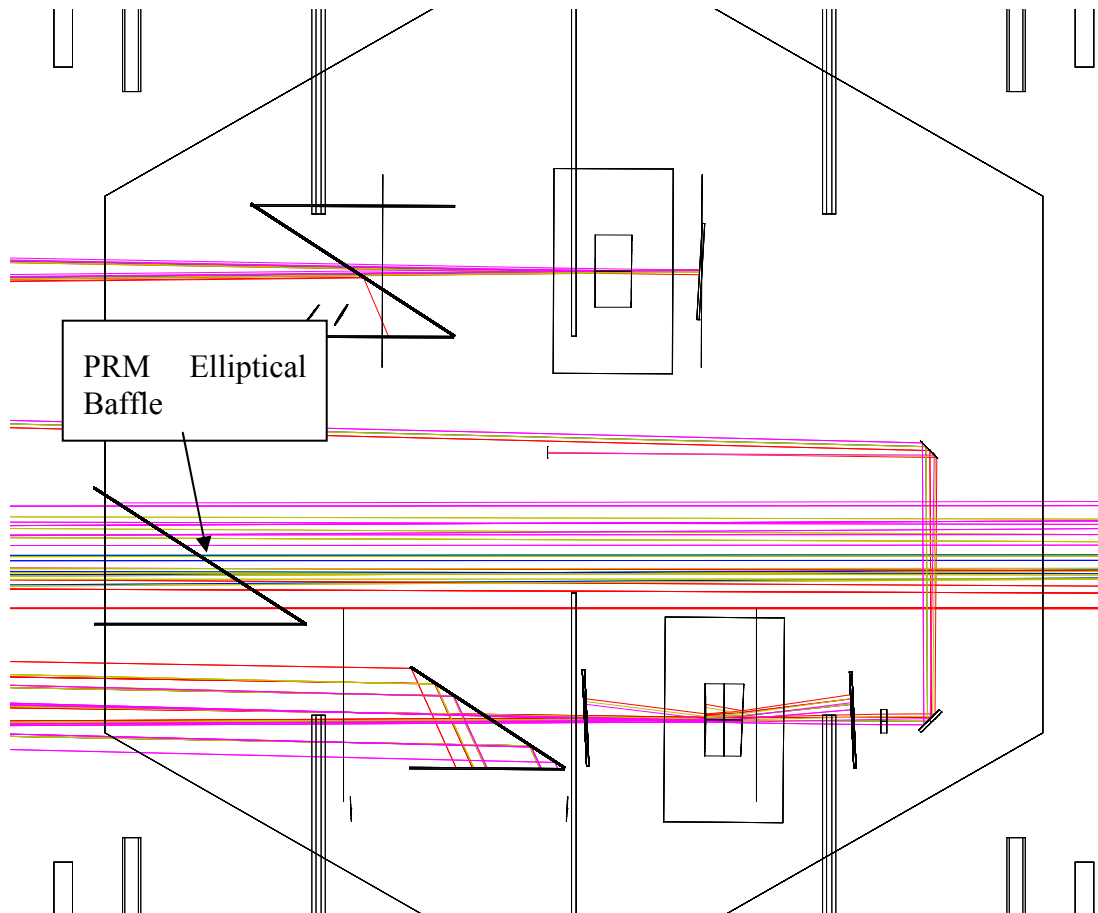


Figure 34: PRM Elliptical Baffle on HAM3

3.2.6.2.1 Motion of PRM Elliptical Baffle

The seismic motion will be the same as the HAM optical table shown in Figure 16.

3.2.6.2.2 Power Hitting the PRM Elliptical Baffle from IO Side

The prompt PSL light that transmits through the PRM and is scraped off by the periphery of the PRM Elliptical Baffle does not build up within the recycling cavity. It is collected by the PR telescope and hits the PRM mirror at an off-axis location where it is re-scattered into the recycling cavity mode.

The irradiance of the IO Gaussian beam incident on the PRM Elliptical Baffle is given by

$$I_{\text{PSL}}(x, y) := 2 \cdot \frac{P_{0\text{psl}}}{\pi \cdot w^2} \cdot e^{-2 \cdot \left(\frac{x^2 + y^2}{w^2} \right)}$$

where $P_{0\text{psl}}$ is the total power in the IO beam, and $w = 0.060$ m is the Gaussian beam radius.

The power passing through the hole in the elliptical baffle is given by

$$P_{\text{hole}} := 4 \cdot \int_0^b \int_0^{a \cdot \sqrt{1 - \frac{y^2}{b^2}}} I_{\text{PSL}}(x, y) \, dx \, dy$$

The power that hits the elliptical baffle is given by

$$P_{\text{prnellbaf}} := P_{\text{psl}} - P_{\text{el}}$$

With a total power input = 125 W, the power hitting the elliptical baffle is = 0.0044 W.

3.2.6.2.3 PRM Elliptical Baffle Surface BRDF

The PRM Elliptical Baffle will be constructed of oxidized polished stainless steel with the first surface inclined at an incidence angle 56 deg and is estimated to have a BRDF < 0.05 sr⁻¹. See T980027-00, Baffling Requirements for the 4K and 2K IFO.

3.2.6.2.4 PRM Elliptical Baffle Reflectivity

The light that is not absorbed by the PRM Elliptical Baffle will reflect from the baffle surface onto the insides of the vacuum chamber. There, it will scatter from the wall, reflect again from the PRM Elliptical Baffle, and enter the recycling cavity mode.

The multi-bounce reflectivity of the PRM Elliptical Baffle is estimated to be 2.4E-5.

3.2.6.2.5 Scattered Light Displacement Noise of PRM Elliptical Baffle

The scattered light displacement noise from both these sources is shown in Figure 35.

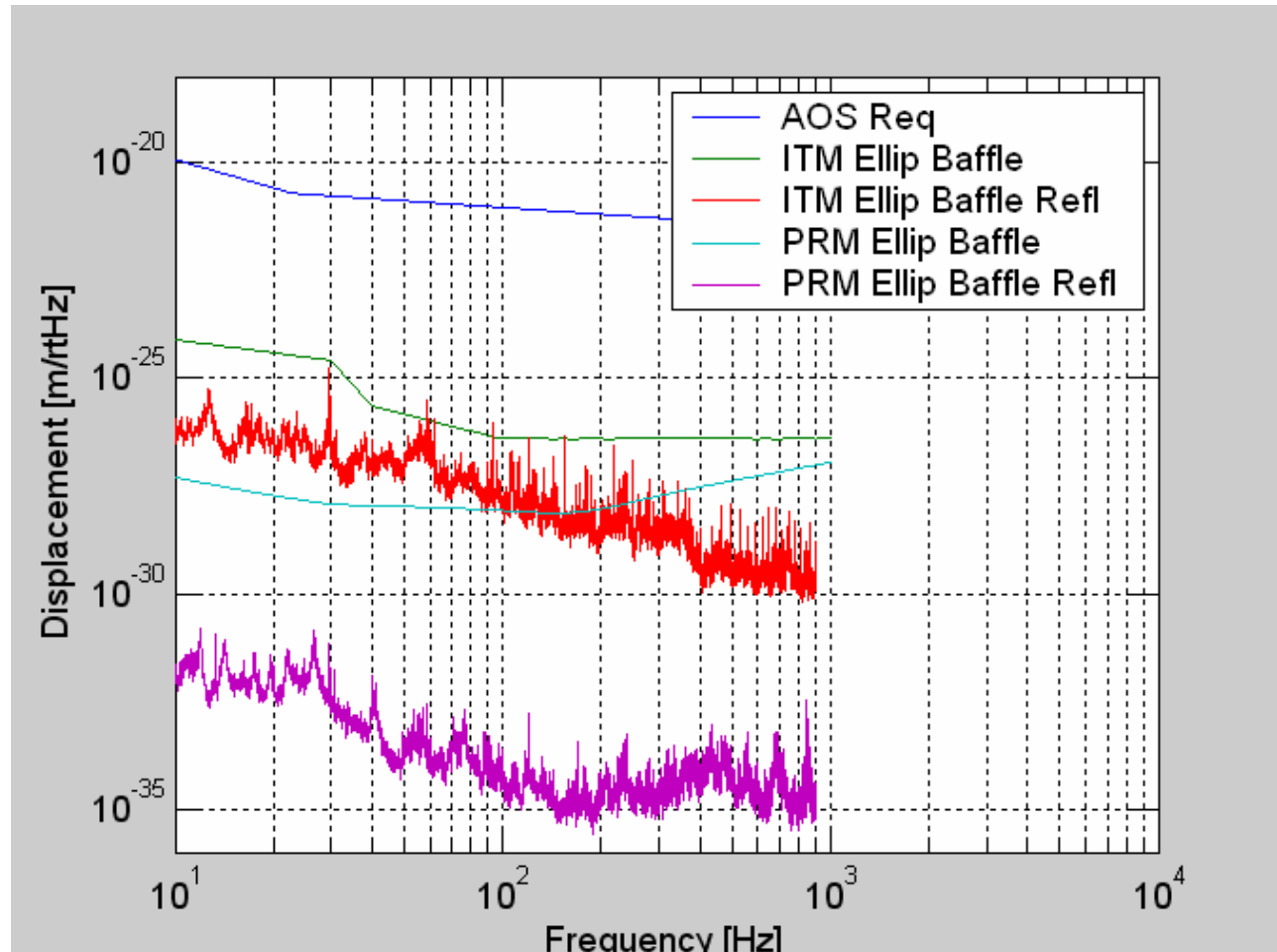


Figure 35: Elliptical Baffle Scattered Light Displacement Noise

3.2.6.2.6 Stay Clear Diameter

The clear aperture of the PRM Elliptical Baffle is 224 mm horizontal diameter and 259 mm vertical diameter. This is approximately the optimum beam profile in the recycling cavity as defined by Hiro. See G070657 LSC-Virgo meeting, 10/24/07, Hiro Yamamoto.

The PRM Elliptical Baffle will be aligned within 4 mm of the beam center.

3.2.7 Wide Angle Scatter from COC

The wide-angle scatter from point defects on the ITM and ETM mirrors is assumed to have a Lambertian distribution with total integrated scattered power equal to 10ppm fraction of the circulating power in the arm cavity. Much of this scattered light will be intercepted by the back of the arm cavity baffle and the associated cylinder baffle; some of the light will pass through the beam holes in the Arm Cavity Baffle and hit the manifold wall and viewport flange at the end of the manifold leading to the cryopump.

3.2.7.1 Manifold Baffle

A manifold baffle, shown in **Figure 36**, will hide the “corner” of the viewport flange surface and avoid the retro-reflection. It will be constructed from oxidized polished stainless steel with the first surface inclined at an incidence angle 56 deg and is estimated to have a BRDF $< 0.05 \text{ sr}^{-1}$. See T980027-00, Baffling Requirements for the 4K and 2K IFO.

3.2.7.1.1 Seismic Motion of Manifold Baffle

The Manifold Baffle has the motion spectrum of the manifold, as shown in Figure 25.

A preliminary FEA vibration analysis shows that the first resonance of the Manifold Baffle occurs at approximately 120 Hz. The Q is expected to be < 1000 , so the motion will be acceptable.

3.2.7.2 Manifold Wall

3.2.7.2.1 Seismic Motion of Manifold Wall

The motion spectrum of the manifold wall is shown in Figure 25.

3.2.7.3 Back of Arm Cavity Baffle and Cylinder

A conceptual design for the Arm Cavity Baffle and the Cylindrical Baffle is shown positioned next to the folded ITM quad suspension in Figure 37.

3.2.7.4 BSC Chamber Wall

3.2.7.4.1 Summary Scattered Light Displacement Noise of Wide-angle COC Scattering

The calculated displacement noise spectrum by light scattered into the IFO mode from 1) total BSC and Manifold Wide Angle scattering, and 2) total back of Arm Cavity Baffle and Cylindrical Baffle wide angle scatter is shown in Figure 38.

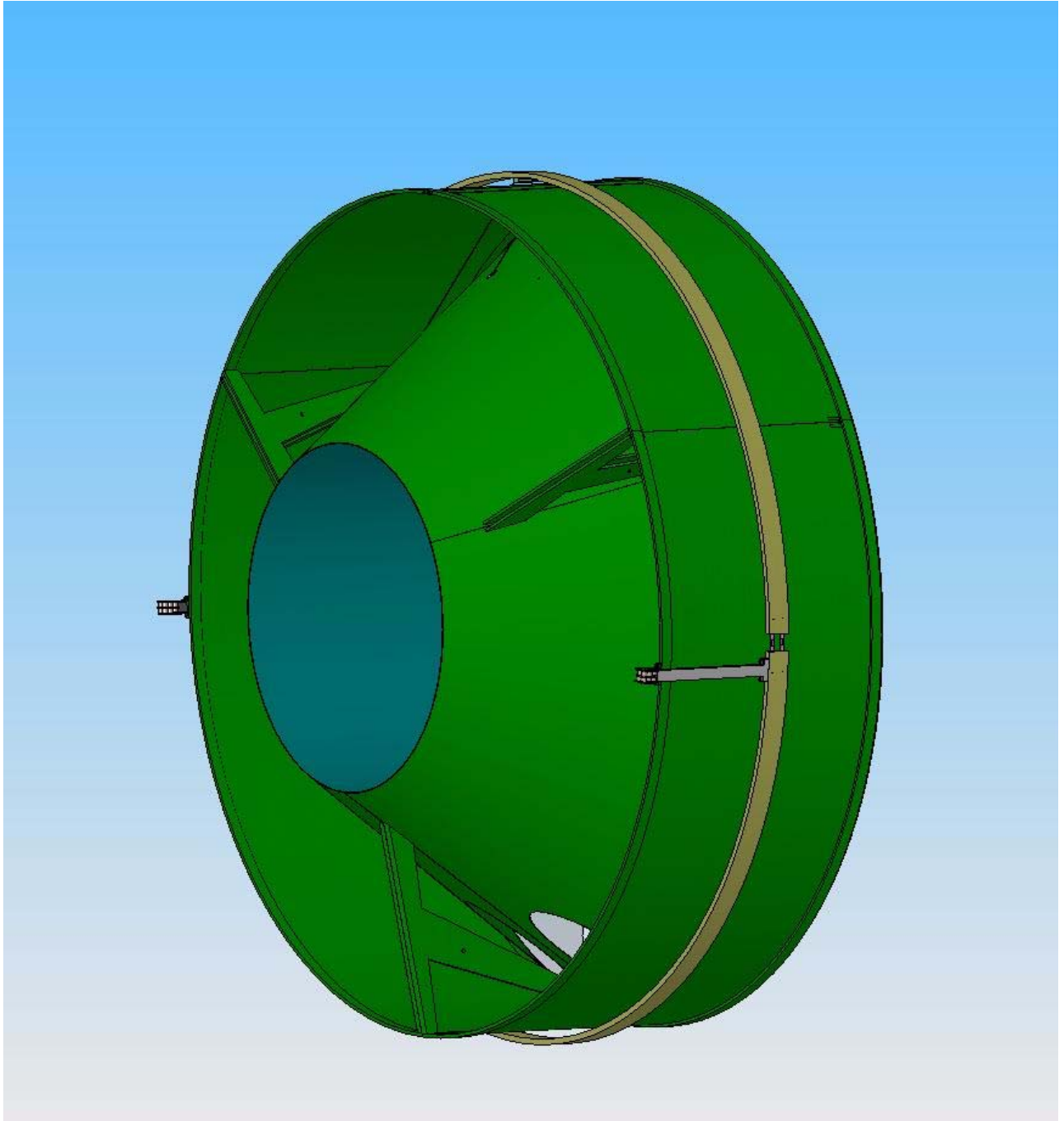


Figure 36: Manifold Baffle

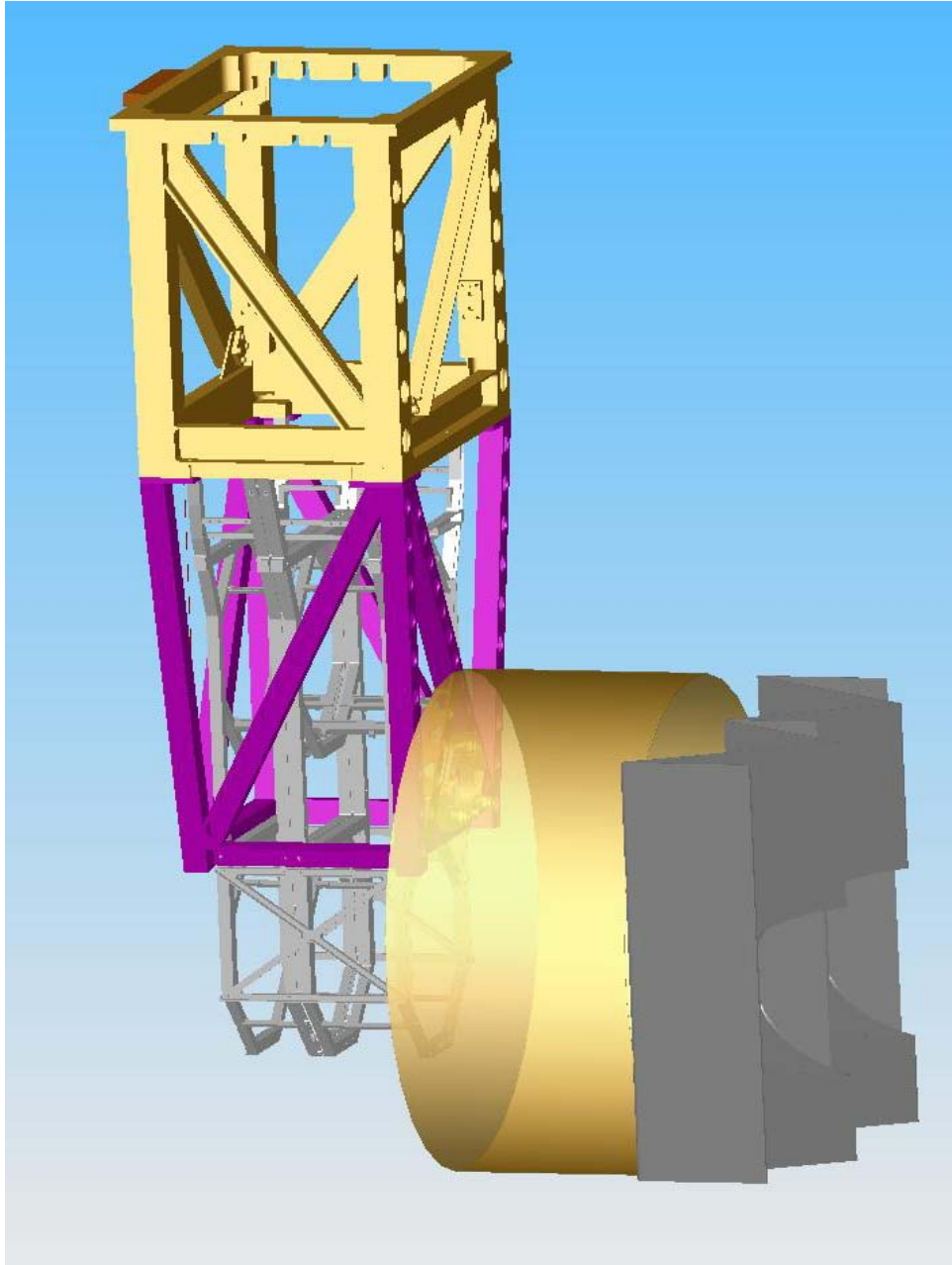


Figure 37: Arm Cavity Baffle with Cylindrical Baffle.

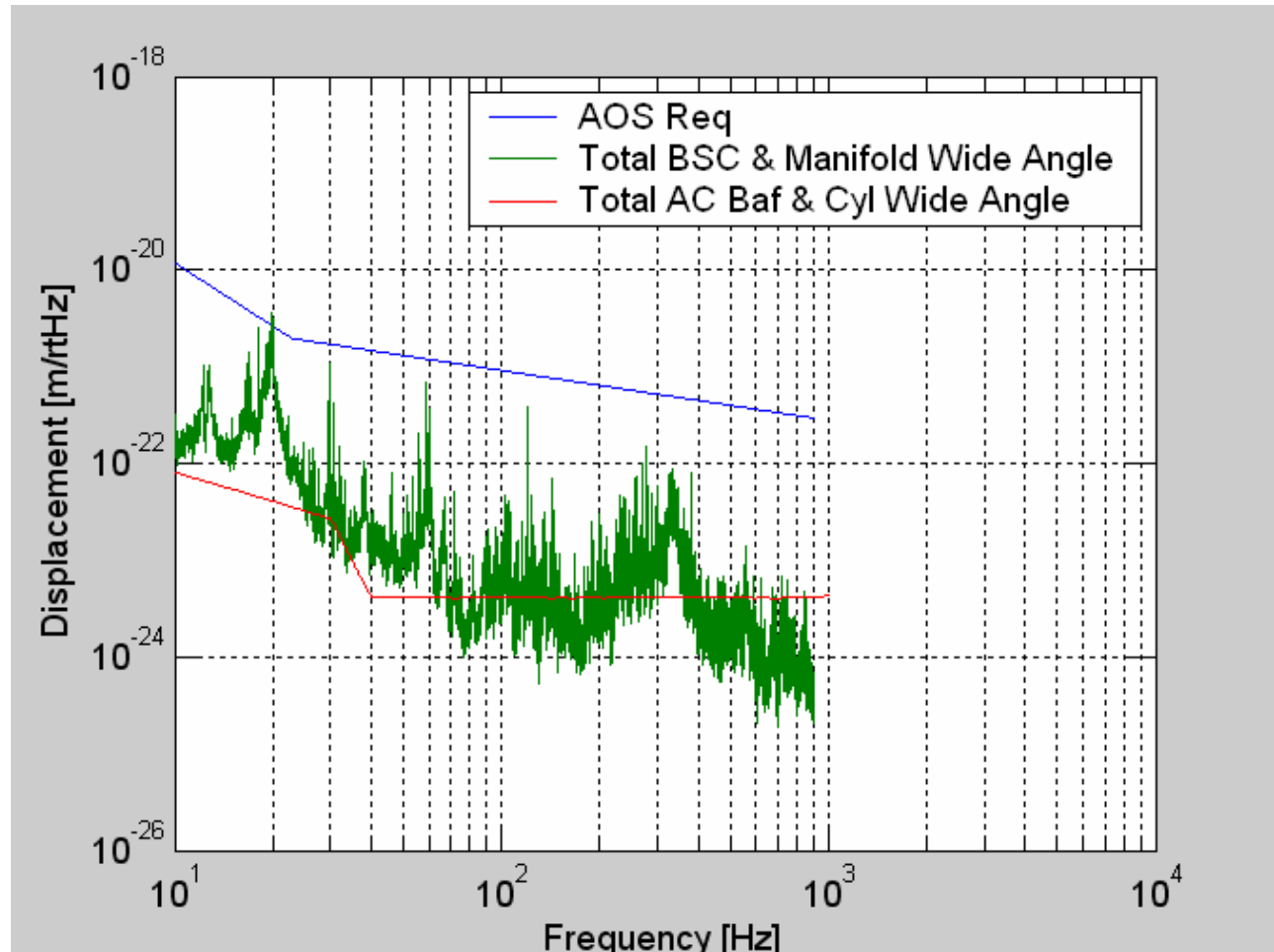


Figure 38: Total wide-Angle COC Scattered Light Displacement Noise

3.2.8 Output Window

Septum Windows for the AS beam, the ITMX PO beam, and the RC PO beam will be mounted to the HAM1, HAM6, HAM7, and HAM12 septum plates, which are mounted to the flange of the HAM chamber, as shown in Figure 39 and Figure 40. The compressible bellows between the Septum Plate assembly and the mounting flange of HAM 6 allows the Septum Windows to be removed without moving any other vacuum enclosures.

In addition, the ITMX and ITMY recycling cavity Hartmann beams will enter and exit the vacuum chamber through vacuum viewports located in HAM4 and HAM10. Part of the AS beam that transmits through the SR2 mirror will leak through the ITMY Hartmann coupling dichroic beam splitter, and part of the ITMX PO beam will leak through the ITMX Hartmann coupling dichroic beam splitter and will scatter from the Hartmann output windows.

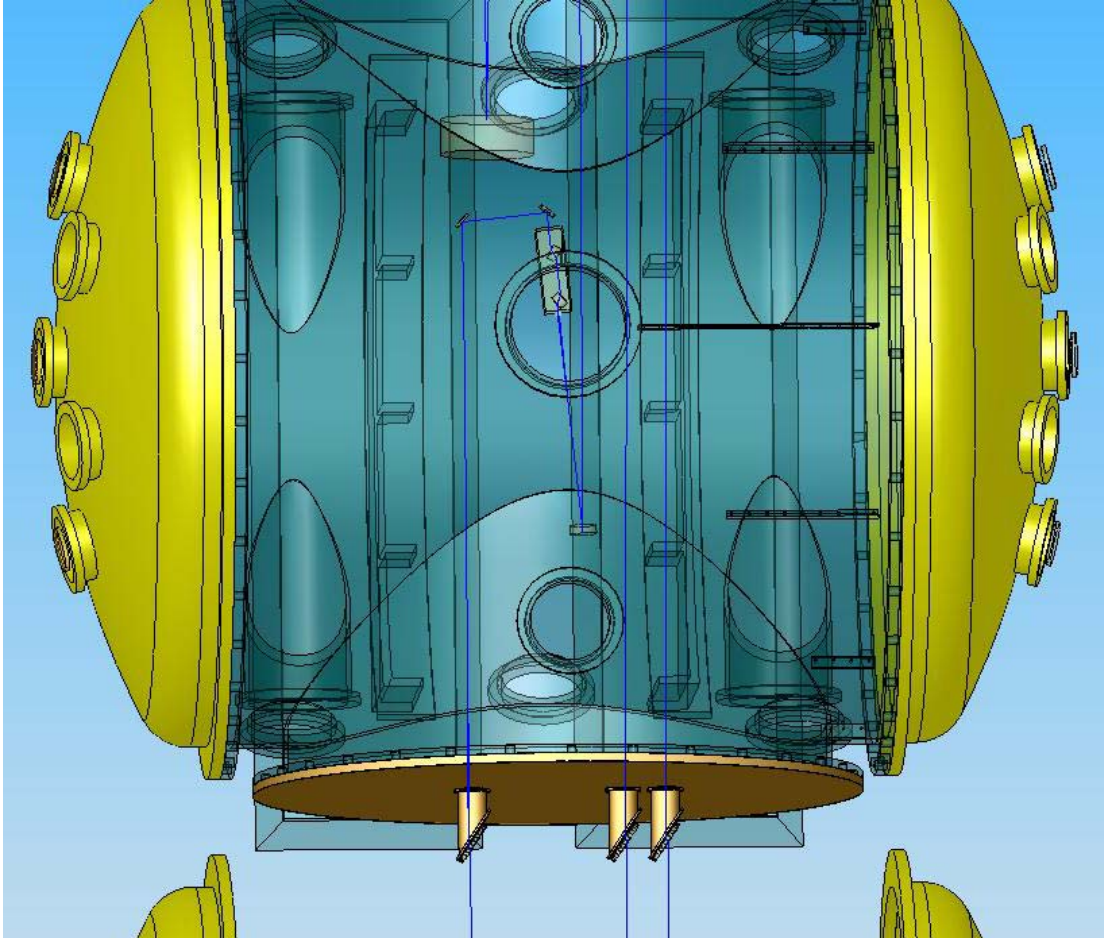


Figure 39: Output Septum Plate

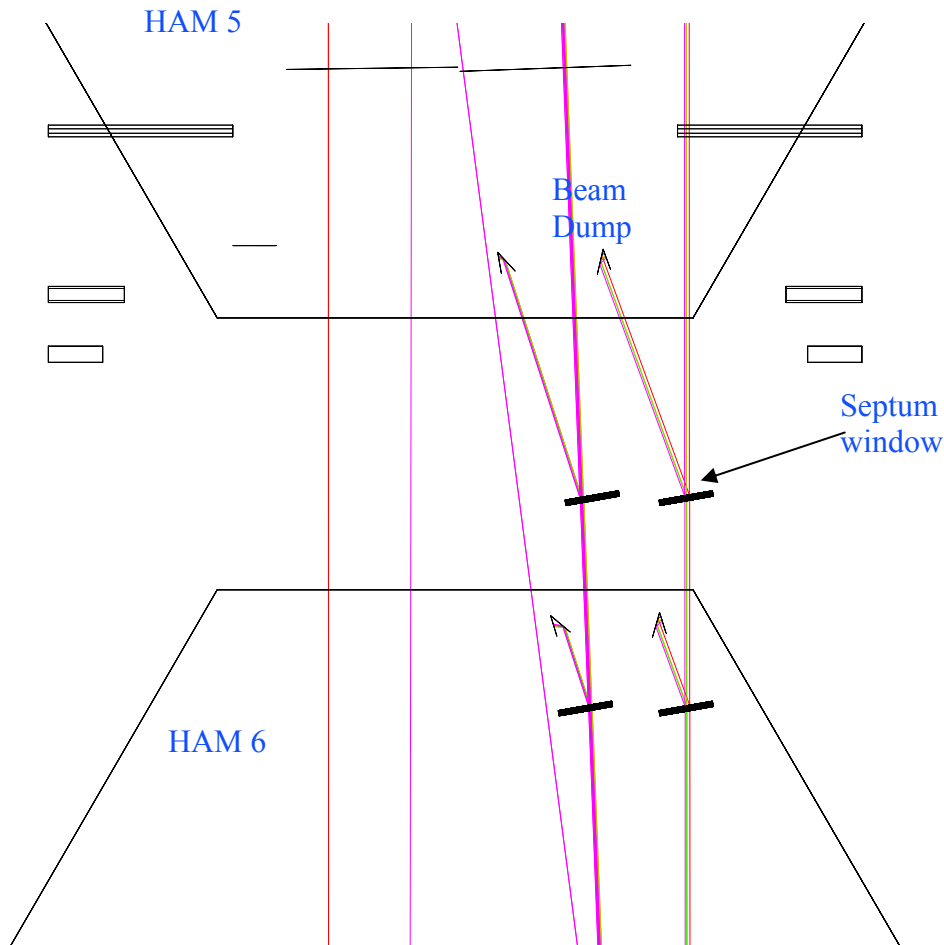


Figure 40: Output Septum Windows

3.2.8.1 Output Window BRDF

The BRDF of the Output Windows were assumed to be the same as the measured BRDF of a super-polished window, $1E-6 \text{ sr}^{-1}$, see T080064-00 Controlling Light Scatter in Advanced LIGO.

The incidence angle on the Septum Window is 10 degrees.

3.2.8.2 Seismic Motion of the Output Windows

The Output Windows are mounted directly to the HAM1, HAM4, HAM6, HAM7, HAM10, and HAM12 septum plates and doors, and will have a displacement spectrum similar to the HAM6 flange, as shown in Figure 41. See Robert Schofield (11/17/06 LHO ILOG).

3.2.8.3 Scattered Light Displacement Noise of Output Window

The scattered light displacement noise from the Output Windows is shown in Figure 42. The scattered light noise from the AS Window exceeds the AOS requirement and also the ADLIGO Science requirement.

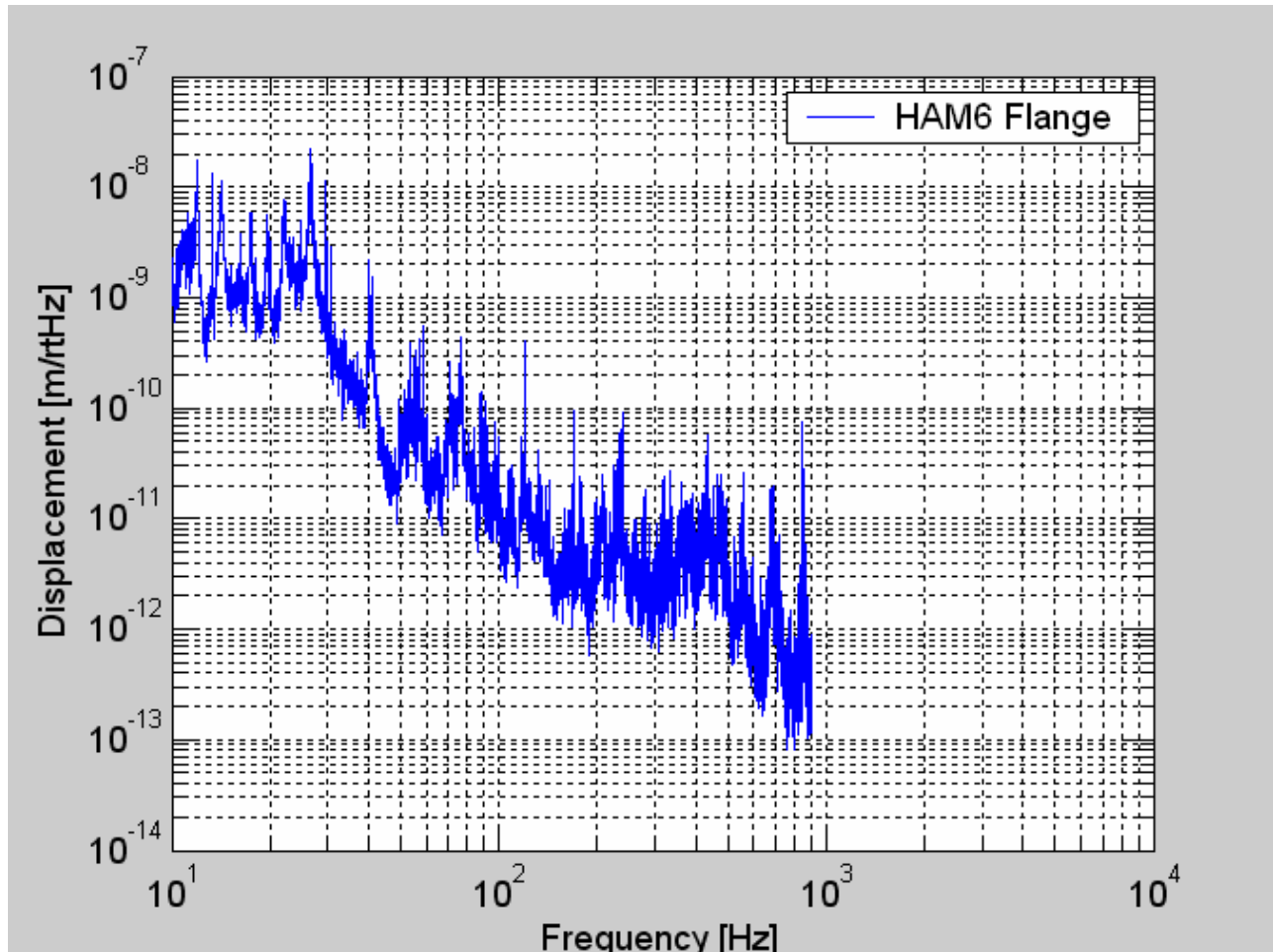


Figure 41: Displacement Spectrum of HAM 6 Flange

3.2.8.4 Reflected Light from AS Output Window

The light that reflects from the two surfaces of the AS Output window will be caught in the cavity beam dumps mounted on HAM chamber optical tables. The cavity beam dump will be made of black glass with the first surface inclined at an incidence angle 56 deg and is estimated to have a BRDF $< 0.005 \text{ sr}^{-1}$. See T980027-00, Baffling Requirements for the 4K and 2K IFO.

The multi-bounce reflectivity of the cavity beam dump is estimated to be $< 2.4\text{E-}5$.

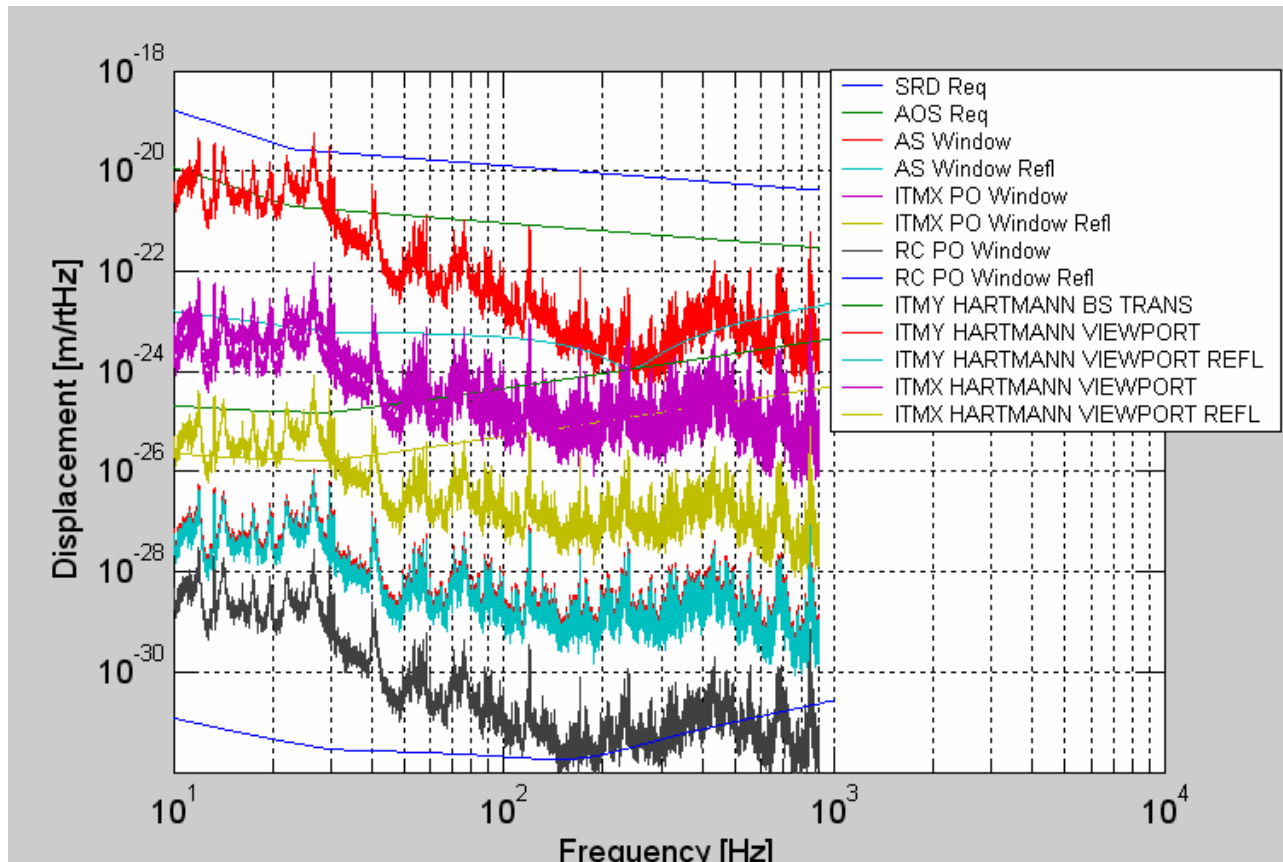


Figure 42: Output Window Scattered Light Displacement noise

3.2.8.5 Output Septum Windows Removal

The Septum Windows are mounted to nozzle pieces with o-rings and a capture flange, and the nozzle piece is mounted independently to the HAM Plenum. Therefore, the nozzle piece can be removed by venting HAM5, with access from the adjoining vented HAM6 chamber, without removing the septum plate.

When the Septum Windows are removed, the total scattered light displacement noise meets the AOS requirement, as shown in Figure 14.

3.2.8.5.1 Stay Clear Diameter

The clear aperture of the Output Window is > 60 mm diameter. The AS beam, the ITMX PO beam, and the RC PO beam have Gaussian diameters approximately 4 mm.

This meets the requirement 4.7 Clear Aperture Requirements.

3.2.9 Hartmann Viewports

The ITMX Hartmann beam is superimposed on the ITMX PO beam with a dichroic beamsplitter that transmits mostly visible light and reflects mostly IR light. However, some of the ITMX PO beam power will transmit through the dichroic beamsplitter and scatter from the ITMX Hartmann Viewport, shown in Figure 43.

Similarly, The ITMY Hartmann beam is superimposed on the beam that leaks through the SR2 HR mirror with a dichroic beamsplitter that reflects mostly visible light and transmits mostly IR light. However, some of the SR2 HR leakage beam power will reflect from the dichroic beamsplitter and scatter from the ITMY Hartmann Viewport

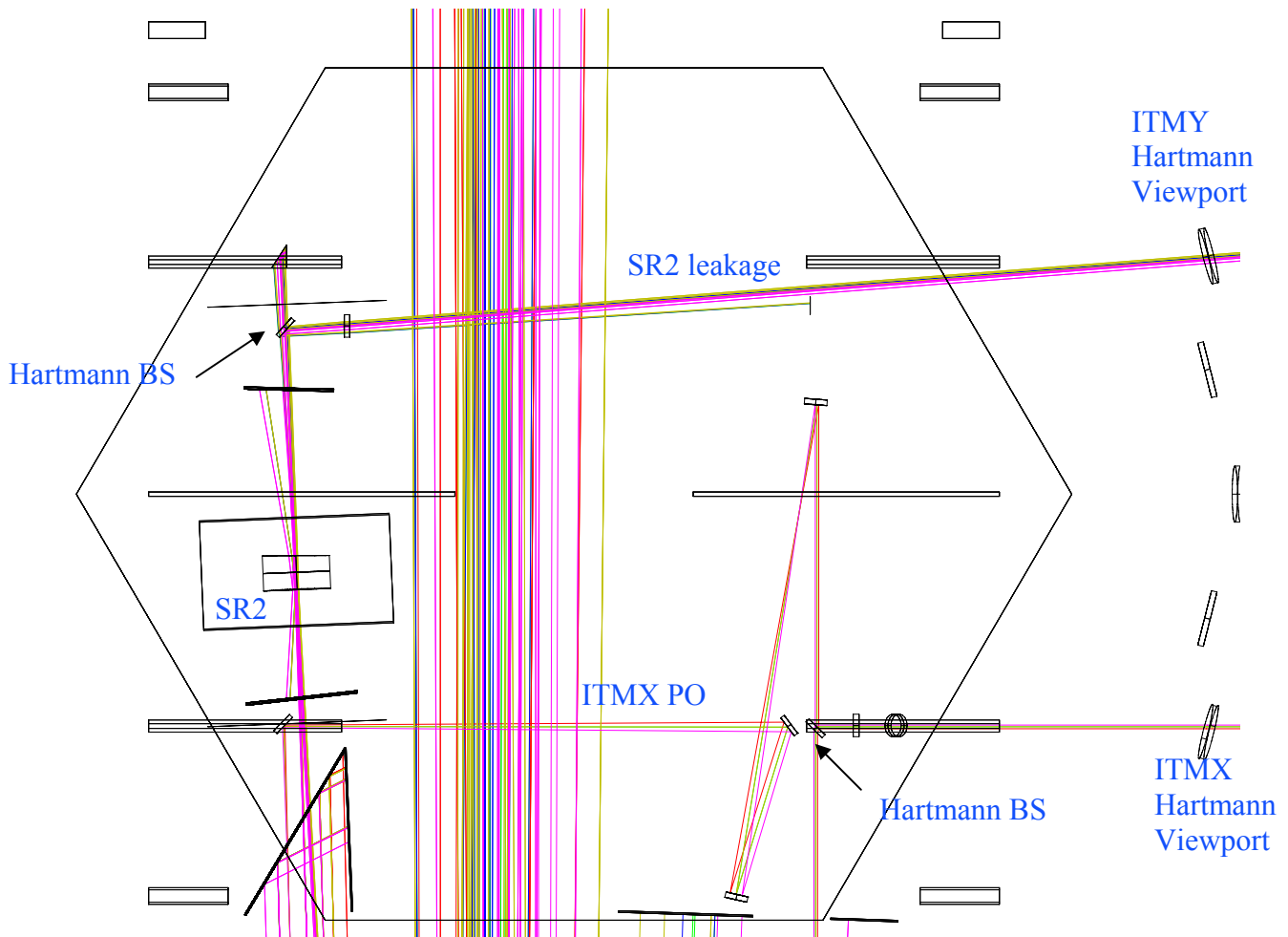


Figure 43: Hartmann Viewports

3.2.9.1 Hartmann Viewport BRDF

The BRDF of the Hartmann Viewport is assumed to be the same as the measured BRDF of a super-polished window, $1\text{E-}6 \text{ sr}^{-1}$, see T080064-00 Controlling Light Scatter in Advanced LIGO.

The incidence angle on the Hartmann Viewport is approximately 10 degrees.

The reflectivity of the Hartmann Viewport is estimated to be $<0.025\%$.

3.2.9.2 Reflected Light from Hartmann Viewport

The light that reflects from the two surfaces of the Hartmann Viewport does not cause excessive displacement noise and will be allowed to hit the walls of the HAM chamber.

3.2.9.2.1 Scattered Light Displacement Noise of Ghost Beams

The scattered light displacement noise from the Hartmann Viewports is shown in Figure 42.

3.2.10 ITM GBAR1, GBAR3, and GBAR4 Ghost Beams

The ITM GBAR1, GBAR3, and GBAR4 Ghost Beams (see Figure 57) are collected by the PR and SR telescopes and will be caught in the scraper cavity beam dumps mounted to the HAM optical table in front of PR2, and SR2 mirrors as shown in Figure 5, and Figure 6.

Some of the ghost beam light will reflect from the cavity beam dumps and scatter from the IO and OUT tube walls, retracing their paths into the recycling cavity beam.

3.2.10.1 PR2/SR2 Cavity Beam Dump BRDF

The PR2/SR2 Cavity Beam Dump will be constructed of oxidized polished stainless steel with the first surface inclined at an incidence angle 56 deg and is estimated to have a BRDF $< 0.05 \text{ sr}^{-1}$. See T980027-00, Baffling Requirements for the 4K and 2K IFO.

3.2.10.2 PR2/SR2 Cavity Beam Dump Reflectivity

The light that is not absorbed by the PR2/SR2 Cavity Beam Dump will reflect from the beam dump surface onto the insides of the manifold. There, it will scatter from the wall, reflect again from the PR2/SR2 Cavity Beam Dump, and enter the recycling cavity mode.

The multi-bounce reflectivity of the PR2/SR2 Cavity Beam Dump is estimated to be $2.4\text{E-}5$.

3.2.10.3 Scattered Light Displacement Noise of Ghost Beams

The scattered light displacement noise from the ITM AR ghost beams is shown in Figure 44.

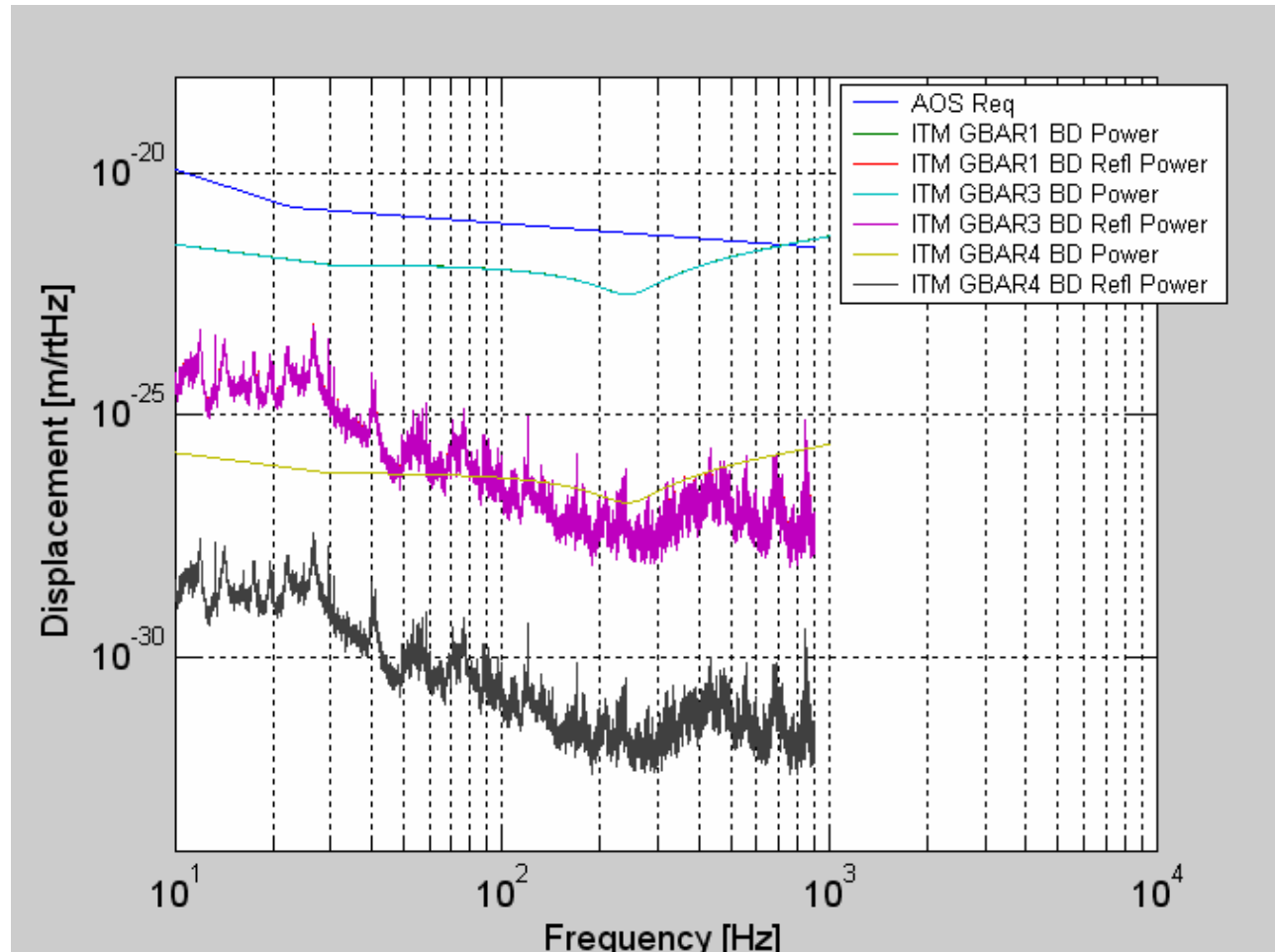


Figure 44: ITM GBAR1, GBAR3, and GBAR4 Beam Dump Scattered Light Displacement Noise

3.2.11 ITM HR, BS AR, AND BS HR Ghost Beams

The ITM HR3, ITM HR4, BS AR3X, BSAR4X, BSHR3X, AND BSHR4X Ghost Beams will pass through the Cryopump Baffle opening and hit the beam tube shark's-tooth baffles inside the arm.

3.2.11.1 Beam Tube Baffle BRDF and Reflectivity

The beam tube shark's-tooth baffles are made from oxidized, polished stainless steel with the first surface inclined at an incidence angle of 55 deg and are estimated to have a BRDF $< 0.05 \text{ sr}^{-1}$. The multi-bounce reflectivity of the PRM Elliptical Baffle is estimated to be $2.4\text{E-}5$. See T980027-00, Baffling Requirements for the 4K and 2K IFO.

3.2.11.2 Scattered Light Displacement Noise of Ghost Beams

The scattered light displacement noise from the ITM HR3 and ITM HR4 ghost beams is shown in Figure 45.

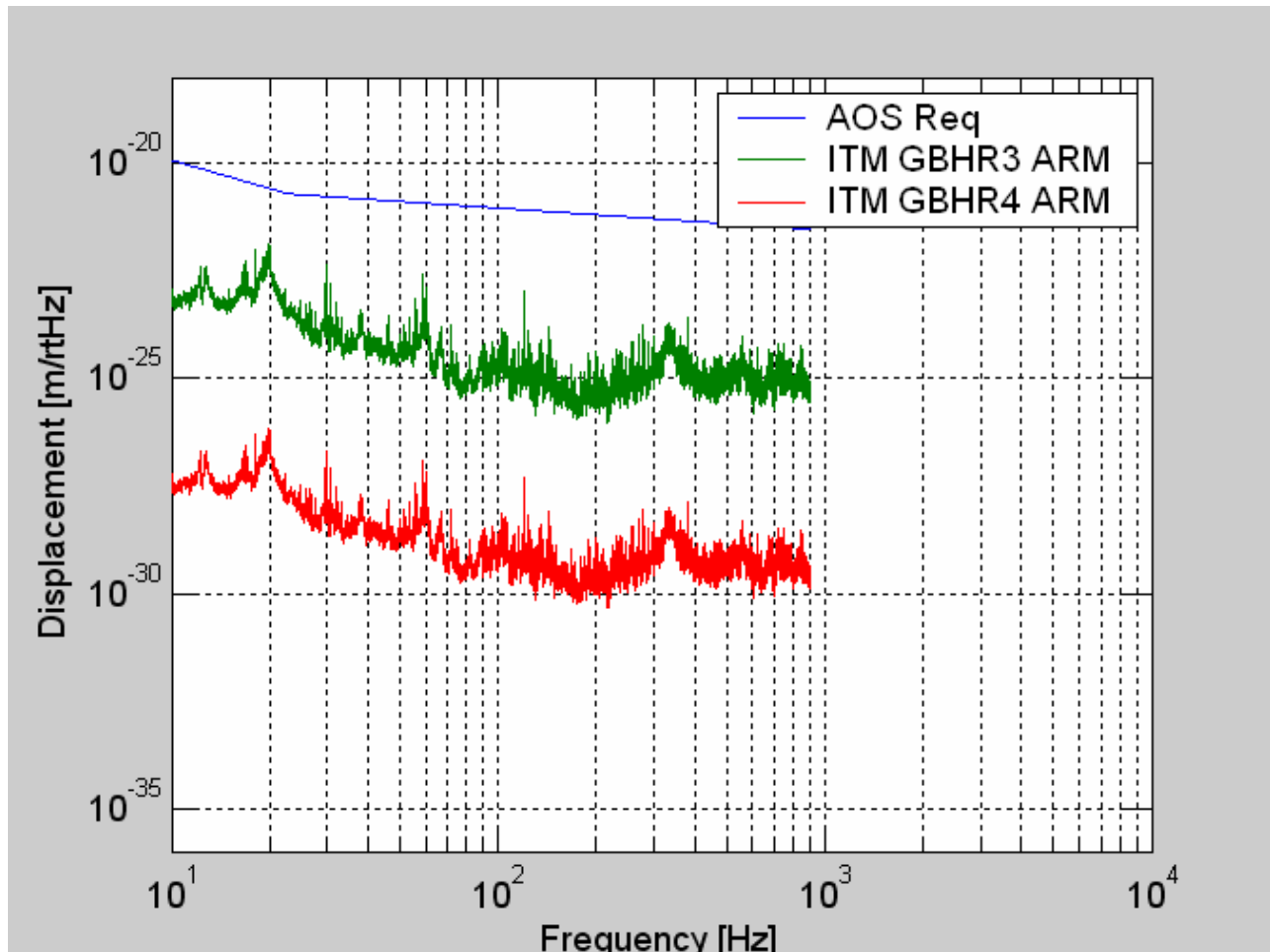


Figure 45: ITM GBHR Beam Dump Scattered Light Displacement Noise

The scattered light displacement noise from the BS AR3X, BSAR4X, BSHR3X, AND BSHR4X ghost beams is shown in Figure 46.

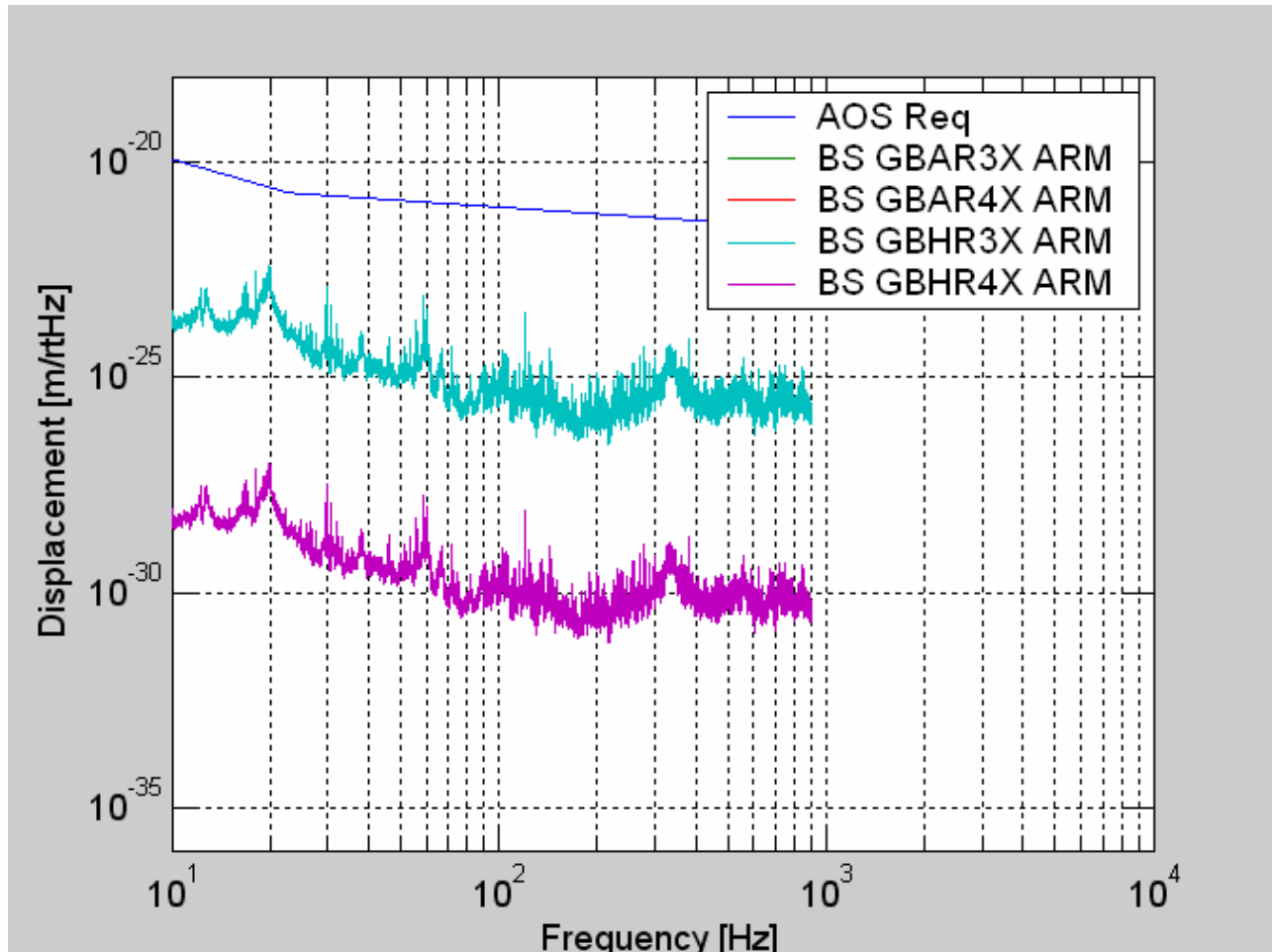


Figure 46: BS GBARX and GBHRX Scattered Light Displacement Noise

3.2.12 BS GBHR3P, BS GBHR

The BS AR3P and, BS HR3P (see Figure 58) are collected by the PR and SR telescopes and will be caught in the scraper cavity beam dumps mounted to the HAM optical table in front of PR2, and SR2 mirrors as shown in Figure 5, and Figure 6.

Some of the ghost beam light will reflect from the cavity beam dumps and scatter from the IO tube and OUT tube walls, retracing their paths into the recycling cavity beam.

3.2.12.1 Scattered Light Displacement Noise of Ghost Beams

The scattered light displacement noise from the BS AR3P and, BS HR3P ghost beams is shown in Figure 47.

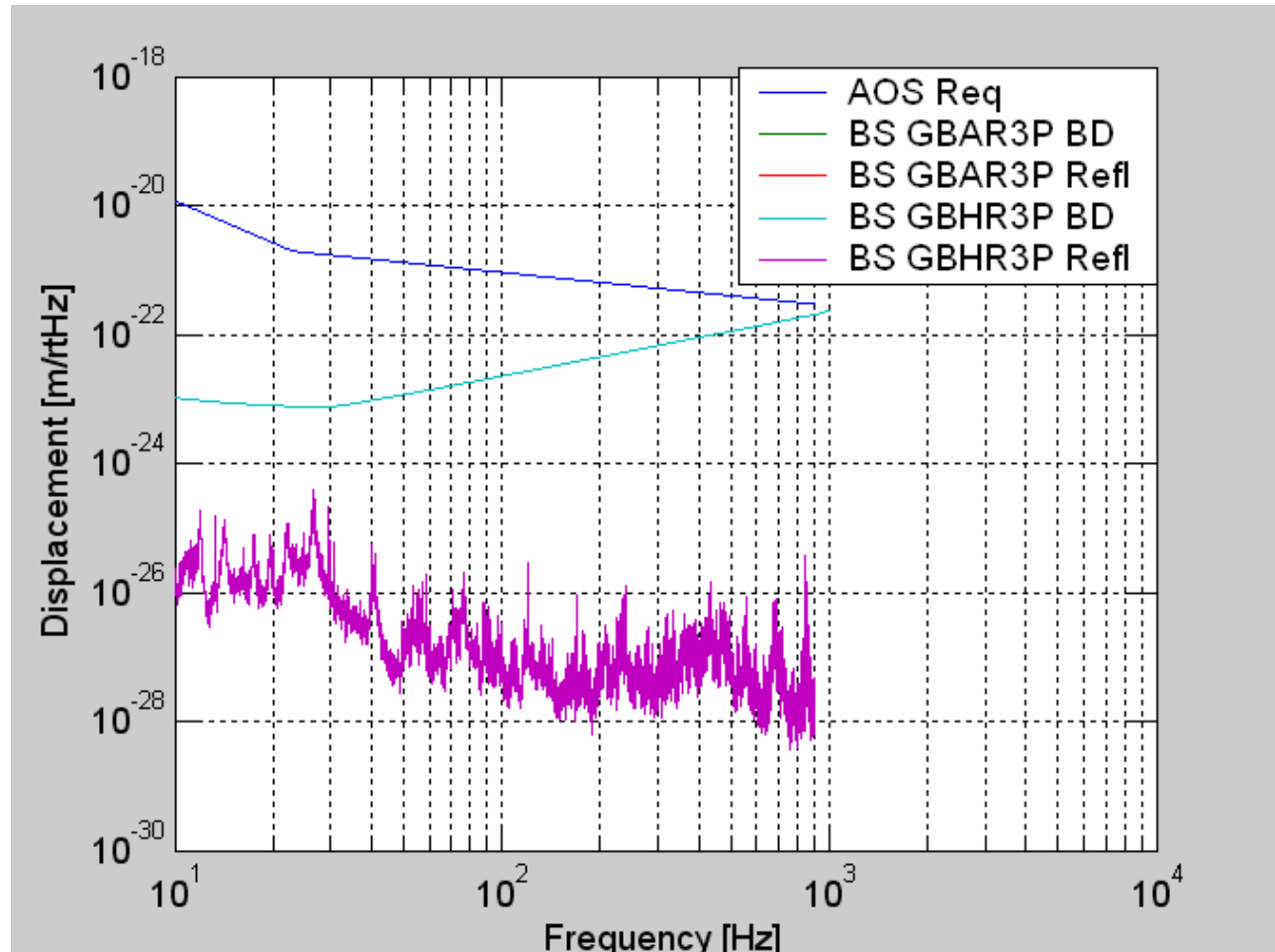


Figure 47: BS GBAR3P and BS GBHR3P Beam Dump Scattered Light Displacement Noise

3.2.13 ITMX PO Beam (BS GBAR1)

The ITMX PO beam (BS GBAR1) hits the center of the signal recycling telescope mirror SR3, see Figure 2, then separates from the main beam and passes through a hole in the scraper beam dump in front of SR2 mirror and is picked off with a small steering mirror, as illustrated in the ZEMAX layout in Figure 43.

3.2.14 PRM Ghost Beams

3.2.14.1 PRM GBAR1

The PRM AR1 Ghost Beam is the reflection of the PSL beam from the AR surface of the PRM. This beam will scatter from the PRM AR Plate Beam Dump shown in Figure 7. A fraction of this scattered light will reflect from the AR surface and head toward the input Faraday isolator. This scattered light will be deflected by the Faraday isolator toward the REFL detection optics where some of it may reflect or scatter back and retrace its path back through the input Faraday isolator and inject noise into the input beam.

3.2.14.2 PRM GBAR3

The PRM AR3 Ghost Beam is the first internal reflection of the recycling cavity beam from the HR and AR surfaces that passes out through the AR surface. This beam will scatter from the PRM AR Plate Beam Dump shown in Figure 7. A fraction of this scattered light will retrace the path and inject noise directly into the recycling cavity.

3.2.14.3 PRM GBHR3

The PRM HR3 Ghost Beam is the first internal reflection of the recycling cavity beam from the AR surface that passes out through the HR surface. This beam will scatter from the PRM HR Plate Beam Dump shown in Figure 7. A fraction of this scattered light will retrace the path and inject noise directly into the recycling cavity.

3.2.14.4 PRM Plate Beam Dump Surface BRDF and Reflectivity

The PRM plate Beam Dump will be constructed of AR-coated black glass. The estimated BRDF is $< 0.05 \text{ sr}^{-1}$. See T980027-00, Baffling Requirements for the 4K and 2K IFO.

The reflectivity of the PRM plate Beam Dump is estimated to be $< 0.025\%$.

3.2.14.5 Scattered Light Displacement Noise of Ghost Beams

The total scattered light displacement noise from the PRM ghost beams is shown in Figure 50.

3.2.15 PR2 Ghost Beams

3.2.15.1 PR2 GBAR0t

The PR2 AR0t Ghost Beam is the leakage through the HR side of the circulating recycling cavity beam from the PRM direction. This beam will scatter from the PR2 GBAR0t Cavity Beam Dump shown in Figure 48. A fraction of this scattered light will pass back through PR2 HR surface and inject noise directly into the recycling cavity.

3.2.15.2 PR2 GBAR0t Cavity Beam Dump Surface BRDF and Reflectivity

The PR2 GBAR0t Cavity Beam Dump will be constructed of oxidized polished stainless steel with the first surface inclined at an incidence angle 56 deg and is estimated to have a BRDF $< 0.05 \text{ sr}^{-1}$. See T980027-00, Baffling Requirements for the 4K and 2K IFO.

The reflectivity of the PR2 GBAR0t Beam Dump is estimated to be $2.4\text{E-}5$.

3.2.15.3 RC PO Beam (PR2 GBARt)

The RC PO Beam (PR2 ARt Ghost Beam), shown in Figure 48, is the leakage through the HR side of the returning recycling cavity beam from the BS. This beam will be steered through a septum window onto the ISC detection bench on HAM1 and HAM7.

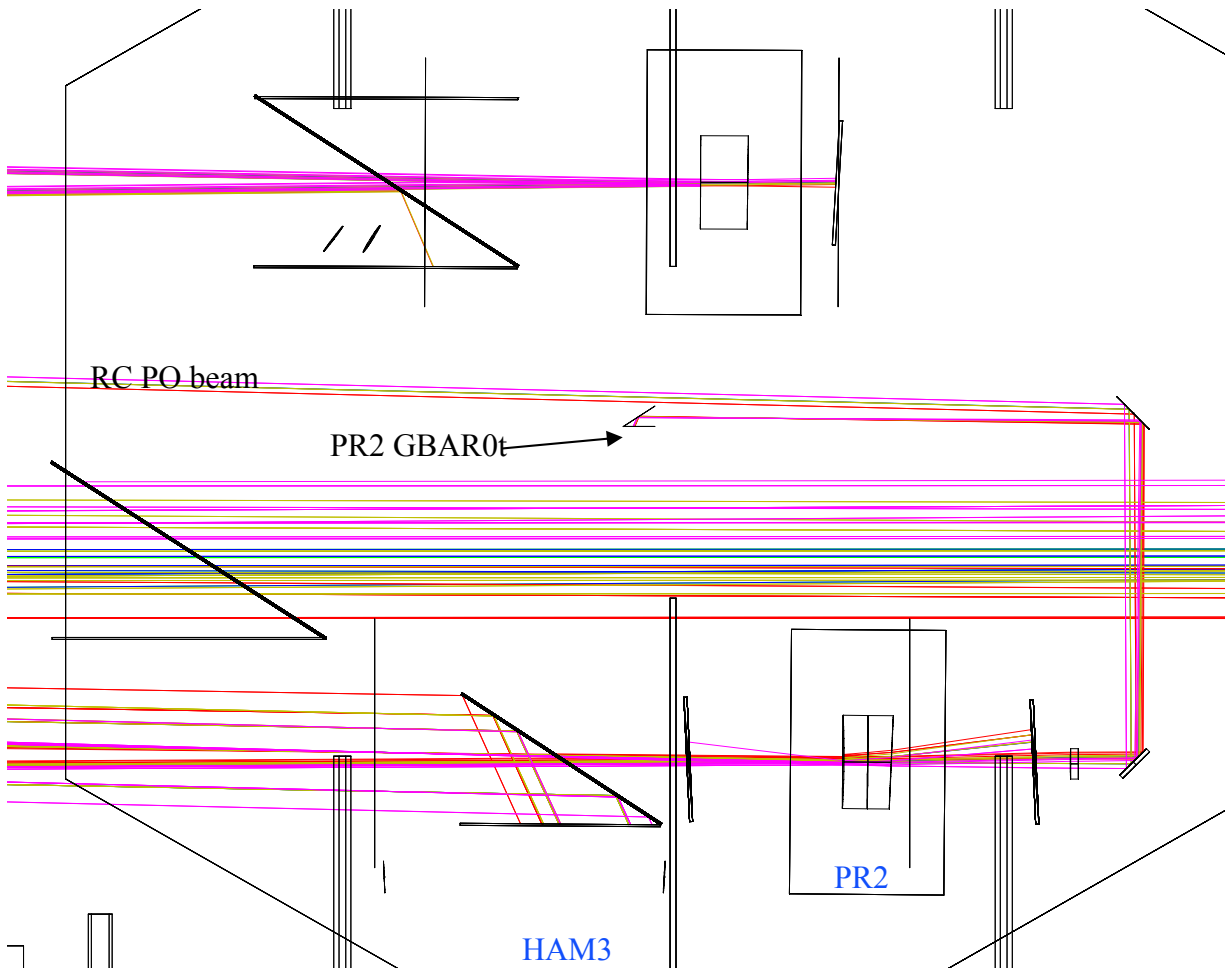


Figure 48: PR2 GBAR0t beam dump

3.2.15.4 PR2 GBAR3

The PR2 AR3 Ghost Beam is the first internal reflection from the HR and AR surfaces that passes out through the AR surface. This beam will scatter from the PR2 AR Plate Beam Dump shown in Figure 9. A fraction of this scattered light will retrace the path and inject noise directly into the recycling cavity.

The recycling cavity beam circulating in the opposite direction undergoes a similar scattering event and injects an additional equal amount of noise into the recycling cavity.

3.2.15.5 PR2 GBHR3

The PR2 HR3 Ghost Beam is the first internal reflection from the AR surface that passes out through the HR surface. This beam will scatter from the PR2 HR Plate Beam Dump shown in Figure 9. A fraction of this scattered light will retrace the path and inject noise directly into the recycling cavity.

The recycling cavity beam circulating in the opposite direction undergoes a similar scattering event and injects an additional equal amount of noise into the recycling cavity.

3.2.15.6 PR2 Plate Beam Dump Surface BRDF and Reflectivity

The PR2 plate Beam Dump will be constructed of AR-coated black glass. The estimated BRDF $< 0.05 \text{ sr}^{-1}$. See T980027-00, Baffling Requirements for the 4K and 2K IFO.

The reflectivity of the PR2 plate Beam Dump is estimated to be $< 0.025\%$.

3.2.15.7 Scattered Light Displacement Noise of Ghost Beams

The total scattered light displacement noise from the PR2 ghost beams is shown in Figure 50.

3.2.16 PR3 Ghost Beams

3.2.16.1 PR3 GBAR0t

The PR3 AR0t Ghost Beam is the transmission of the circulating recycling cavity beam from PR2 direction. This beam will scatter from the PR3 AR Plate Beam Dump shown in Figure 11. A fraction of this scattered light will pass back through PR3 HR surface and inject noise directly into the recycling cavity.

The recycling cavity beam circulating in the opposite direction undergoes a similar scattering event and injects an additional equal amount of noise into the recycling cavity.

3.2.16.2 PR3 GBAR3

The PR3 AR3 Ghost Beam is the first internal reflection from the HR and AR surfaces that passes out through the AR surface. This beam will scatter from the PR3 AR Plate Beam Dump shown in Figure 11. A fraction of this scattered light will retrace the path and inject noise directly into the recycling cavity.

The recycling cavity beam circulating in the opposite direction undergoes a similar scattering event and injects an additional equal amount of noise into the recycling cavity.

3.2.16.3 PR3 GBHR3

The PR3 HR3 Ghost Beam is the first internal reflection from the AR surface that passes out through the HR surface. This beam will be allowed to hit the IO beam tube wall. A fraction of this scattered light will retrace the path and inject noise directly into the recycling cavity.

The recycling cavity beam circulating in the opposite direction undergoes a similar scattering event and injects an additional equal amount of noise into the recycling cavity.

3.2.16.4 PR3 Plate Beam Dump Surface BRDF and Reflectivity

The PR3 plate Beam Dump will be constructed of AR-coated black glass. The estimated BRDF $< 0.05 \text{ sr}^{-1}$. See T980027-00, Baffling Requirements for the 4K and 2K IFO.

The reflectivity of the PR3 plate Beam Dump is estimated to be $< 0.025\%$.

3.2.16.5 Scattered Light Displacement Noise of PR3 Ghost Beams

The scattered light displacement noise from the PR3 AR and PR3 HR ghost beams are shown in Figure 50.

3.2.17 SRM Ghost Beams

3.2.17.1 SRM GBAR3

The SRM AR3 Ghost Beam is the first internal reflection from the HR and AR surfaces that passes out through the AR surface. This beam will scatter from the SRM AR Plate Beam Dump shown in Figure 8. A fraction of this scattered light will retrace the path and inject noise directly into the signal recycling cavity.

The signal recycling cavity beam circulating in the opposite direction undergoes a similar scattering event and injects an additional equal amount of noise into the recycling cavity.

3.2.17.2 SRM GBHR3

The SRM HR3 Ghost Beam is the first internal reflection from the AR surface that passes out through the HR surface. This beam will scatter from the SRM HR Plate Beam Dump shown in Figure 8. A fraction of this scattered light will reflect internally from the AR surface and inject noise directly into the recycling cavity.

The signal recycling cavity beam circulating in the opposite direction undergoes a similar scattering event and injects an additional equal amount of noise into the signal recycling cavity.

3.2.17.3 SRM Plate Beam Dump Surface BRDF and Reflectivity

The SRM plate Beam Dump will be constructed of AR-coated black glass. The estimated BRDF $< 0.05 \text{ sr}^{-1}$. See T980027-00, Baffling Requirements for the 4K and 2K IFO.

The reflectivity of the SRM plate Beam Dump is estimated to be $< 0.025\%$.

3.2.17.4 Scattered Light Displacement Noise of Ghost Beams

The total scattered light displacement noise from the SRM ghost beams is shown in Figure 50.

3.2.18 SR2 Ghost Beams

3.2.18.1 SR2 GBAR0t

The SR2 AR0t Ghost Beam is the leakage through the HR side of the circulating signal recycling cavity beam from the SR3 direction. This beam will scatter from the SR2 GBAR0t Plate Beam Dump shown in Figure 49. A fraction of this scattered light will retrace the path and inject noise directly into the signal recycling cavity.

The signal recycling cavity beam circulating in the opposite direction undergoes a similar scattering event and injects an additional equal amount of noise into the recycling cavity.

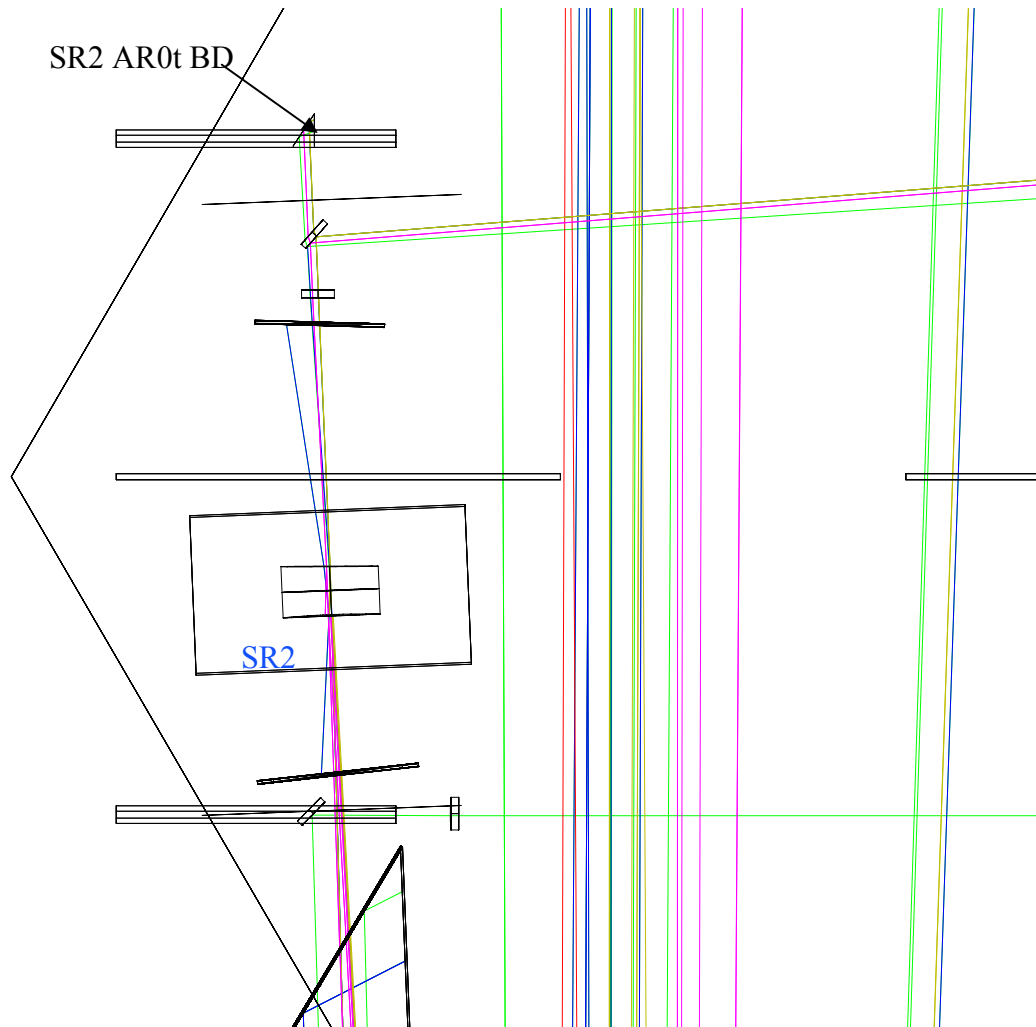


Figure 49: SR2 AR0t beam dump

3.2.18.2 SR2 GBAR3

The SR2 AR3 Ghost Beam is the first internal reflection from the HR and AR surfaces that passes out through the AR surface. This beam will scatter from the SR2 AR Plate Beam Dump shown in Figure 10. A fraction of this scattered light will retrace the path and inject noise directly into the recycling cavity.

The recycling cavity beam circulating in the opposite direction undergoes a similar scattering event and injects an additional equal amount of noise into the recycling cavity.

3.2.18.3 SR2 GBHR3

The SR2 HR3 Ghost Beam is the first internal reflection from the AR surface that passes out through the HR surface. This beam will scatter from the SR2 HR Plate Beam Dump shown in Figure 10. A fraction of this scattered light will retrace the path and inject noise directly into the recycling cavity.

The recycling cavity beam circulating in the opposite direction undergoes a similar scattering event and injects an additional equal amount of noise into the recycling cavity.

3.2.18.4 SR2 Plate Beam Dump Surface BRDF and Reflectivity

The SR2 plate Beam Dump will be constructed of AR-coated black glass. The estimated BRDF $< 0.05 \text{ sr}^{-1}$. See T980027-00, Baffling Requirements for the 4K and 2K IFO.

The reflectivity of the SR2 plate beam dump is estimated to be $< 0.025\%$.

3.2.18.5 Scattered Light Displacement Noise of Ghost Beams

The total scattered light displacement noise from the SR2 ghost beams is shown in Figure 50.

3.2.19 SR3 Ghost Beams

3.2.19.1 SR3 GBAR0t

The SR3 AR0t Ghost Beam is the transmission of the circulating signal recycling cavity beam from the BS direction. This beam will scatter from the SR3 AR Plate Beam Dump shown in Figure 12. A fraction of this scattered light will retrace the path and inject noise directly into the recycling cavity.

The signal recycling cavity beam circulating in the opposite direction undergoes a similar scattering event and injects an additional equal amount of noise into the signal recycling cavity.

3.2.19.2 SR3 GBAR3

The SR3 AR3 Ghost Beam is the first internal reflection from the HR and AR surfaces that passes out through the AR surface. This beam will scatter from the SR3 AR Plate Beam Dump shown in Figure 12. A fraction of this scattered light will retrace the path and inject noise directly into the recycling cavity.

The signal recycling cavity beam circulating in the opposite direction undergoes a similar scattering event and injects an additional equal amount of noise into the signal recycling cavity.

3.2.19.3 SR3 GBHR3

The SR3 HR3 Ghost Beam is the first internal reflection from the AR surface that passes out through the HR surface. This beam will be allowed to hit the OUT beam tube wall. A fraction of this scattered light will retrace the path and inject noise directly into the recycling cavity.

The recycling cavity beam circulating in the opposite direction undergoes a similar scattering event and injects an additional equal amount of noise into the recycling cavity.

3.2.19.4 SR3 Plate Beam Dump Surface BRDF and Reflectivity

The SR3 plate Beam Dump will be constructed of AR-coated black glass. The estimated BRDF $< 0.05 \text{ sr}^{-1}$. See T980027-00, Baffling Requirements for the 4K and 2K IFO.

The reflectivity of the SR3 Beam Dump is estimated to be $< 0.025\%$.

3.2.19.5 Scattered Light Displacement Noise of SR3 Ghost Beams

The scattered light displacement noise from the SR3 AR and SR3 HR ghost beams are shown in Figure 50.

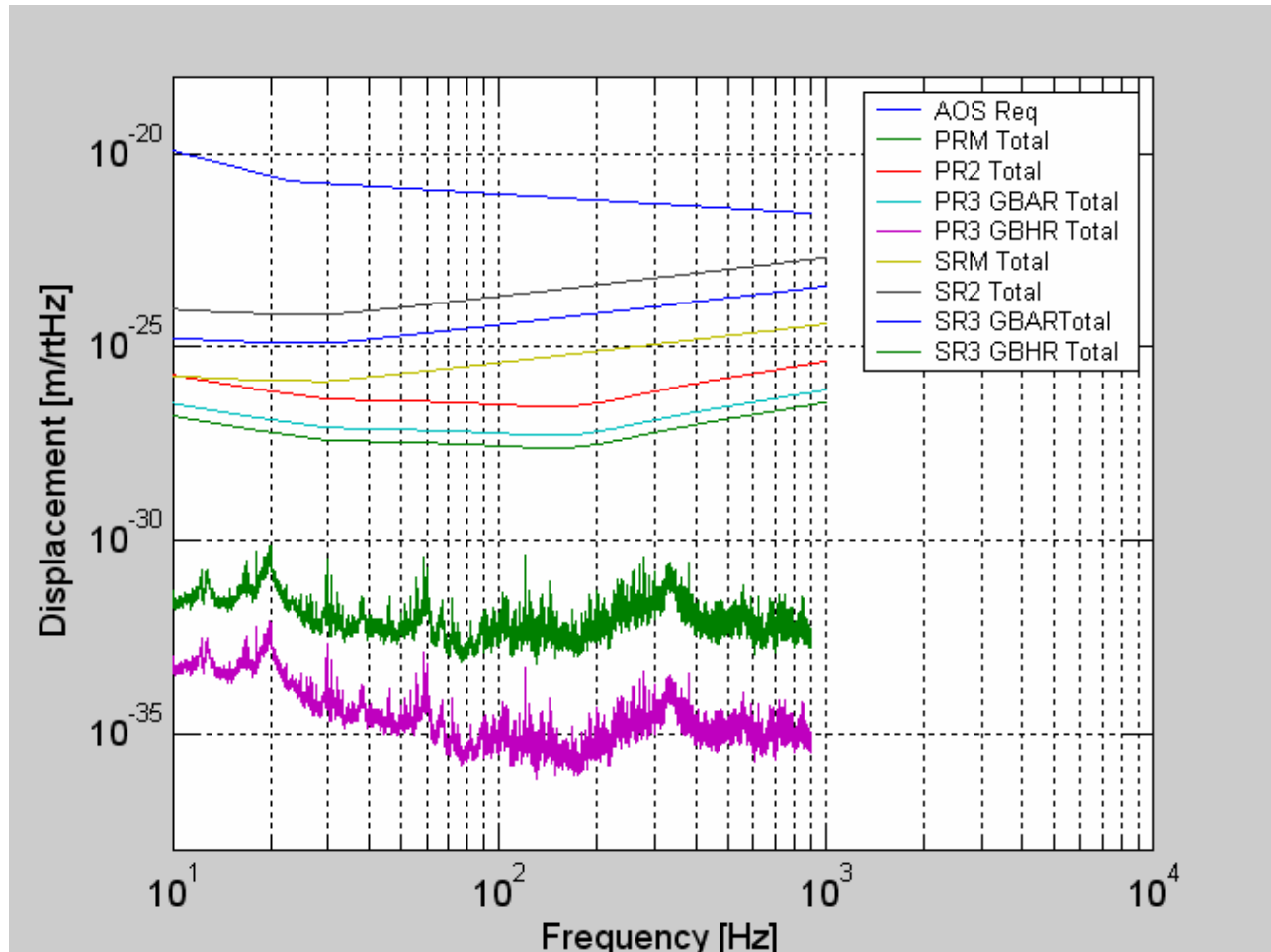


Figure 50: PRM, PR2, PR3, SRM, SR2, SR3, Scattered Light Displacement Noise

3.2.20 ETM Telescope Baffle

The ETM Telescope Baffle is mounted to the front of the ETM telescope, as shown in Figure 51. The baffle blocks all the transmitted light from the ETM except for the central region. The baffle will be constructed of black glass tilted at 10 deg with a high-efficiency AR coating. Most of the light will be absorbed by the baffle. Less than 0.0025 of the light incident on the baffle will be reflected at an angle toward the ETM. The reflected light will bounce back and forth between the ETM and the baffle until it eventually hits the chamber walls.

The ETM Telescope Baffle will be mounted concentrically with the optical axis of the ETM Telescope within 0.5 mm. The aperture in the baffle is the same as the clear aperture of the ETM Telescope (TBD).

This will meet the requirement 4.7 Clear Aperture Requirements.

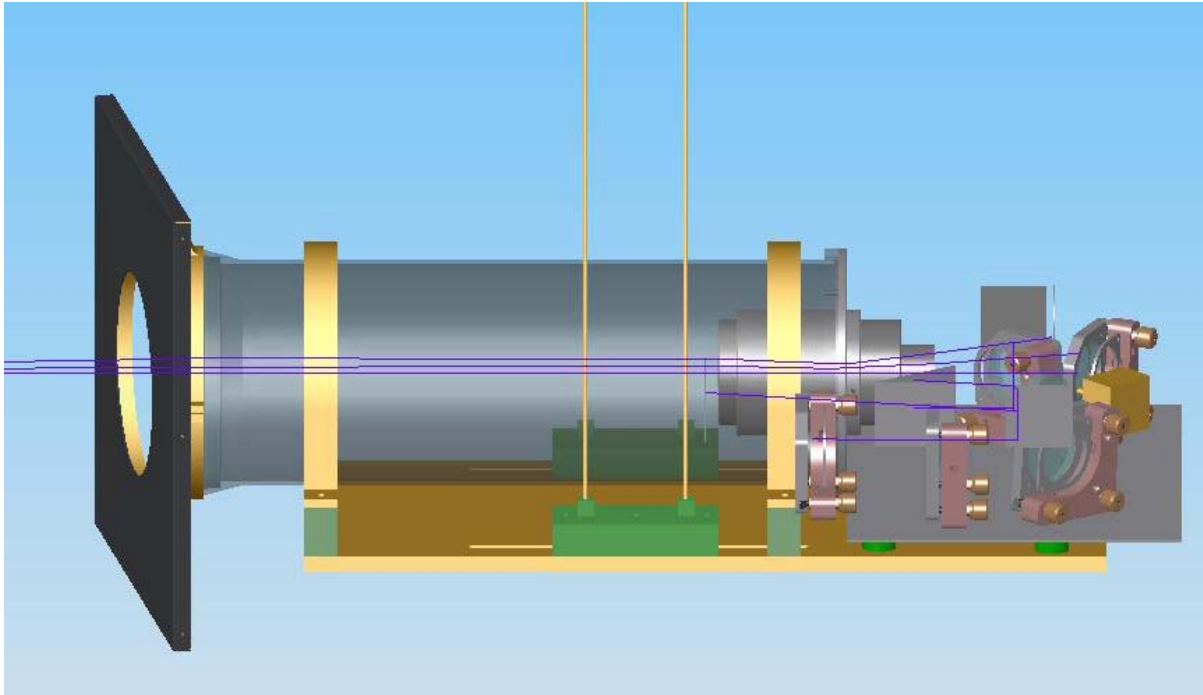


Figure 51: ETM Telescope Baffle

3.2.20.1 ETM Telescope Baffle Motion Requirements

The motion requirement for the ETM Telescope Baffle was determined using the scattered light model. The ETM Telescope Baffle requires no further motion isolation than that provided by the BSC optical table seismic requirement.

3.2.20.2 ETM Telescope Baffle Surface BRDF

The ETM Telescope Baffle will be constructed of oxidized polished stainless steel with the first surface inclined at an incidence angle 56 deg and is estimated to have a BRDF $< 0.05 \text{ sr}^{-1}$. See T980027-00, Baffling Requirements for the 4K and 2K IFO.

3.2.20.3 ETM Telescope Baffle Reflectivity

The light that is not absorbed by the ETM Telescope Baffle will reflect from the baffle surface onto the insides of the vacuum chamber. There, it will scatter from the chamber, reflect again from the ETM Telescope Baffle, and enter the IFO mode.

The requirement for the reflectivity of the ETM Telescope Baffle was calculated using the scattered light model. The reflectivity of the ETM Telescope Baffle must be < 0.07 . This requirement will be met by using oxidized polished stainless steel.

3.2.20.4 Seismic Motion of the ETM Telescope Baffle Scattering Surfaces

The light that reflects from the ETM Telescope Baffle will scatter from the vacuum chamber, which has the seismic motion shown in Figure 25.

3.2.20.5 Scattered Light Displacement Noise of Suspended ETM Telescope Baffle

The scattered light noise from the two ETM Telescope Baffle sources is shown in Figure 52.

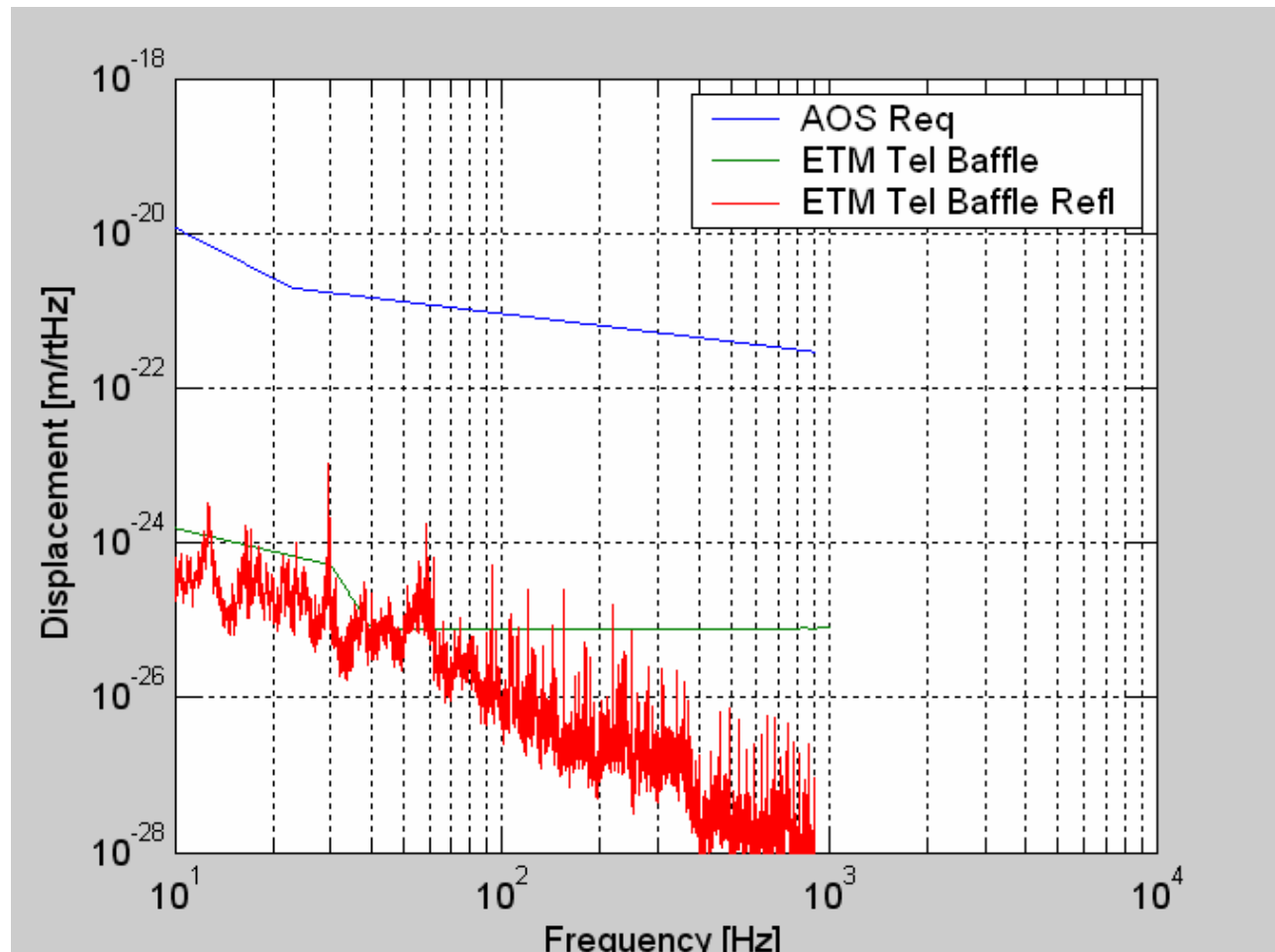


Figure 52: Scattered Light Displacement Noise of ETM Telescope Baffle

3.3 Stray Light Control Physical Characteristics

3.3.1 Faraday Isolator

Table 4: Faraday Isolator Characteristics

Parameter	Value
Configuration	Single Faraday isolator
Wavelength	1064 nm
Clear Aperture	20 mm
Rotator material	TGG crystal
Rotator crystal wedge angle front and back surface	1 deg
Total wavefront distortion	$<1 \lambda @ 633 \text{ nm}$
Rotator transmissivity across clear aperture	$>97 \%$
Input/output polarizer	Calcite, air-spaced Brewster's angle
Polarizer transmissivity per surface	$>99.9 \%$
Half-wave rotation plate	Zero-order quartz

Table 5 : Faraday Isolator Suspension Characteristics

Parameter	Value
Frame	Modified LOS
Suspension	Four wire marionette
Amplitude response	See Figure 17
Damping	Eddy current
Height adjustment	manual
Yaw adjustment	manual
Pitch adjustment	Remote, Pico Motor

3.3.2 Arm Cavity Baffle

Table 6: Arm Cavity Baffle Characteristics

Parameter	Value
Aperture diameter	346 mm
Outer diameter blockage	$>850 \text{ mm}$
Material	Oxidized polished stainless steel
BRDF	$<0.05 \text{ sr}^{-1}$

Parameter	Value
Reflectivity	<0.05
Weight	TBD kg

Table 7: Arm Cavity Baffle Suspension

Parameter	Value
Frame	Aluminum frame
Suspension	Two wire, suspended from HEPI stage “0”
Amplitude response	See Figure 22, Figure 23, Figure 24
Damping	$Q < 1000$

3.3.3 Arm Cavity Baffle Cylinder

Table 8: Arm Cavity Baffle Cylinder Characteristics

Parameter	Value
diameter	1400 mm
Length	500 mm
Material	Oxidized polished stainless steel
BRDF	$<0.05 \text{ sr}^{-1}$
Reflectivity	<0.05
Weight	TBD kg

Table 9: Arm Cavity Baffle Suspension

Parameter	Value
Frame	TBD
Suspension	Two wire, suspended from HEPI stage “0”
Amplitude response	TBD
Damping	$Q < 1000$

3.3.4 Elliptical Baffle

3.3.4.1 ITM Elliptical Baffle

Table 10: ITM Elliptical Baffle Characteristics

Parameter	Value
Suspension	Single pendulum SUS from BSC optical table or HEPI stage “0”
Damping	$Q < 1000$
Aperture major diameter	259 mm
Aperture minor diameter	224 mm
Material	Oxidized polished stainless steel
BRDF	$< 0.05 \text{ sr}^{-1}$
Reflectivity	$< 3\text{E-}5$
Weight	TBD kg

3.3.4.2 PRM Elliptical Baffle

Table 11: PRM Elliptical Baffle Characteristics

Parameter	Value
Suspension	Attached to HAM optics table
Damping	none
Aperture major diameter	259 mm
Aperture minor diameter	224 mm
Material	Oxidized polished stainless steel
BRDF	$< 0.05 \text{ sr}^{-1}$
Reflectivity	$< 3\text{E-}5$
Weight	TBD kg

3.3.5 Manifold Baffle

Table 12: Manifold Baffle

Parameter	Value
Suspension	Mounted to manifold wall
Damping	none
Aperture	769 mm radius
Outer diameter	1860 mm
Material	Oxidized polished stainless steel
BRDF	$<0.05 \text{ sr}^{-1}$
Reflectivity	$<3\text{E-}5$
Weight	TBD kg

3.3.6 Septum Window

Table 13: Septum Window Characteristics

Parameter	Value
Clear aperture diameter	60 mm @ 56 deg incidence
Wavefront distortion	$<0.14 \lambda$ @ 633 nm
BRDF @ 56 deg incidence	$< 5\text{E-}6 \text{ sr}^{-1}$
Reflectivity	$<2.5\text{E-}3$
Diameter of substrate	TBD
Thickness	TBD
Material	Grade A fused silica, super polished
Attachment to Flange	O-ring seal

3.3.7 PR2/SR2 Cavity Beam Dump

Table 14: Cavity Beam Dump Characteristics

Parameter	Value
Suspension	Direct to HAM table
Damping	none
Aperture	TBD
Material	Oxidized polished stainless steel

Parameter	Value
BRDF	<0.05 sr ⁻¹
Reflectivity	<3E-5
Weight	TBD kg

3.3.8 Cryopump Baffle

Table 15: Cryopump Baffle Characteristics

Parameter	Value
Location	Corner Station-- x arm, y arm End Station-- x arm, y arm
Suspension	Single pendulum
Aperture diameter	769 mm
Outer diameter	conical
Material	Oxidized polished stainless steel
BRDF	<0.05 sr ⁻¹
Reflectivity	<3E-5
Weight	TBD

3.3.9 ETM Telescope Baffle

Table 16: ETM Telescope Baffle Characteristics

Parameter	Value
Aperture diameter	TBD
Outer dimensions	340 mm x 340 mm
Material	Oxidized polished stainless steel
BRDF	<0.05 sr ⁻¹
Reflectivity	<0.07
Weight	TBD

3.4 Stray Light Control Interface Definitions

3.4.1 Interfaces to other LIGO detector subsystems

3.4.1.1 Mechanical Interfaces

The beam dumps will attach to the optical tables or be suspended from the HEPI stage “0” in the HAM and BSC chambers, without interfering with the COC mirror structures. Earthquake stops will attach to the chamber wall.

The ITM Elliptical Baffle will hang from the BSC optics table or from the HEPI stage “0” and will have earthquake stops attached to the chamber wall.

The PRM Elliptical Baffle will mount directly to the HAM optical table.

The Arm Cavity Baffles will hang from the ITM and ETM HEPI stage “0” and will have earthquake stops attached to the chamber wall.

The Cryopump Baffle will be suspended from a mounting ring that is held in position inside the manifold piece by means of compressive forces.

The Manifold Baffle will be held in position inside the manifold by means of compressive forces.

3.4.1.2 Electrical Interfaces

3.4.1.2.1 Suspended Baffles and Beam Dumps

All the suspended baffles and beam dumps are passively damped and will require no electrical interfaces.

3.4.1.2.2 Faraday Isolator

The Faraday Isolator will be suspended from a modified LOS, and appropriate electronic control signals to the Pico Motor will be used for pitch steering.

3.4.1.3 Optical Interfaces

The Cavity Beam Dumps will intercept the ghost beams while maintaining adequate clearance from the main recycling cavity beams.

The PRM elliptical baffle will vignette the main beam incident onto the BS from the PRM direction to an elliptical cross section as described in 3.2.6.2.5.

The ITM elliptical baffle will vignette the main beam incident onto the BS from the ITM direction to an elliptical cross section as described in 3.2.6.1.6.

3.4.1.4 Stay Clear Zone

3.4.1.4.1 Arm Cavity Baffle

The aperture of the Arm Cavity Baffle will be 346 mm, which is larger than the diameter of the ITM and ETM COC. The aperture will be concentric with the COC within 4 mm.

3.4.1.4.2 ITMX, ITMY, and BS Beam Dump

The Cavity Beam Dumps will have a stay clear zone of >25 mm from the elliptical edges of the main recycling cavity beam.

3.4.1.4.3 Cryopump Baffle

The Cryopump Baffle will be concentric to the spool piece diameter within 4 mm. The clearance between the 1 ppm edge of the main beam and the centered Cryopump Baffle aperture will be > 7 mm.

3.4.1.4.4 ETM Telescope Baffle

The clear aperture diameter of the ETM Telescope Baffle is TBD mm, which is the same as the clear aperture of the ETM telescope. The ETM Telescope Baffle will be concentric with the entrance aperture of the ETM telescope to within 0.5 mm.

3.4.1.4.5 Elliptical Baffle

The Elliptical Baffles will be concentric with the centerline of the IFO main beam within 4 mm.

3.4.2 Interfaces external to LIGO detector subsystems

There are no interfaces external to the LIGO detector.

3.5 Stray Light Control Reliability

All Stray Light Control baffles and beam dumps are passive and are expected to have 100% availability. The MTBF is expected to be equal to the life of the IFO.

The Faraday Isolator will be suspended by a modified LOS. The typical MTBF of an LOS will apply **TBD**.

3.6 Stray Light Control Maintainability

The following components are susceptible to failure:

- 1) Pico Motor. Both the Faraday Isolator suspension and the ETM Telescope suspension use Pico Motors for initial alignment.

If this component fails, the failure will be ignored until a major realignment of the beam path requires that the ETM Telescope and the Faraday Isolator be realigned. At which time, an incursion into the vacuum chamber will be required.

3.7 Stray Light Control Environmental Conditions

3.7.1.1.1.1 Natural Environment

3.7.1.1.1.1.1 Temperature and Humidity

The SLC assemblies are designed to operate in the high vacuum environment of the IFO and in the controlled LVEA environment during installation.

Table 17 Environmental Performance Characteristics

Operating	Non-operating (storage)	Transport
+20C to +25C, 20-70% RH, non- condensing	0C to +60C, 10-90% RH, non-condensing	0C to +60C, 10-90% RH, non- condensing

3.7.1.1.1.1.2 Atmospheric Pressure

The Brewster's window will function with a differential pressure of 1 atmosphere under normal atmospheric pressure conditions.

3.7.1.1.1.1.3 Seismic Disturbance

The suspended SLC assemblies and the assemblies mounted to the vacuum chambers will withstand ground seismic disturbances.

3.7.1.1.1.2 Induced Environment

3.7.1.1.1.2.1 Electromagnetic Radiation

NA

3.7.1.1.1.2.2 Acoustic

NA

3.7.1.1.1.2.3 Mechanical Vibration

NA

3.8 Stray Light Control Transportability

All items will be transportable by commercial carrier without degradation in performance. As necessary, provisions will be made for measuring and controlling environmental conditions (temperature and accelerations) during transport and handling. Special shipping containers, shipping and handling mechanical restraints, and shock isolation will be utilized to prevent damage. All containers will be movable for forklift. All items over 100 lbs. that must be moved into place within LIGO buildings will have appropriate lifting eyes and mechanical strength to be lifted by cranes.

4 Stray Light Control Design and Construction

The design and construction of the Stray Light Control subsystem allow adequate cleaning, either on site or at an appropriate outside vendor, and will fit inside the vacuum baking ovens on site.

4.1.1.1 Materials and Processes

The materials and processes used in the fabrication of the Stray Light Control subsystem will be compatible with the LIGO approved materials list.

Metal components will have quality finishes on all surfaces, suitable for vacuum finishes. Aluminum components used in the vacuum will not have anodized surfaces.

4.1.1.1.1 Materials

A list of currently approved materials for use inside the LIGO vacuum envelope can be found in LIGO Vacuum Compatible Materials List (LIGO-E960022). All fabricated metal components exposed to vacuum will be made from stainless steel, copper, or aluminum. Other metals are subject to LIGO approval. Pre-baked viton (or fluorel) may be used subject to LIGO approval. All materials used inside the vacuum chamber will comply with LIGO Vacuum Compatibility, Cleaning Methods and Procedures (LIGO-E960022-00-D).

The only lubricating films permitted within the vacuum are dry plating of vacuum compatible materials such as silver and gold.

4.1.1.1.2 Processes

4.1.1.1.2.1 Cleaning

All materials used inside the vacuum chambers will be cleaned in accordance LIGO-E960022-00-D or LIGO-E000007-00, and Specification Guidance for Seismic Component Cleaning, Baking, and Shipping Preparation (LIGO-L970061-00-D). To facilitate final cleaning procedures, parts will be cleaned after any processes that result in visible contamination from dust, sand or hydrocarbon films.

Materials will be joined in such a way as to facilitate cleaning and vacuum preparation procedures; i.e. internal volumes will be provided with adequate openings to allow for wetting, agitation and draining of cleaning fluids and for subsequent drying.

4.1.1.1.3 Component Naming

All components will be identified using the LIGO Naming Convention (LIGO-E950111-A-E). This will include identification (part or drawing number, revision number, serial number) physically stamped on all components, in all drawings and in all related documentation.

4.1.1.2 Stray Light Control Workmanship

All components will be manufactured according to good commercial practice.

4.1.1.3 Stray Light Control Interchangeability

Common elements with ordinary dimensional tolerances will be interchangeable.

4.1.1.4 Stray Light Control Safety

This item will meet all applicable NSF and other Federal safety regulations, plus those applicable State, Local and LIGO safety requirements. A hazard/risk analysis will be conducted in accordance with guidelines set forth in the LIGO Project System Safety Management Plan LIGO-M950046-F, section 3.3.2.

4.1.1.5 Stray Light Control Human Engineering

NA

4.1.2 Stray Light Control Assembly and Maintenance

Assembly fixtures and installation procedures will be developed in conjunction with the Stray Light Control hardware design. These will include (but not be limited to) fixtures and procedures for:

- installation and assembly of beam dumps and baffles into the vacuum
- assembly of the in vacuum components in a clean room (class 100) environment

4.1.3 Stray Light Control Documentation

The documentation will consist of working drawings, assembly drawings, and alignment procedures

4.1.3.1 Stray Light Control Specifications

Specifications for the purchase of specialized components and assemblies such as Faraday isolator, optical mirrors, windows, and lenses will be developed.

4.1.3.2 Stray Light Control Design Documents

The following documents will be produced:

- LIGO Stray Light Control Preliminary Design Document (including supporting technical design and analysis documentation)
- LIGO Stray Light Control Final Design Document (including supporting technical design and analysis documentation)
- LIGO Stray Light Control Installation Procedures

4.1.3.3 Stray Light Control Engineering Drawings and Associated Lists

A complete set of drawings suitable for fabrication will be provided along with Bill of Material (BOM) and drawing tree lists. The drawings will comply with LIGO standard formats and will be provided in electronic format. All documents will use the LIGO drawing numbering system, be drawn using LIGO Drawing Preparation Standards, etc.

4.1.3.4 Stray Light Control Technical Manuals and Procedures

4.1.3.4.1 Procedures

Procedures will be provided for the installation, and final alignment of the Stray Light Control elements.

4.1.3.5 Stray Light Control Documentation Numbering

All documents will be numbered and identified in accordance with the LIGO documentation control numbering system LIGO document TBD

4.1.3.6 Stray Light Control Test Plans and Procedures

All test plans and procedures will be developed in accordance with the LIGO Test Plan Guidelines, LIGO document TBD.

4.1.4 Stray Light Control Logistics

The design will include a list of all recommended spare parts and special test equipment required.

4.1.5 Stray Light Control Precedence

The relative importance of the positioning of the beam dumps and baffles will be as follows:

- 1) satisfy the stay clear requirements
- 2) align the baffles and beam dumps with the centers of the ghost beams

4.1.6 Stray Light Control Qualification

N/A

5 Quality Assurance Provisions

This section includes all of the examinations and tests to be performed in order to ascertain that the fabricated SLC elements conform to the requirements in section 3.

5.1 General

5.1.1 Responsibility for Tests

AOS will conduct tests to verify the as-delivered performance specifications of the sub-system.

5.1.2 Special Tests

5.1.2.1 Engineering Tests

5.1.2.1.1 Witness Sample Scattering Tests of Baffle and Beam Dump Material

5.1.2.1.2 ETM Telescope Performance Test

5.1.2.1.3 ETM Telescope Suspension Damping Test

5.1.2.1.4 Faraday Isolator Performance Test

5.1.2.1.5 Faraday Isolator Suspension Damping Test

5.1.2.1.6 TBD

5.1.2.2 Reliability Testing

No reliability testing is anticipated.

5.1.3 Configuration Management

Configuration control of specifications and designs will be in accordance with the LIGO Detector Implementation Plan.

5.2 Quality conformance inspections

Design and performance requirements identified in this specification and referenced specifications will be verified by inspection, analysis, demonstration, similarity, test or a combination thereof per the Verification Matrix, Appendix 1 (TBD). Verification method selection shall be specified by individual specifications, and documented by appropriate test and evaluation plans and procedures. Verification of compliance to the requirements of this and subsequent specifications will be accomplished by the following methods or combination of methods:

5.2.1 Inspections

Manufactured parts with LIGO identification numbers or marks will be inspected to determine conformity with the procurement specification.

Witness samples will be acceptable proof of the properties of HR and AR coatings applied to the optical surfaces.

5.2.2 Demonstration

The required attenuation and transmissivity characteristics of the assembled Faraday isolator will be demonstrated before installation.

The resonance and damping characteristics of the suspended beam dumps and baffles will be demonstrated before installation.

5.2.3 Test

Appropriate tests will be implemented to verify the specifications of the purchased components.

TBD

6 Preparation for Delivery

Packaging and marking of equipment for delivery will be in accordance with the Packaging and Marking procedures specified herein.

6.1 Preparation

- Vacuum preparation procedures as outlined in E960022-B LIGO Vacuum Compatibility, Cleaning Methods and Qualification Procedures will be followed for all components intended for use in vacuum. After wrapping vacuum parts as specified in this document, an additional, protective outer wrapping and provisions for lifting shall be provided.
- Electronic components will be wrapped according to standard procedures for such parts.

6.2 Packaging

Procedures for packaging will ensure cleaning, drying, and preservation methods adequate to prevent deterioration, appropriate protective wrapping, adequate package cushioning, and proper containers. Proper protection will be provided for shipping loads and environmental stress during transportation, hauling and storage. The shipping crates used for large items will use for guidance military specification MIL-C-104B, Crates, Wood; Lumber and Plywood Sheathed, Nailed and Bolted. Passive shock witness gauges will accompany the crates during all transits.

For the viewports, the shipping preparation will include double bagging with Ameristat 1.5TM plastic film (heat sealed seams as practical, with the exception of the inner bag, or tied off, or taped with care taken to insure that the tape does not touch the cleaned part). The bag will be purged with dry nitrogen before sealing.

6.3 Marking

Appropriate identification of the product, both on packages and shipping containers; all markings necessary for delivery and for storage, if applicable; all markings required by regulations, statutes, and common carriers; and all markings necessary for safety and safe delivery will be provided.

Identification of the material will be maintained through all manufacturing processes. Each component will be uniquely identified. The identification will enable the complete history of each component to be maintained (in association with Documentation “travelers”). A record for the optical lever support structures will indicate all weld repairs and fabrication abnormalities.

The specification for marking will state that marking fluids, die stamps and/or electro-etching is not permitted. A vibratory tool with a minimum tip radius of 0.005" is acceptable for marking on surfaces that are not hidden from view. Engraving and stamping are also permitted.

7 Appendix A—Scattered Light Noise Theory

7.1 Scattered Light Requirement

A DARM signal is obtained when the differential arm length is modulated as a result of a gravity wave strain. The DARM signal was calculated in reference T060073-00 Transfer Functions of Injected Noise, and is defined by the following expression:

$$V_{\text{signal}} := \text{DARM} \cdot L \cdot h_{\text{SRD}} \cdot \sqrt{P_0}$$

Where L is the arm length, h_{SRD} is the minimum SRD gravity wave strain spectral density requirement, P_0 is the input laser power into the IFO, and DARM is the signal transfer function.

In a similar manner, an apparent signal (scattered light noise) occurs when a scattered light field with a phase shift is injected into the IFO at some particular location, e.g. through the back of the ETM mirror. The scattered light noise is defined by the following expression:

$$V_{\text{noise}} := \text{SNXXX} \cdot \delta_{\text{SN}} \cdot \sqrt{P_{\text{SNi}}}$$

P_{SNi} is the scattered light power injected into the IFO mode, δ_{SN} is the phase shift of the injected field, and SNXXX is the noise transfer function for that particular injection location.

The phase shift spectral density of the injected field due to the motion of the scattering surface is given by

$$\delta_{\text{SNi}} := \frac{4 \cdot \pi \cdot x_s}{\lambda}$$

where x_s is the spectral density of the longitudinal motion of the scattering surface.

In general, the different scattering sources are not coherent and must be added in quadrature. The requirement for total scattered light displacement noise can be stated with the following inequality:

$$\sqrt{\sum_{i=1}^n \left(\frac{\text{SNXXX}}{\text{DARM}} \cdot \frac{4 \cdot \pi \cdot x_s}{\lambda} \cdot \sqrt{\frac{P_{\text{SNi}}}{P_0}} \right)^2} < \frac{1}{10} \cdot L \cdot h_{\text{SRD}}$$

The SNXXX/DARM scattered light noise transfer functions for various injection locations within the IFO were calculated by Hiro (T060073-00 Transfer Functions of Injected Noise) and are shown in Figure 53: Scattered Light Noise Transfer Functions.

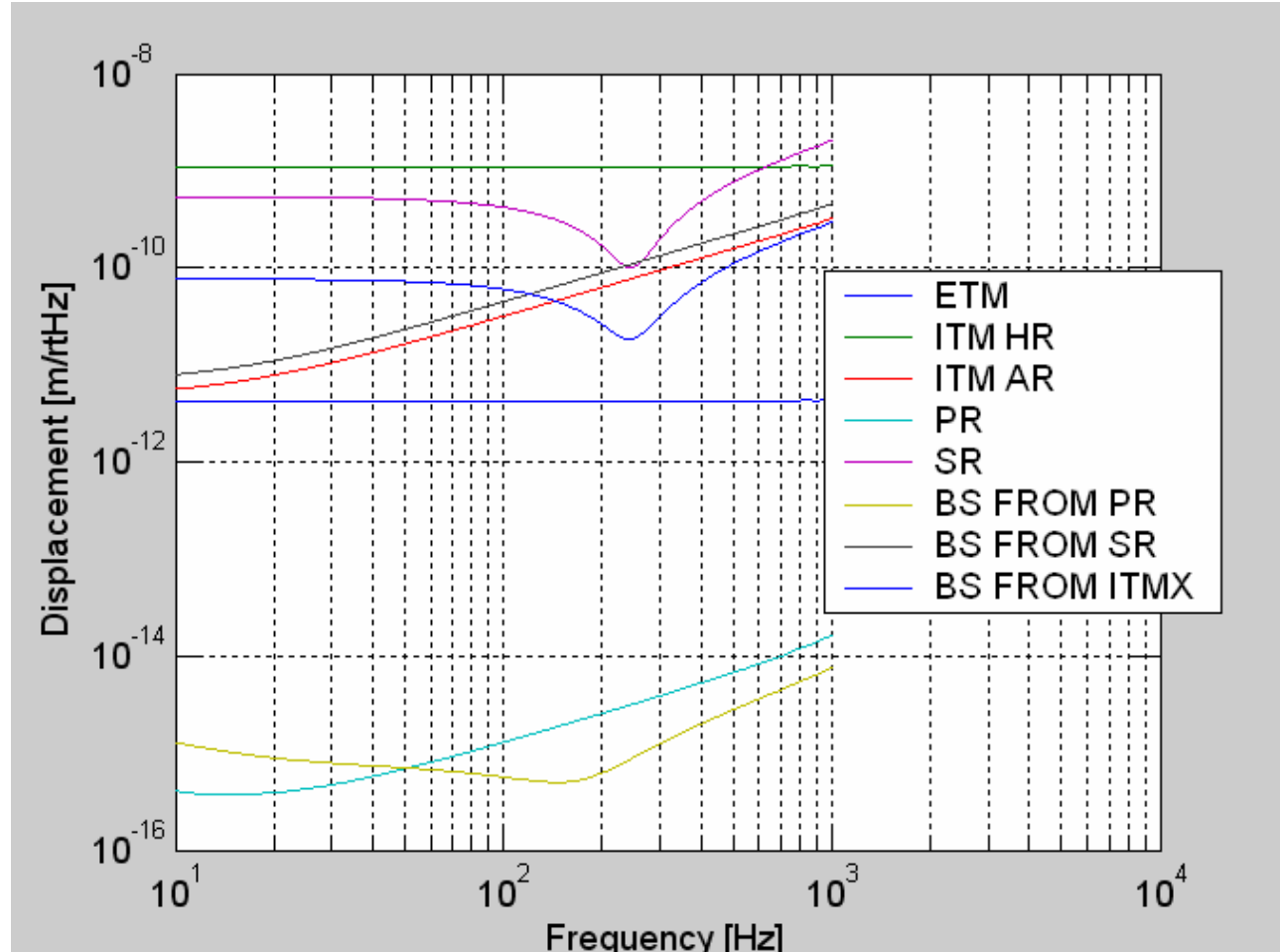


Figure 53: Scattered Light Noise Transfer Functions

7.2 Scattered Power into the IFO

The light power scattered into the interferometer from the i th source is calculated as follows:

$$P_{\text{SN}i} := P_{\text{in}} \cdot \text{BRDF} \cdot \Delta\Omega \cdot \frac{w_{\text{IFO}}^2}{w_{\text{SN}}^2} \cdot T$$

Where P_{in} is the power incident on the scattering surface, BRDF is the fraction of incident light that is scattered per unit solid angle, $\Delta\Omega$ is the solid angle subtended by the mode inside the IFO arm, w_{IFO} is the beam waist of the mode inside the arm, w_{SN} is the beam waist of the beam incident on the scattering surface, and T is the transmissivity of the path from the scattering surface to the injection point in the IFO.

The effective solid angle increases whenever the IFO beam waist has been transformed to a smaller waist by an AOS telescope or some other focusing element in the ISC detection system, because the product of solid angle and beam waist cross-sectional area is proportional to the total radiant

flux, which is an optical invariant. Therefore, as the area of the beam waist decreases the effective solid angle increases proportionally.

7.2.1 Output Faraday Isolator Scatter

The power incident on the Faraday isolator is given by

$$P_{Flin} := P_0 \cdot G_{AS}$$

G_{AS} is the dark port signal ratio.

The light power scattered into the IFO from the five surfaces before the Faraday rotator magnet is given by

$$P_{FIs} := 5 \cdot P_{Flin} \cdot BRDF_{FI} \cdot \Delta\Omega_{IFO} \cdot \frac{w_0^2}{w_{FI}^2}$$

The scattering surface has the seismic motion of the HAM requirement, attenuated by the motion transfer function of the Faraday Isolator requirement.

The scattered light is injected into the SRM mirror, and the appropriate scattered light noise transfer function is 'SRM'. The displacement noise (m/rt Hz) is

$$DN_{faradsifo} := TF_{sr} \cdot \left(\frac{P_{farads}}{P_{psl}} \right)^{0.5} \cdot x_{ham} \cdot 2 \cdot k \cdot faradisolre$$

7.2.2 Arm Cavity Baffle Surface Scatter

The small angle scattered power from the far arm cavity mirror passes through the beam tube to the near arm cavity mirror. The power in the annulus between the cryopump baffle and the ITM (ETM) outside diameter will hit the Arm Cavity Baffle. See Figure 54.

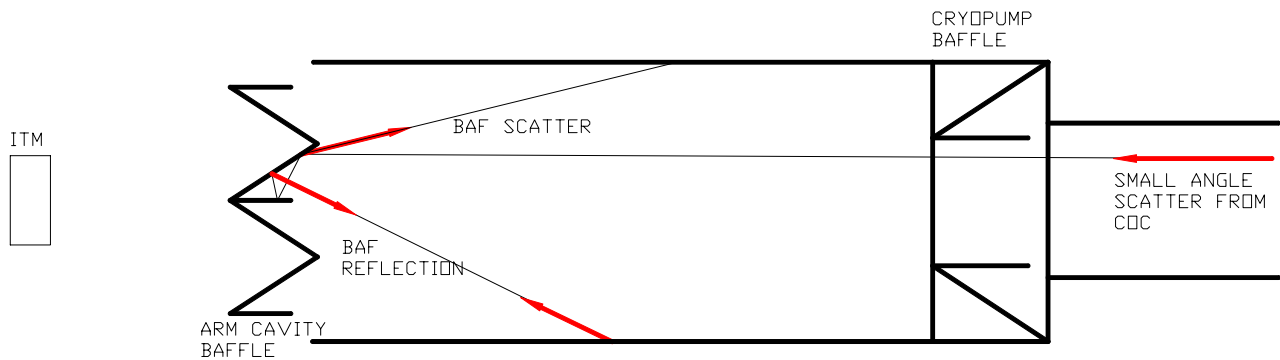


Figure 54: ARM CAVITY BAFFLE SCATTER

The offset between the arm cavity mirror and the beam tube axis will be ignored.

$$P_{acb} := P_a \cdot \int_{\theta_{ac}}^{\theta_{cp}} 2 \cdot \pi \cdot \theta \cdot BRDF_1(\theta) d\theta$$

The half-angle from the beam tube centerline to the AC baffle inner edge is

$$\theta_{ac} := \frac{R_{ac}}{L}$$

The half-angle from the beam tube centerline to the cryopump baffle outer edge is

$$\theta_{cp} := \frac{R_{cp}}{L}$$

P_a is the circulating power in each arm.

The light power scattered from four Arm Cavity Baffles into the mode cross section and re-scattered by the far COC into the IFO mode is given by

$$P_{acbfafs} := \sqrt{4} \cdot P_{acb} \cdot BRDF_{bd} \cdot \frac{\pi \cdot w_{ifo}^2}{L^2} \cdot BRDF_1(30 \cdot 10^{-6}) \cdot \Delta_{ifc}$$

The scattering surface is suspended from the BSC HEPI ring and has the seismic motion of the HEPI requirement, attenuated by the motion transfer function of the Arm Cavity Baffle requirement.

The scattered light is injected into the arm cavity, and the appropriate scattered light noise transfer function is 'ITM_HR'. The displacement noise (m/rt Hz) is

$$DN_{acbf} := TF_{itmhr} \left(\frac{P_{acbfafs}}{P_{psl}} \right)^{0.5} \cdot x_{hepi} \cdot 2 \cdot k \cdot acbatter$$

7.2.3 Arm Cavity Baffle Reflected Light

The power reflected from the Arm Cavity Baffle and incident on the vacuum manifold wall is given by

$$P_{armbafrefl} = P_{acb} \cdot R_{bd}$$

where R_{bd} is the net reflectivity of the baffle.

This light will scatter from the wall, reflect again from the Arm Cavity Baffle toward the far COC, and finally scatter from the COC into the mode of the IFO. The scattered power is given by

$$P_{armbafrefls} := R_{bd} \cdot P_{armbafrefl} \cdot BRDF_{wall} \cdot \frac{\pi \cdot w_{ifo}^2}{L^2} \cdot BRDF_1(30 \cdot 10^{-6}) \cdot \Delta_{ifc}$$

The scattering surface has the seismic motion of the beam tube.

The scattered light is injected into the arm cavity, and the appropriate scattered light noise transfer function is 'ITM_HR'. The displacement noise (m/rt Hz) is

$$DN_{\text{armbafrefls}} = TF_{\text{itmhr}} \left(\frac{P_{\text{armbafrefls}}}{P_{\text{psl}}} \right)^{0.5} \cdot x_{\text{beamtube}} \cdot 2 \cdot k$$

7.2.4 ITM Elliptical Baffle Surface Scatter

See Figure 55. When the IFO arm cavity is on resonance, the power exiting the arm cavity into the recycling cavity through the ITM is exactly twice the power incident on the ITM from the recycling cavity side. The two counter-propagating beams are exactly 180 degrees out of phase and they interfere at the surface of the ITM. The resultant beam, with a power equal to the power recycling cavity arm power, appears to reflect from the ITM back into the power recycling cavity.

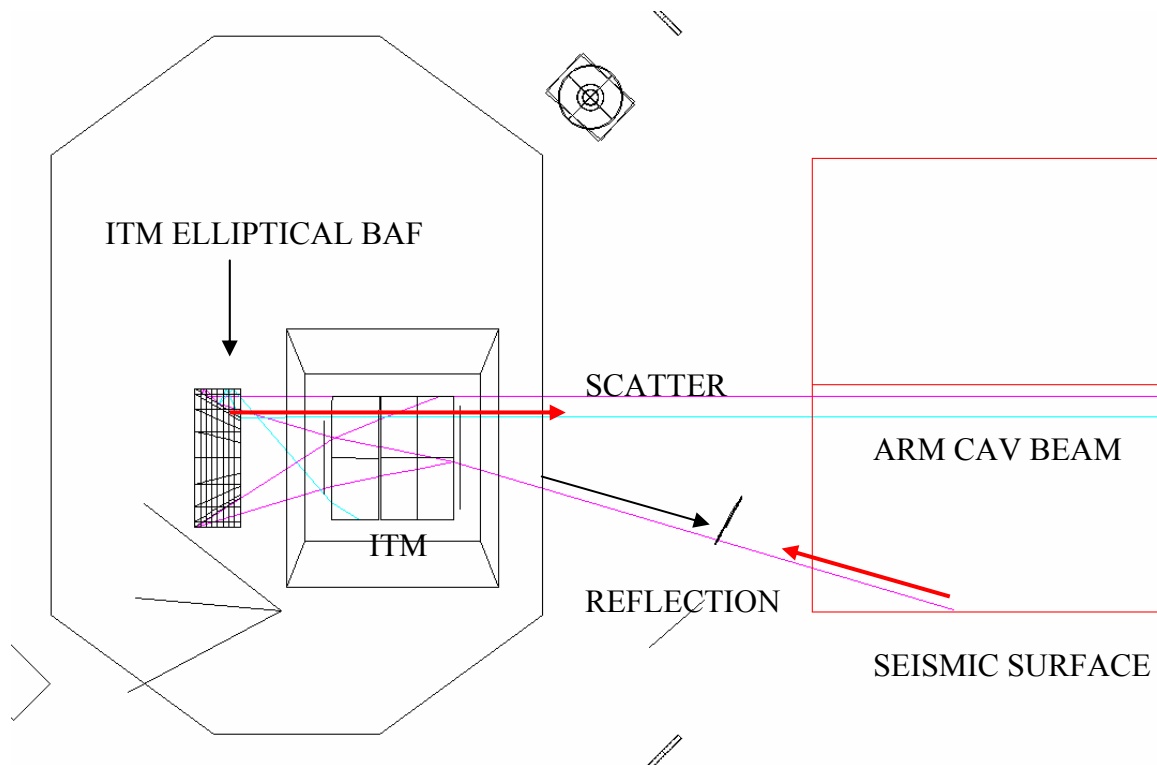


Figure 55: ITM ELLIPTICAL BAFFLE SCATTER AND REFLECTION

However, in the actual LIGO IFO the recycling cavity beam has a truncated Gaussian profile with an elliptical cross section. Beyond the edges of the sharp elliptical boundary, the Gaussian shaped

beam exiting from the arm cavity is not opposed with a Gaussian power recycling cavity beam and will strike the elliptical baffle with twice the irradiance of the power recycling cavity beam.

The Gaussian irradiance parameter, P_{0itm} , of the beam exiting the ITM is twice the irradiance parameter, P_{0rc} , of the recycling cavity beam.

$$P_{0itm} := 2 \cdot P_{0rc}$$

The exitance function from the ITM is given by

$$I_{ITM}(x, y) := 2 \cdot \frac{P_{0itm}}{\pi \cdot w^2} \cdot e^{-2 \cdot \left(\frac{x^2 + y^2}{w^2} \right)}$$

and the irradiance function inside the power recycling cavity arm is given by

$$I_{rc}(x, y) := 2 \cdot \frac{P_{0rc}}{\pi \cdot w^2} \cdot e^{-2 \cdot \left(\frac{x^2 + y^2}{w^2} \right)}$$

The total power exiting from the ITM is

$$P_{itm} := \int_0^R I_{itm}(r) \cdot 2 \cdot \pi \cdot r \, dr$$

$$P_{itm} = 2.1084 \times 10^3$$

The total power from the exiting ITM beam that passes through the elliptical baffle is

$$P_{ell} := 4 \cdot \int_0^b \int_0^{a \cdot \sqrt{1 - \frac{y^2}{b^2}}} I_{ITM}(x, y) \, dx \, dy$$

Then, the power that hits the elliptical baffle from the ITM side is the difference

$$P_{ellbaf} := P_{itm} - P_{ell}$$

The light power scattered from the two Elliptical Baffles and then re-scattered into the IFO mode at the far COC is given by

$$P_{itmellbaf} = \sqrt{2} \cdot T_{itmhr} \cdot P_{itmellbaf} \cdot BRDF_{ellbaf} \frac{\pi \cdot w_{ifo}^2}{L^2} \cdot BRDF_1(30 \cdot 10^{-6}) \cdot \Delta_{ifc}$$

where T_{itmhr} is the transmissivity of the ITM mirror, and the scattering BRDF from the far COC mirror is evaluated at the incidence angle $30E-6$ rad.

The scattering surface is suspended from the BSC HEPI ring and has the seismic motion of the HEPI requirement, attenuated by the motion transfer function of the ITM Elliptical Baffle requirement.

The scattered light is injected into the arm cavity, and the appropriate scattered light noise transfer function is 'ITM_HR'. The displacement noise (m/rt Hz) is

$$DN_{itmellbaf} = TF_{itmhr} \left(\frac{P_{itmellbaf}}{P_{psl}} \right)^{0.5} \cdot x_{hepi} \cdot ellipbafatter2 \cdot k$$

7.2.5 ITM Elliptical Baffle Reflected Light

The power reflected from the ITM Elliptical Baffle and incident on the vacuum manifold wall is given by

$$P_{ellbafRin} = P_{ellbaf} R_{ellbaf}$$

where R_{ellbaf} is the reflectivity of the baffle surface.

The light will scatter from the wall, reflect from the Elliptical Baffle, and transmit through the ITM into the mode of the IFO at the far COC. The scattered power is given by

$$P_{elleRs} = P_{ellbafRin} \cdot BRDF_{VAC} \cdot R_{ellbaf} \cdot T_{itm} \frac{\pi \cdot w_0^2}{L^2}$$

The scattering surface has the seismic motion of the BSC chamber wall.

The scattered light is injected into the arm cavity, and the appropriate scattered light noise transfer function is 'ITM_HR'. The displacement noise (m/rt Hz) is

$$DN_{itmellbafrefl} = TF_{itmhr} \left(\frac{P_{itmellbafrefl}}{P_{psl}} \right)^{0.5} \cdot x_{bscchamber} \cdot 2 \cdot k$$

7.2.6 PRM Elliptical Baffle

The prompt Gaussian beam that enters the power recycling cavity through the PRM HR surface is expanded by the PRM telescope (PR2 and PR3) and is vignettted into an elliptical cross section by the PRM Elliptical Baffle.

The expanded Gaussian irradiance functions at the PRM Elliptical Baffle, given in terms of radius and Cartesian coordinates, are

$$I_{\text{psl}}(r) := 2 \cdot \frac{T_{\text{prmhr}} P_{\text{psl}}}{\pi \cdot w^2} \cdot e^{-2 \cdot \left(\frac{r^2}{w^2} \right)}$$

$$I_{\text{psl}}(x, y) := 2 \cdot \frac{T_{\text{prmhr}} P_{\text{psl}}}{\pi \cdot w^2} \cdot e^{-2 \cdot \left(\frac{x^2 + y^2}{w^2} \right)}$$

The total power passing through the PR3 mirror is

$$P_{\text{pr3}} := \int_0^{r_{\text{pr3}}} I_{\text{psl}}(r) \cdot 2 \cdot \pi \cdot r \cdot dr$$

The total power passing through the PRM Elliptical Baffle is

$$P_{\text{pr3rc}} := 4 \cdot \int_0^b \int_0^{a \cdot \sqrt{1 - \frac{y^2}{b^2}}} I_{\text{psl}}(x, y) \, dx \, dy$$

The power hitting the baffle is the difference

$$P_{\text{prmellbaf}} := P_{\text{pr3}} - P_{\text{pr3rc}}$$

This power scatters back through the PRM telescope onto the PRM HR surface, where it re-scatters into the de-magnified mode volume of the recycling cavity. The scattering from the PRM will be evaluated at the maximum scattering angle at the surface of the PRM

$$\theta_{\text{prmellbafs}} := m \cdot \frac{w_{\text{ifo}}}{L}$$

where m is the magnification of the PRM telescope.

The scattered power into the IFO is given by

$$P_{\text{prmellbafs}} := P_{\text{prmellbaf}} \cdot \text{BRDF}_{\text{ellbaf}} \cdot \frac{\pi \cdot w_{\text{rc}}^2}{L_{\text{prm2}}} \cdot \text{BRDF}_1 \left(\theta_{\text{prmellbafs}} \right) \cdot \frac{w_{\text{ifo}}^2}{w_{\text{rc}}^2} \cdot \Delta_{\text{ifc}}$$

where L_{prm2} is the distance from the recycling cavity beam waist (near PR2) and PRM, w_{rc} is the demagnified beam radius in the power recycling cavity.

The PRM Elliptical Baffle scattering surface is mounted to the HAM table and has the seismic motion of the HAM requirement.

The scattered light is injected into the BS from the PR side, and the appropriate scattered light noise transfer function is 'BS_from_PR'. The displacement noise (m/rt Hz) is

$$DN_{\text{prmeffbaf}} = TF_{\text{prbs}} \left(\frac{P_{\text{prmeffbafs}}}{P_{\text{psl}}} \right)^{0.5} \cdot x_{\text{ham}} \cdot 2 \cdot k$$

7.2.7 ITM (ETM) Wide-Angle Scatter

Point defects in the coatings and dust particles on the surface of the arm cavity mirrors will cause wide-angle scattered light. The scattering function appears to be Lambertian. See T070089-02 Wide-angle Scatter from LIGO Arm Cavities.

The wide-angle scattered light will predominately hit the back of the Arm Cavity Baffle and the Cylindrical Baffle between the mirror and the Arm Cavity Baffle. Some of the light will pass through the hole in the Arm Cavity Baffle and hit the manifold wall and the manifold baffle. Some of the light will hit the BSC chamber.

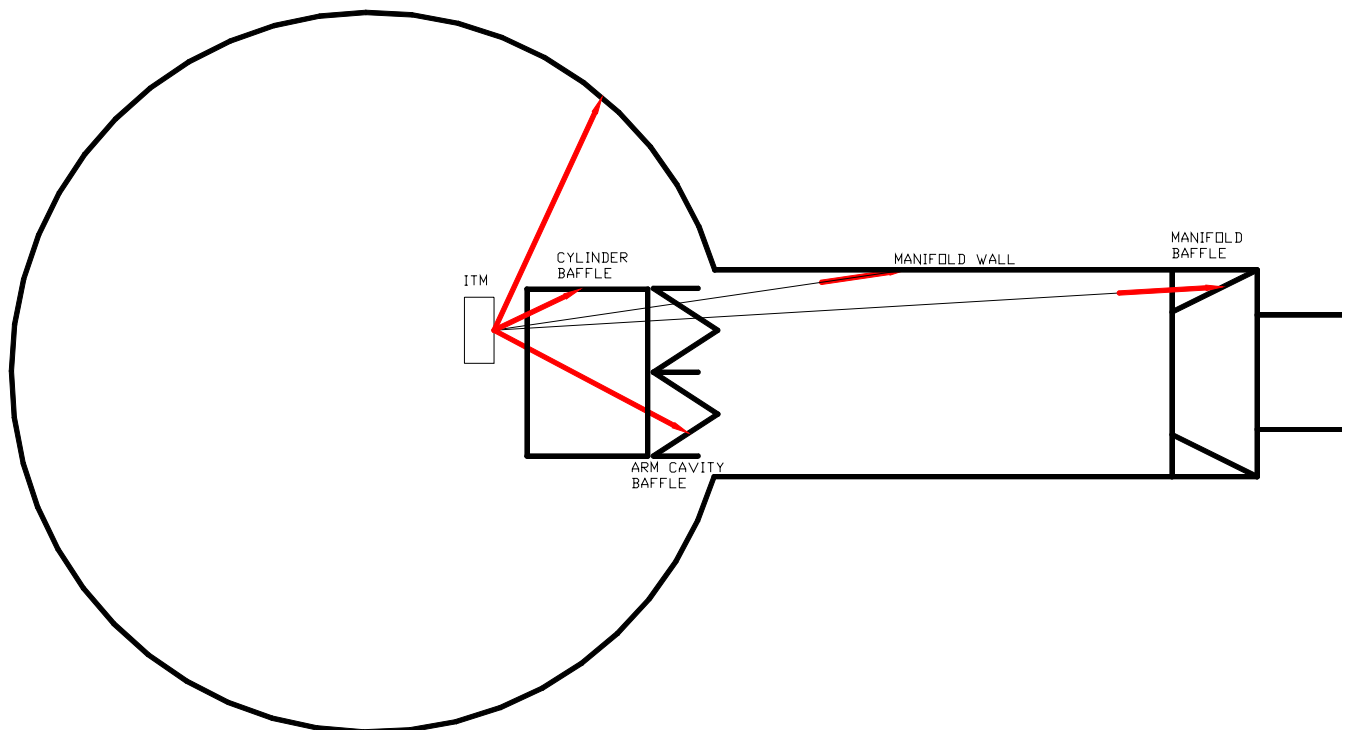


Figure 56: Wide-angle Scatter from ITM (ETM)

7.2.7.1 Scattering from the Back of Arm Cavity Baffle

In the following calculations, the offset of the ITM from the centerline of the arm cavity is ignored. The wide-angle scattered light hitting the back of the Arm Cavity Baffle is given by

$$P_{\text{acbback}}(L_{\text{acb}}, r_{\text{acbo}}) := P_a \cdot \int_{\theta_{\text{acbi}}(L_{\text{acb}})}^{\theta_{\text{acbo}}(L_{\text{acb}}, r_{\text{acbo}})} \frac{\alpha_{\text{ws}} \cdot \cos(\theta)}{\pi} \cdot 2 \cdot \pi \cdot \sin(\theta) \, d\theta$$

Where, the half-angle from the ITM centerline to the Arm Cavity Baffle outer edge is

$$\theta_{\text{acbo}}(L_{\text{acb}}, r_{\text{acbo}}) := \text{atan}\left(\frac{r_{\text{acbo}}}{L_{\text{acb}}}\right)$$

The half-angle from the ITM centerline to the Arm Cavity Baffle inner edge is

$$\theta_{\text{acbi}}(L_{\text{acb}}) := \text{atan}\left(\frac{r_{\text{acbi}}}{L_{\text{acb}}}\right)$$

and L_{acb} is the distance from the ITM to the Arm Cavity Baffle.

The power scattered onto the back of the Arm Cavity Baffle is

$$P_{\text{acbbackifo}}(L_{\text{acb}}, r_{\text{acbo}}) := \sqrt{4} \cdot P_a \cdot \left(C_2(L_{\text{acb}}, r_{\text{acbo}}) \cdot \alpha_{\text{ws}}^2 \cdot \frac{\lambda^2}{L_{\text{acb}}^2} \cdot \text{BRDF}_{\text{wall}} \right)$$

Where the geometric function is

$$C_2(L_{\text{acb}}, r_{\text{acbo}}) := \frac{2}{\pi} \cdot \int_{\theta_{\text{acbi}}(L_{\text{acb}})}^{\theta_{\text{acbo}}(L_{\text{acb}}, r_{\text{acbo}})} \cos(\theta)^5 \cdot \sin(\theta) \, d\theta$$

7.2.7.2 Scattering from the Cylindrical Baffle

The wide-angle scattered light hitting the inside of the Cylinder Baffle is

$$P_{\text{accyl}}(L_{\text{acb}}, r_{\text{acbo}}, L_{\text{cyl}}) := P_a \cdot \int_{\theta_{\text{acbo}}(L_{\text{acb}}, r_{\text{acbo}})}^{\theta_{\text{accyl}}(L_{\text{acb}}, r_{\text{acbo}}, L_{\text{cyl}})} \frac{\alpha_{\text{ws}} \cdot \cos(\theta)}{\pi} \cdot 2 \cdot \pi \cdot \sin(\theta) \, d\theta$$

Where the half-angle from the ITM centerline to the Cylinder Baffle is

$$\theta_{\text{accyl}}(L_{\text{acb}}, r_{\text{acbo}}, L_{\text{cyl}}) := \text{atan}\left(\frac{r_{\text{acbo}}}{L_{\text{acb}} - L_{\text{cyl}}}\right)$$

and L_{acb} is the length of the Arm Cavity Baffle, and L_{cyl} is the length of the Cylindrical Baffle.

The power scattered into the IFO mode is given by

$$P_{\text{wsaccylifo}}(L_{\text{acb}}, r_{\text{acbo}}, L_{\text{cyl}}) := \sqrt{4} \cdot P_{\text{a}} \cdot \left(C_4(L_{\text{acb}}, r_{\text{acbo}}, L_{\text{cyl}}) \cdot \alpha_{\text{ws}}^2 \cdot \frac{\lambda^2}{r_{\text{acbo}}^2} \cdot \text{BRDF}_{\text{cyl}} \right)$$

Where the geometric function is

$$C_4(L_{\text{acb}}, r_{\text{acbo}}, L_{\text{cyl}}) := \frac{2}{\pi} \cdot \int_{\theta_{\text{acbo}}(L_{\text{acb}}, r_{\text{acbo}})}^{\theta_{\text{accyl}}(L_{\text{acb}}, r_{\text{acbo}}, L_{\text{cyl}})} \cos(\theta)^2 \cdot \sin(\theta)^3 d\theta$$

7.2.7.3 Total Scattered Light Displacement Noise from Arm Cavity Baffle and Cylindrical Baffle

The total scattered light from the Arm Cavity Baffle and the Cylindrical Baffle into the IFO is

$$P_{\text{totalacbbacyl}}(L_{\text{acb}}, r_{\text{acbo}}, L_{\text{cyl}}) := P_{\text{acbbacifo}}(L_{\text{acb}}, r_{\text{acbo}}) + P_{\text{wsaccylifo}}(L_{\text{acb}}, r_{\text{acbo}}, L_{\text{cyl}})$$

The total scattered light displacement noise is

$$\text{DN}_{\text{totalacbbacyl}} := \text{TF}_{\text{itmhr}} \cdot \left(\frac{P_{\text{totalacbbacyl}}(L_{\text{acb}}, r_{\text{acbo}}, L_{\text{cyl}})}{P_{\text{psl}}} \right)^{0.5} \cdot x_{\text{hepr}} \cdot 2 \cdot k \cdot \text{acbatter}$$

7.2.7.4 Scattering from the Manifold Baffle

The wide-angle scattered light hitting the Manifold Baffle is

$$P_{\text{mb}} := P_{\text{a}} \cdot \int_{\theta_{\text{cp}}}^{\theta_{\text{mbo}}} \frac{\alpha_{\text{ws}} \cdot \cos(\theta)}{\pi} \cdot 2 \cdot \pi \cdot \sin(\theta) d\theta$$

Where the half-angle from the ITM centerline to the Manifold Baffle is

$$\theta_{\text{mbo}} := \text{atan}\left(\frac{r_{\text{m}}}{L_{\text{m}}}\right)$$

and L_{m} is the distance from the ITM to the Manifold Baffle.

The power scattered into the IFO mode is given by

$$P_{\text{wsmbifo}} := \sqrt{4} \cdot P_a \cdot \left(C_1 \cdot \alpha_{\text{ws}}^2 \cdot \frac{\lambda^2}{r_m} \cdot \text{BRDF}_{\text{bd}} \right)$$

Where the geometric function is

$$C_1 := \frac{2}{\pi} \cdot \int_{\theta_{\text{cp}}}^{\theta_{\text{mbo}}} \cos(\theta)^2 \cdot \sin(\theta)^3 d\theta$$

7.2.7.5 Scatter from ITM Manifold Wall

The wide-angle scattered light hitting the Manifold wall is

$$P_{\text{mw}}(L_{\text{acb}}) := P_a \cdot \int_{\theta_{\text{mbo}}}^{\theta_{\text{acbi}}(L_{\text{acb}})} \frac{\alpha_{\text{ws}} \cdot \cos(\theta)}{\pi} \cdot 2 \cdot \pi \cdot \sin(\theta) d\theta$$

The power scattered into the IFO mode is given by

$$P_{\text{wsmbifo}} := \sqrt{4} \cdot P_a \cdot \left(C_1 \cdot \alpha_{\text{ws}}^2 \cdot \frac{\lambda^2}{r_m} \cdot \text{BRDF}_{\text{bd}} \right)$$

Where the geometric function is

$$C_3(L_{\text{acb}}) := \frac{2}{\pi} \cdot \int_{\theta_{\text{mbo}}}^{\theta_{\text{acbi}}(L_{\text{acb}})} \cos(\theta)^2 \cdot \sin(\theta)^3 d\theta$$

7.2.7.6 Scattering from BSC Chamber Walls

The wide-angle scattered light hitting the BSC chamber wall is

$$P_{\text{bsc}}(L_{\text{acb}}, r_{\text{acbo}}, L_{\text{cyl}}) := P_a \cdot \int_{\theta_{\text{accyl}}(L_{\text{acb}}, r_{\text{acbo}}, L_{\text{cyl}})}^{\frac{\pi}{2}} \frac{\alpha_{\text{ws}} \cdot \cos(\theta)}{\pi} \cdot 2 \cdot \pi \cdot \sin(\theta) d\theta$$

The power scattered into the IFO mode is given by

$$P_{\text{wsbscifd}}(L_{\text{acb}}, r_{\text{acbo}}, L_{\text{cyl}}) := \sqrt{4} \cdot P_a \cdot \left(C_5(L_{\text{acb}}, r_{\text{acbo}}, L_{\text{cyl}}) \cdot \alpha_{\text{ws}}^2 \cdot \frac{\lambda^2}{r_{\text{bsc}}^2} \cdot \text{BRDF}_{\text{wall}} \right)$$

where the geometric function is

$$C_5(L_{\text{acb}}, r_{\text{acbo}}, L_{\text{cyl}}) := \frac{2}{\pi} \cdot \int_{\theta_{\text{accyl}}(L_{\text{acb}}, r_{\text{acbo}}, L_{\text{cyl}})}^{\frac{\pi}{2}} \cos(\theta)^2 \cdot \sin(\theta)^3 d\theta$$

7.2.7.7 Total Wide-Angle Scattered Light Displacement Noise from BSC Chamber, Manifold Walls, and Manifold Baffle

The total scattered light from the BSC Chamber, Manifold Walls, and Manifold Baffle into the IFO is

$$P_{\text{totalbscman}}(L_{\text{acb}}, r_{\text{acbo}}, L_{\text{cyl}}) := P_{\text{wsbscifd}}(L_{\text{acb}}, r_{\text{acbo}}, L_{\text{cyl}}) + P_{\text{wsmanif}}(L_{\text{acb}}) + P_{\text{wsmbif}}$$

The scattered light is injected into the arm cavity, and the appropriate scattered light noise transfer function is ‘ITM_HR’. The displacement noise (m/rt Hz) is

$$\text{DN}_{\text{wsbscmanif}}(L_{\text{acb}}, r_{\text{acbo}}, L_{\text{cyl}}) := \text{TF}_{\text{itmhr}} \left(\frac{P_{\text{totalbscman}}(L_{\text{acb}}, r_{\text{acbo}}, L_{\text{cyl}})}{P_{\text{psl}}} \right)^{0.5} \cdot x_{\text{manifold}}^{2 \cdot k}$$

7.2.8 Septum Window Scatter

7.2.8.1 AS Output Window

The power incident on the AS output Window is given by

$$P_{\text{assp}} := P_{\text{farad}}$$

The light power scattered into the IFO mode from the two surfaces of the AS Output Window is given by

$$P_{\text{assps}} := N_{\text{sp}} \cdot P_{\text{assp}} \cdot \text{BRDF}_{\text{sp}} \cdot \frac{w_{\text{ifo}}^2}{w_{\text{rc}}} \cdot \Delta_{\text{ifo}} \cdot \text{faradatter}$$

The scattered light is injected through the SRM, and the appropriate scattered light noise transfer function is ‘SRM’. The displacement noise (m/rt Hz) is

$$DN_{\text{asspsifo}} := TF_{\text{sr}} \left(\frac{P_{\text{assps}}}{P_{\text{psl}}} \right)^{0.5} \cdot x_{\text{hamflange}}^{2 \cdot k}$$

7.2.8.2 AS Output Window Reflection

The reflected power incident on the AS Output Window beam dump is given by

$$P_{\text{asspbd}} := R_{\text{sp}} \cdot P_{\text{assp}}$$

where R_{sp} is the Fresnel reflectivity of the window surfaces.

The light power scattered into the IFO mode from the AS Output Window beam dump is given by

$$P_{\text{assprefls}} := N_{\text{sp}} \cdot P_{\text{asspbd}} \cdot BRDF_{\text{bd}} \cdot \frac{w_{\text{ifo}}^2}{w_{\text{rc}}^2} \cdot \Delta_{\text{ifo}} \cdot R_{\text{sp}} \cdot \text{faradatter}$$

The total scattered light displacement noise is

$$DN_{\text{asspreflsifo}} := TF_{\text{sr}} \left(\frac{P_{\text{assprefls}}}{P_{\text{psl}}} \right)^{0.5} \cdot x_{\text{ham}}^{2 \cdot k}$$

7.2.8.3 ITMX PO Septum Window

The power incident on the ITMX PO Septum Window is given by

$$P_{\text{itmposp}} := R_{\text{bsar}} \cdot P_{\text{rca}}$$

The light power scattered into the IFO mode from the two surfaces of the ITMX PO Septum Window is given by

$$P_{\text{itmposps}} := N_{\text{sp}} \cdot P_{\text{itmposp}} \cdot BRDF_{\text{sp}} \cdot \frac{w_{\text{ifo}}^2}{w_{\text{rc}}^2} \cdot \Delta_{\text{ifo}} \cdot R_{\text{bsar}}$$

The scattered light is injected into the ITM AR, and the appropriate scattered light noise transfer function is 'ITM_AR. The displacement noise (m/rt Hz) is

$$DN_{\text{itmpospsifo}} := TF_{\text{itmar}} \left(\frac{P_{\text{itmposps}}}{P_{\text{psl}}} \right)^{0.5} \cdot x_{\text{hamflange}}^{2 \cdot k}$$

7.2.8.4 ITMX PO Septum Window Reflection

The reflected power incident on the ITMX PO Septum Window beam dump is given by

$$P_{\text{itmuposbd}} := R_{\text{sp}} \cdot P_{\text{itmupos}}$$

The light power scattered into the IFO mode from the ITMX PO Septum Window beam dump is given by

$$P_{\text{itmuposprefls}} := N_{\text{sp}} \cdot P_{\text{itmuposbd}} \cdot \text{BRDF}_{\text{bd}} \cdot \frac{w_{\text{ifo}}^2}{w_{\text{rc}}} \cdot \Delta_{\text{ifo}} \cdot R_{\text{sp}} \cdot R_{\text{bsar}}$$

The total scattered light displacement noise is

$$\text{DN}_{\text{itmupospreflsifo}} := \text{TF}_{\text{itmar}} \left(\frac{P_{\text{itmuposprefls}}}{P_{\text{psl}}} \right)^{0.5} \cdot x_{\text{ham}} \cdot 2 \cdot k$$

7.2.8.5 RC PO Septum Window

The power incident on the RC PO Septum Window is given by

$$P_{\text{rcposp}} := G_{\text{refl}} P_{\text{psl}} (1 - R_{\text{pr2hr}}) (1 - R_{\text{pr2ar}})$$

where R_{pr2hr} and R_{pr2ar} are the Fresnel reflectivity of the HR and AR surfaces of the PR2 mirror, and G_{refl} is the reflected port signal ratio.

The light power scattered into the IFO mode from the two surfaces of the RC PO Septum Window is given by

$$P_{\text{rcposps}} := N_{\text{sp}} \cdot P_{\text{rcposp}} \cdot \text{BRDF}_{\text{sp}} \cdot \frac{w_{\text{ifo}}^2}{w_{\text{rc}}} \cdot \Delta_{\text{ifo}} (1 - R_{\text{pr2hr}}) (1 - R_{\text{pr2ar}})$$

The scattered light is injected into the RC from the PRM direction, and the appropriate scattered light noise transfer function is 'BS_FROM_PRM'. The displacement noise (m/rt Hz) is

$$\text{DN}_{\text{rcpospsifo}} := \text{TF}_{\text{prbs}} \left(\frac{P_{\text{rcposps}}}{P_{\text{psl}}} \right)^{0.5} \cdot x_{\text{hamflange}} \cdot 2 \cdot k$$

7.2.8.6 RC PO Septum Window Reflection

The reflected power incident on the RC PO Septum Window beam dump is given by

$$P_{\text{rcposbd}} := R_{\text{sp}} \cdot P_{\text{rcposp}}$$

The light power scattered into the IFO mode from the RC PO Septum Window beam dump is given by

$$P_{\text{rcposprefls}} := N_{\text{sp}} \cdot P_{\text{rcpospbd}} \cdot \text{BRDF}_{\text{bd}} \cdot \frac{w_{\text{ifo}}^2}{w_{\text{rc}}} \cdot \Delta_{\text{ifo}} \cdot R_{\text{sp}} \cdot [(1 - R_{\text{pr2hr}}) \cdot (1 - R_{\text{pr2ar}})]$$

The total scattered light displacement noise is

$$\text{DN}_{\text{rcpospreflsifo}} := \text{TF}_{\text{prbs}} \cdot \left(\frac{P_{\text{rcposprefls}}}{P_{\text{psl}}} \right)^{0.5} \cdot x_{\text{ham}} \cdot 2 \cdot k$$

7.2.9 ITMY Hartmann Viewport

The power transmitted through the SR2 HR surface is

$$P_{\text{hartytransbd}} := G_{\text{as}} \cdot P_{\text{psl}} \cdot (1 - R_{\text{sr2hr}}) \cdot (1 - R_{\text{sr2ar}})$$

The power incident on the Hartmann viewport is

$$P_{\text{hartyvp}} := P_{\text{hartytransbd}} \cdot R_{\text{hartybs}}$$

where R_{hartybs} is the reflectivity of the Hartmann beam splitter.

The light power scattered into the IFO mode from the Hartmann viewport is given by

$$P_{\text{hartyvps}} := N_{\text{sp}} \cdot P_{\text{hartyvp}} \cdot \text{BRDF}_{\text{sp}} \cdot \frac{w_{\text{ifo}}^2}{w_{\text{rc}}} \cdot \Delta_{\text{ifo}} \cdot R_{\text{hartybs}} \cdot [(1 - R_{\text{sr2hr}}) \cdot (1 - R_{\text{sr2ar}})]$$

The scattered light is injected into the BS from the SRM direction, and the appropriate scattered light noise transfer function is 'BS_FROM_SRM'. The displacement noise (m/rt Hz) is

$$\text{DN}_{\text{hartyvpsifo}} := \text{TF}_{\text{srbs}} \cdot \left(\frac{P_{\text{hartyvps}}}{P_{\text{psl}}} \right)^{0.5} \cdot x_{\text{hamflange}} \cdot 2 \cdot k$$

7.2.10 ITMX Hartmann Viewport

The power incident on the Hartmann viewport is

$$P_{\text{hartxvp}} := P_{\text{itmposp}} \cdot T_{\text{hartxb}}$$

where T_{hartxb} is the transmissivity of the Hartmann beam splitter.

The light power scattered into the IFO mode from the Hartmann viewport is given by

$$P_{\text{hartxvps}} := N_{\text{sp}} \cdot P_{\text{hartxvp}} \cdot \text{BRDF}_{\text{sp}} \cdot \frac{w_{\text{ifo}}^2}{w_{\text{rc}}} \cdot \Delta_{\text{ifo}} \cdot T_{\text{hartxb}}$$

The total scattered light displacement noise is

$$DN_{\text{hartxvpsifo}} = TF_{\text{itmar}} \left(\frac{P_{\text{hartxvps}}}{P_{\text{psl}}} \right)^{0.5} \cdot x_{\text{hamflange}}^{2 \cdot k}$$

7.2.11 Ghost Beams

7.2.11.1 Ghost Beam Naming Convention

The ghost beam naming conventions for the COC mirrors and the beam splitter are shown in the following figures.

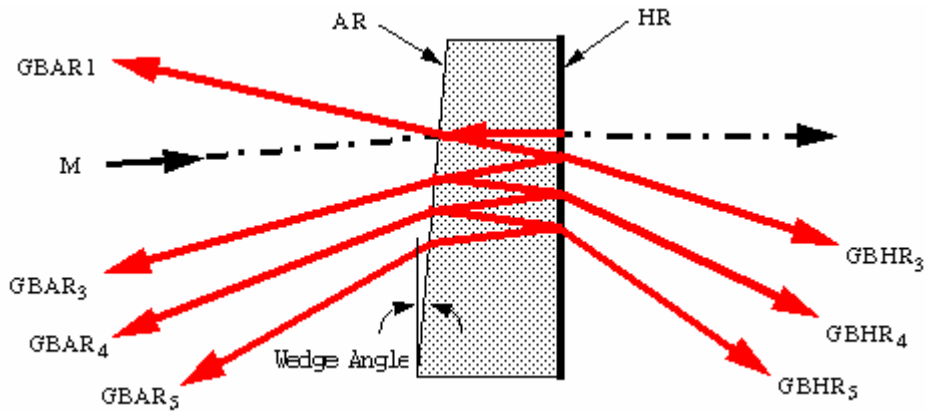


Figure 57: PRM, SRM, ITM, and ETM ghost beam naming convention

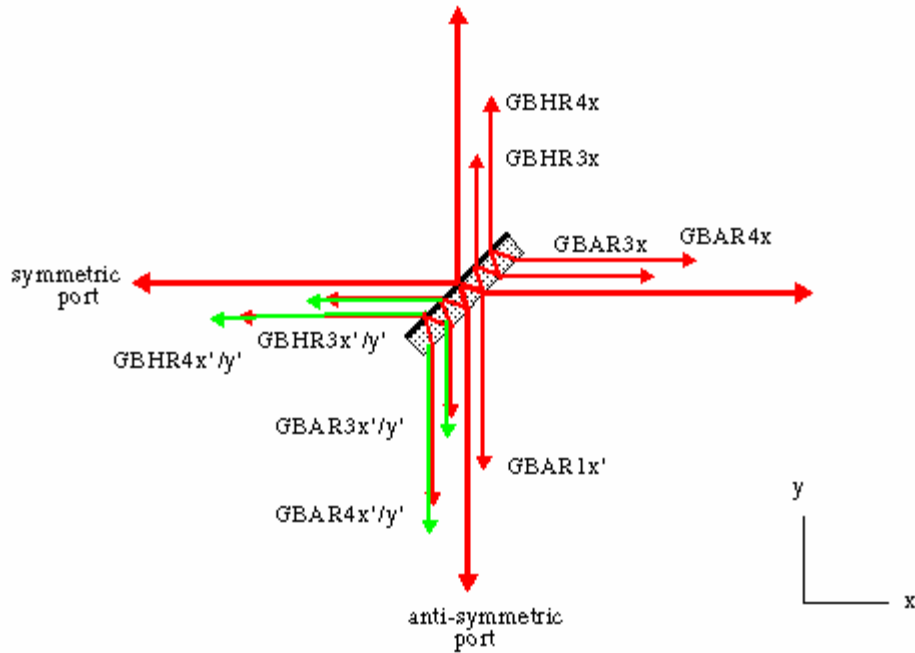


Figure 58: BS ghost beam naming convention

The GBAR3x'/y' are superimposed, and are renamed GBAR3P. Likewise, the other superimposed pairs are renamed GBAR4P, GBHR3P, and GBAR4P.

7.2.11.2 ITMAR1

The ITMAR1 ghost beam is collected by the PRM and SRM telescopes and hits the beam dumps in front of PR2 and SR2. The power incident on ITMAR1 Beam Dumps is given by

$$P_{itmar1bd} := P_{rca} \cdot R_{itma}$$

where R_{itmar} is the reflectivity of the AR surface of the ITM.

The light power scattered into the IFO from the ITM Beam Dump is given by

$$P_{itmar1bds} := \sqrt{2} \cdot P_{itmar1bd} \cdot BRDF_{bd} \cdot \frac{w_{ifo}^2}{2} \cdot \Delta_{ifo} \cdot R_{itma}$$

The scattered light displacement noise is

$$DN_{itmar1bd} := TF_{itmbs} \left(\frac{P_{itmar1bds}}{P_{psl}} \right)^{0.5} \cdot x_{ham} \cdot 2 \cdot k$$

7.2.11.3 ITMAR1 REFL

The power reflected from the ITMAR1 Beam Dump and incident on the IO tube wall is given by

$$P_{\text{itmar1bdrefl}} = P_{\text{itmar1bd}} R_{\text{bd}}$$

The light power scattered into the IFO from the wall is given by

$$P_{\text{itmar1bdrefls}} = \sqrt{2} \cdot R_{\text{bd}} \cdot P_{\text{itmar1bdrefl}} \cdot \text{BRDF}_{\text{wall}} \cdot \frac{w_{\text{ifo}}^2}{w_{\text{rc}}^2} \cdot \Delta_{\text{ifo}} \cdot R_{\text{itma}}$$

The scattered light displacement noise is

$$\text{DN}_{\text{itmar1bdrefl}} = \text{TF}_{\text{itmbs}} \left(\frac{P_{\text{itmar1bdrefls}}}{P_{\text{psl}}} \right)^{0.5} \cdot x_{\text{hamflange}}^{2 \cdot k}$$

7.2.11.4 ITMAR3

The ITMAR3 ghost beam is collected by the PRM and SRM telescopes and hits the beam dumps in front of PR2 and SR2. The power incident on ITMAR3 Beam Dumps is given by

$$P_{\text{itmar3bd}} = P_{\text{rca}} \cdot R_{\text{itmhr}}^2 \cdot R_{\text{itmar}} (1 - R_{\text{itmar}})^2$$

where R_{itmhr} is the reflectivity of the HR surface of the ITM.

The light power scattered into the IFO from the ITM Beam Dump is given by

$$P_{\text{itmar3bds}} = \sqrt{2} \cdot P_{\text{itmar3bd}} \cdot \text{BRDF}_{\text{bd}} \cdot \frac{w_{\text{ifo}}^2}{w_{\text{rc}}^2} \cdot \Delta_{\text{ifo}} \cdot R_{\text{itmhr}}^2 \cdot R_{\text{itmar}} (1 - R_{\text{itmar}})^2$$

The scattered light displacement noise is

$$\text{DN}_{\text{itmar3bd}} = \text{TF}_{\text{itmbs}} \left(\frac{P_{\text{itmar3bds}}}{P_{\text{psl}}} \right)^{0.5} \cdot x_{\text{ham}}^{2 \cdot k}$$

7.2.11.5 ITMAR3 REFL

The power reflected from the ITMAR3 Beam Dump and incident on the IO tube wall is given by

$$P_{\text{itmar3bdrefl}} = P_{\text{itmar3bd}} R_{\text{bd}}$$

The light power scattered into the IFO from the wall is given by

$$P_{\text{itmar3bdrefls}} := \sqrt{2} \cdot R_{\text{bd}} \cdot P_{\text{itmar3bdrefl}} \cdot \text{BRDF}_{\text{wall}} \frac{w_{\text{ifo}}^2}{w_{\text{rc}}} \cdot \Delta_{\text{ifo}} \cdot R_{\text{itmhr}}^2 \cdot R_{\text{itmar}} (1 - R_{\text{itmar}})^2$$

The scattered light displacement noise is

$$\text{DN}_{\text{itmar3bdrefl}} := \text{TF}_{\text{itmbs}} \left(\frac{P_{\text{itmar3bdrefls}}}{P_{\text{psl}}} \right)^{0.5} \cdot x_{\text{hamflange}}^{2 \cdot k}$$

7.2.11.6 ITMHR3

The ITMHR3 ghost beam passes into the arm beam tube and hits the beam tube baffle. The ITMHR3 ghost beam power incident on Beam Tube Baffle in the arm is given by

$$P_{\text{itmhr3btbaf}} := P_{\text{rca}} \cdot (1 - R_{\text{itmar}}) \cdot R_{\text{itmhr}} \cdot R_{\text{itmar}} \cdot T_{\text{itmhr}}$$

where T_{itmhr} is the transmissivity of the HR surface of the ITM.

The light power scattered into the recycling cavity through the ITM from the Beam Tube Baffle is given by

$$P_{\text{itmhr3btbafs}} := \sqrt{2} \cdot P_{\text{itmhr3btbaf}} \cdot \text{BRDF}_{\text{bd}} \cdot \Delta_{\text{ifo}} \cdot [(1 - R_{\text{itmar}}) \cdot R_{\text{itmhr}} \cdot R_{\text{itmar}} \cdot T_{\text{itmhr}}]$$

The scattered light displacement noise is

$$\text{DN}_{\text{itmhr3btbaf}} := \text{TF}_{\text{itmbs}} \left(\frac{P_{\text{itmhr3btbafs}}}{P_{\text{psl}}} \right)^{0.5} \cdot x_{\text{beamtube}}^{2 \cdot k}$$

7.2.11.7 BSAR3

The BSAR3 ghost beam passes into the arm beam tube and hits the beam tube baffle. The BSAR3 ghost beam power incident on Beam Tube Baffle in the arm is given by

$$P_{\text{bsar3btbaf}} := 2 \cdot P_{\text{rca}} \cdot (1 - R_{\text{bshr}}) \cdot R_{\text{bsar}} \cdot R_{\text{bshr}} \cdot (1 - R_{\text{bsar}}) \cdot (1 - R_{\text{itmhr}})$$

where R_{bshr} is the reflectivity of the HR surface of the BS and R_{bsar} is the reflectivity of the AR surface of the BS.

The light power scattered into the IFO from the Beam Tube Baffle is given by

$$P_{\text{bsar3btbafs}} := P_{\text{bsar3btbaf}} \cdot \text{BRDF}_{\text{bd}} \cdot \Delta_{\text{ifo}} \cdot [(1 - R_{\text{bshr}}) \cdot R_{\text{bsar}} \cdot R_{\text{bshr}} \cdot (1 - R_{\text{bsar}}) \cdot (1 - R_{\text{itmhr}})]$$

The scattered light displacement noise is

$$\text{DN}_{\text{bsar3btbaf}} := \text{TF}_{\text{itmbs}} \left(\frac{P_{\text{bsar3btbafs}}}{P_{\text{psl}}} \right)^{0.5} \cdot x_{\text{beamtube}}^{2 \cdot k}$$

7.2.11.8 BSHR3

The BSHR3 ghost beam passes into the arm beam tube and hits the beam tube baffle. The power incident on Beam Tube Baffle is given by

$$P_{\text{bshr3btbaf}} := 2 \cdot P_{\text{rca}} \cdot (1 - R_{\text{bshr}}) \cdot R_{\text{bsar}} \cdot (1 - R_{\text{bshr}}) \cdot (1 - R_{\text{itmhr}})$$

The light power scattered into the IFO from the Beam Tube Baffle is given by

$$P_{\text{bshr3btbafs}} := P_{\text{bshr3btbaf}} \cdot \text{BRDF}_{\text{bd}} \cdot \Delta_{\text{ifo}} \cdot (1 - R_{\text{bshr}}) \cdot R_{\text{bsar}} \cdot (1 - R_{\text{bshr}}) \cdot (1 - R_{\text{itmhr}})$$

The scattered light displacement noise is

$$\text{DN}_{\text{bshr3btbaf}} := \text{TF}_{\text{itmbs}} \left(\frac{P_{\text{bshr3btbafs}}}{P_{\text{psl}}} \right)^{0.5} \cdot x_{\text{beamtube}} \cdot 2 \cdot k$$

7.2.11.9 BSAR3P

The BSAR3P ghost beam is collected by the SRM telescope and hits the beam dump in front of SR2. The power incident on the BSAR3P beam dump from the two collinear beams is given by

$$P_{\text{bsar3pbd}} := 2 \cdot P_{\text{rca}} \cdot \left[(1 - R_{\text{bsar}})^2 \cdot R_{\text{bshr}}^2 \cdot R_{\text{bsar}} + (1 - R_{\text{bshr}}) \cdot R_{\text{bsar}} \cdot R_{\text{bshr}} \cdot (1 - R_{\text{bsar}}) \right]$$

The light power scattered into the IFO from the BSAR3P beam dump is given by

$$P_{\text{bsar3pbds}} := P_{\text{bsar3pbd}} \cdot \text{BRDF}_{\text{bd}} \cdot \frac{w_{\text{ifo}}^2}{2} \cdot \Delta_{\text{ifo}} \cdot \left[(1 - R_{\text{bsar}})^2 \cdot R_{\text{bshr}}^2 \cdot R_{\text{bsar}} + (1 - R_{\text{bshr}}) \cdot R_{\text{bsar}} \cdot R_{\text{bshr}} \cdot (1 - R_{\text{bsar}}) \right] \cdot \frac{1}{w_{\text{rc}}}$$

The scattered light displacement noise is

$$\text{DN}_{\text{bsar3pbd}} := \text{TF}_{\text{itmar}} \left(\frac{P_{\text{bsar3pbds}}}{P_{\text{psl}}} \right)^{0.5} \cdot x_{\text{ham}} \cdot 2 \cdot k$$

7.2.11.10 BSAR3P REFL

The power reflected from the BSAR3P Beam Dump and incident on the OUT tube wall is given by

$$P_{\text{bsar3pbdrefl}} := P_{\text{bsar3pbd}} \cdot R_{\text{bd}}$$

The light power scattered into the IFO from the wall is given by

$$P_{\text{bsar3pbdrefls}} := R_{\text{bd}} \cdot P_{\text{bsar3pbdrefl}} \cdot \text{BRDF}_{\text{wall}} \cdot \frac{w_{\text{ifo}}^2}{2} \cdot \Delta_{\text{ifo}} \cdot \left[(1 - R_{\text{bsar}})^2 \cdot R_{\text{bshr}}^2 \cdot R_{\text{bsar}} + (1 - R_{\text{bshr}}) \cdot R_{\text{bsar}} \cdot R_{\text{bshr}} \cdot (1 - R_{\text{bsar}}) \right] \cdot \frac{1}{w_{\text{rc}}}$$

The scattered light displacement noise is

$$DN_{\text{bsar3pbdrefl}} := TF_{\text{itmar}} \left(\frac{P_{\text{bsar3pbdrefls}}}{P_{\text{psl}}} \right)^{0.5} \cdot x_{\text{hamflange}}^{2 \cdot k}$$

7.2.11.11 BSHR3P

The BSHR3P ghost beam is collected by the PRM telescope and hits the beam dump in front of PR2. The power incident on the BSHR3P beam dump from the two collinear beams is given by

$$P_{\text{bshr3pbd}} := 2 \cdot P_{\text{rca}} \cdot \left[(1 - R_{\text{bsar}}) \cdot R_{\text{bshr}} \cdot R_{\text{bsar}} \cdot (1 - R_{\text{bshr}}) + (1 - R_{\text{bshr}})^2 \cdot R_{\text{bsar}} \right]$$

The light power scattered into the IFO from the BSHR3P beam dump is given by

$$P_{\text{bshr3pbd}} := P_{\text{bshr3pbd}} \cdot BRDF_{\text{bd}} \cdot \frac{w_{\text{ifo}}^2}{w_{\text{rc}}} \cdot \Delta_{\text{ifo}} \left[(1 - R_{\text{bsar}}) \cdot R_{\text{bshr}} \cdot R_{\text{bsar}} \cdot (1 - R_{\text{bshr}}) + (1 - R_{\text{bshr}})^2 \cdot R_{\text{bsar}} \right]$$

The scattered light displacement noise is

$$DN_{\text{bshr3pbd}} := TF_{\text{itmar}} \left(\frac{P_{\text{bshr3pbd}}}{P_{\text{psl}}} \right)^{0.5} \cdot x_{\text{ham}}^{2 \cdot k}$$

7.2.11.12 BSHR3P REFL

The power reflected from the BSHR3P Beam Dump and incident on the IO tube wall is given by

$$P_{\text{bshr3pbdrefl}} := P_{\text{bshr3pbd}} \cdot R_{\text{bd}}$$

The light power scattered into the IFO from the wall is given by

$$P_{\text{bshr3pbdrefls}} := R_{\text{bd}} \cdot P_{\text{bshr3pbdrefl}} \cdot BRDF_{\text{wall}} \cdot \frac{w_{\text{ifo}}^2}{w_{\text{rc}}} \cdot \Delta_{\text{ifo}} \left[(1 - R_{\text{bsar}}) \cdot R_{\text{bshr}} \cdot R_{\text{bsar}} \cdot (1 - R_{\text{bshr}}) + (1 - R_{\text{bshr}})^2 \cdot R_{\text{bsar}} \right]$$

The scattered light displacement noise is

$$DN_{\text{bshr3pbdrefls}} := TF_{\text{itmar}} \left(\frac{P_{\text{bshr3pbdrefls}}}{P_{\text{psl}}} \right)^{0.5} \cdot x_{\text{hamflange}}^{2 \cdot k}$$

7.2.12 PRM

7.2.12.1 PRMAR1

The power incident on the PRMAR1 beam dump is given by

$$P_{\text{prmar1bd}} := P_{\text{psl}} \cdot R_{\text{prmar}}$$

The light power scattered into the IFO from the PRMAR1 beam dump is given by

$$P_{\text{prmar1bds}} := P_{\text{prmar1bd}} \cdot \text{BRDF}_{\text{platebd}} \cdot \frac{w_{\text{ifo}}^2}{w_{\text{rc}}} \cdot \Delta_{\text{ifo}} \cdot R_{\text{prmar}} \cdot \text{faradatten} \cdot T_{\text{prmar}} \cdot T_{\text{prmh}}$$

7.2.12.2 PRMAR3

The power incident on the PRMAR3 beam dump is given by

$$P_{\text{prmar3bd}} := P_{\text{rct}} \cdot T_{\text{prmhr}} \cdot R_{\text{prmar}} \cdot R_{\text{prmhr}} \cdot T_{\text{prmar}}$$

The light power scattered into the IFO from the PRMAR3 beam dump is given by

$$P_{\text{prmar3bds}} := P_{\text{prmar3bd}} \cdot \text{BRDF}_{\text{platebd}} \cdot \frac{w_{\text{ifo}}^2}{w_{\text{rc}}} \cdot \Delta_{\text{ifo}} \cdot (T_{\text{prmhr}} \cdot R_{\text{prmar}} \cdot R_{\text{prmhr}} \cdot T_{\text{prmar}})$$

7.2.12.3 PRMHR3

The power incident on the PRMHR3 beam dump is given by

$$P_{\text{prmhr3bd}} := P_{\text{rct}} \cdot T_{\text{prmhr}}^2 \cdot R_{\text{prmar}}$$

The light power scattered into the IFO from the PRMHR3 beam dump is given by

$$P_{\text{prmhr3bds}} := P_{\text{prmhr3bd}} \cdot \text{BRDF}_{\text{platebd}} \cdot \frac{w_{\text{ifo}}^2}{w_{\text{rc}}} \cdot \Delta_{\text{ifo}} \cdot (T_{\text{prmhr}}^2 \cdot R_{\text{prmar}})$$

7.2.12.4 Total Displacement Noise from PRM

The total light power scattered into the IFO from the PRM beam dumps is given by

$$P_{\text{prmtotals}} := P_{\text{prmar1bds}} + 2 \cdot (P_{\text{prmar3bds}} + P_{\text{prmhr3bds}})$$

The scattered light displacement noise is

$$DN_{prmsifo} := TF_{prbs} \cdot \left(\frac{P_{prmtotals}}{P_{psl}} \right)^{0.5} \cdot x_{ham} \cdot 2 \cdot k$$

7.2.13 PRM2

7.2.13.1 PR2AR0t

The circulating power in the recycling cavity that transmits through the PR2 mirror from the PRM mirror and is incident on the PR2AR0t beam dump is given by

$$P_{pr20tbd} := P_{rct} \cdot T_{pr2hr} \cdot T_{pr2ar}$$

The light power scattered into the IFO from the PR2AR0t beam dump is given by

$$P_{pr20tbd} := P_{pr20tbd} \cdot BRDF_{bd} \cdot \frac{w_{ifo}^2}{w_{rc}^2} \cdot \Delta_{ifo} (T_{pr2hr} \cdot T_{pr2ar})$$

7.2.13.2 PR2AR3

The power incident on the PR2AR3 beam dump is given by

$$P_{pr2ar3bd} := P_{rct} \cdot T_{pr2hr} \cdot R_{pr2ar} \cdot R_{pr2hr} \cdot T_{pr2ar}$$

The light power scattered into the IFO from the PR2AR3 beam dump is given by

$$P_{pr2ar3bd} := P_{pr2ar3bd} \cdot BRDF_{platebd} \cdot \frac{w_{ifo}^2}{w_{rc}^2} \cdot \Delta_{ifo} (T_{pr2hr} \cdot R_{pr2ar} \cdot R_{pr2hr} \cdot T_{pr2ar})$$

7.2.13.3 PR2HR3

The power incident on the PR2HR3 beam dump is given by

$$P_{pr2hr3bd} := P_{rct} \cdot T_{pr2hr}^2 \cdot R_{pr2ar}$$

The light power scattered into the IFO from the PR2HR3 beam dump is given by

$$P_{pr2hr3bd} := P_{pr2hr3bd} \cdot BRDF_{platebd} \cdot \frac{w_{ifo}^2}{w_{rc}^2} \cdot \Delta_{ifo} (T_{pr2hr}^2 \cdot R_{pr2ar})$$

7.2.13.4 Total Displacement Noise from PR2

The total light power scattered into the IFO from the PR2 beam dumps is given by

$$P_{\text{pr2totals}} := 2 \cdot (P_{\text{pr20tbds}} + P_{\text{pr2ar3bds}} + P_{\text{pr2hr3bds}})$$

The scattered light displacement noise is

$$\text{DN}_{\text{pr2sifo}} := \text{TF}_{\text{prbs}} \cdot \left(\frac{P_{\text{pr2totals}}}{P_{\text{psl}}} \right)^{0.5} \cdot x_{\text{ham}} \cdot 2 \cdot k$$

7.2.14 PRM3

7.2.14.1 PR3AR0t

The circulating power in the recycling cavity that transmits through the PR3 mirror from the PR2 mirror and is incident on the PR3AR0t beam dump is given by

$$P_{\text{pr30tbd}} := P_{\text{rct}} \cdot T_{\text{pr3hr}} \cdot T_{\text{pr3ar}}$$

The light power scattered into the IFO from the PR3AR0t beam dump is given by

$$P_{\text{pr30tbds}} := P_{\text{pr30tbd}} \cdot \text{BRDF}_{\text{platebd}} \cdot \Delta_{\text{ifo}} (T_{\text{pr3hr}} \cdot T_{\text{pr3ar}})$$

7.2.14.2 PR3AR3

The power incident on the PR3AR3 beam dump is given by

$$P_{\text{pr3ar3bd}} := P_{\text{rct}} \cdot T_{\text{pr3hr}} \cdot R_{\text{pr3ar}} \cdot R_{\text{pr3hr}} \cdot T_{\text{pr3ar}}$$

The light power scattered into the IFO from the PR3AR3 beam dump is given by

$$P_{\text{pr3ar3bds}} := P_{\text{pr3ar3bd}} \cdot \text{BRDF}_{\text{platebd}} \cdot \Delta_{\text{ifo}} (T_{\text{pr3hr}} \cdot R_{\text{pr3ar}} \cdot R_{\text{pr3hr}} \cdot T_{\text{pr3ar}})$$

7.2.14.3 PR3HR3

The power incident on the PR3HR3 beam dump is given by

$$P_{\text{pr3hr3bd}} := P_{\text{rct}} \cdot T_{\text{pr3hr}}^2 \cdot R_{\text{pr3ar}}$$

The light power scattered into the IFO from the PR3HR3 beam dump is given by

$$P_{\text{pr3hr3bds}} := P_{\text{pr3hr3bd}} \cdot \text{BRDF}_{\text{wall}} \cdot \Delta_{\text{ifo}} (T_{\text{pr3hr}}^2 \cdot R_{\text{pr3ar}})$$

7.2.14.4 Total Displacement Noise from PR3

The total light power scattered into the IFO from the PR3 beam dumps is given by

$$P_{pr3ars} := 2 \cdot (P_{pr30tbd} + P_{pr3ar3bds})$$

The scattered light displacement noise is

$$DN_{pr3arsifo} := TF_{prbs} \cdot \left(\frac{P_{pr3ars}}{P_{psl}} \right)^{0.5} \cdot x_{ham} \cdot 2 \cdot k$$

7.2.15 SRM

7.2.15.1 SRMAR3

The power incident on the SRMAR3 beam dump is given by

$$P_{srmr3bd} := P_{sc} \cdot T_{srmhr} \cdot R_{srmr} \cdot R_{srmhr} \cdot T_{srma}$$

The light power scattered into the IFO from the SRMAR3 beam dump is given by

$$P_{srmr3bds} := P_{srmr3bd} \cdot BRDF_{platebd} \cdot \frac{w_{ifo}^2}{w_{rc}} \cdot \Delta_{ifo} \cdot (T_{srmhr} \cdot R_{srmr} \cdot R_{srmhr} \cdot T_{srma})$$

7.2.15.2 SRMHR3

The power incident on the SRMHR3 beam dump is given by

$$P_{srmhr3bd} := P_{sc} \cdot T_{srmhr}^2 \cdot R_{srma}$$

The light power scattered into the IFO from the PRMAR1 beam dump is given by

$$P_{srmhr3bds} := P_{srmhr3bd} \cdot BRDF_{platebd} \cdot \frac{w_{ifo}^2}{w_{rc}} \cdot \Delta_{ifo} \cdot (T_{srmhr}^2 \cdot R_{srma})$$

7.2.15.3 Total Displacement Noise from SRM

The total light power scattered into the IFO from the SRM beam dumps is given by

$$P_{srmtotals} := 2 \cdot (P_{srmr3bds} + P_{srmhr3bds})$$

The scattered light displacement noise is

$$DN_{\text{srmsifo}} := TF_{\text{srbs}} \cdot \left(\frac{P_{\text{srmtotals}}}{P_{\text{psl}}} \right)^{0.5} \cdot x_{\text{ham}} \cdot 2 \cdot k$$

7.2.16 SRM2

7.2.16.1 SR2AR0t

The circulating power in the signal recycling cavity that transmits through the SR2 mirror from the SRM mirror and is incident on the SR2AR0t beam dump is given by

$$P_{\text{sr20tbd}} := P_{\text{sc}} \cdot T_{\text{sr2hr}} \cdot T_{\text{sr2ar}}$$

The light power scattered into the IFO from the SR2AR0t beam dump is given by

$$P_{\text{sr20tbds}} := P_{\text{sr20tbd}} \cdot BRDF_{\text{bd}} \cdot \frac{w_{\text{ifo}}^2}{w_{\text{rc}}^2} \cdot \Delta_{\text{ifo}} \cdot (T_{\text{sr2hr}} \cdot T_{\text{sr2ar}})$$

7.2.16.2 SR2AR3

The power incident on the SRMAR3 beam dump is given by

$$P_{\text{sr2ar3bd}} := P_{\text{sc}} \cdot T_{\text{sr2hr}} \cdot R_{\text{sr2ar}} \cdot R_{\text{sr2hr}} \cdot T_{\text{sr2ar}}$$

The light power scattered into the IFO from the SRMAR3 beam dump is given by

$$P_{\text{sr2ar3bds}} := P_{\text{sr2ar3bd}} \cdot BRDF_{\text{platebd}} \cdot \frac{w_{\text{ifo}}^2}{w_{\text{rc}}^2} \cdot \Delta_{\text{ifo}} \cdot (T_{\text{sr2hr}} \cdot R_{\text{sr2ar}} \cdot R_{\text{sr2hr}} \cdot T_{\text{sr2ar}})$$

7.2.16.3 SR2HR3

The power incident on the SRMHR3 beam dump is given by

$$P_{\text{sr2hr3bd}} := P_{\text{sc}} \cdot T_{\text{sr2hr}}^2 \cdot R_{\text{sr2ar}}$$

The light power scattered into the IFO from the SRMHR3 beam dump is given by

$$P_{\text{sr2hr3bds}} := P_{\text{sr2hr3bd}} \cdot BRDF_{\text{platebd}} \cdot \frac{w_{\text{ifo}}^2}{w_{\text{rc}}^2} \cdot \Delta_{\text{ifo}} \cdot (T_{\text{sr2hr}}^2 \cdot R_{\text{sr2ar}})$$

7.2.16.4 Total Displacement Noise from SR2

The total light power scattered into the IFO from the SR2 beam dumps is given by

$$P_{\text{sr2totals}} := 2 \cdot (P_{\text{sr20tbds}} + P_{\text{sr2ar3bds}} + P_{\text{sr2hr3bds}})$$

The scattered light displacement noise is

$$DN_{sr2sifo} := TF_{srbs} \cdot \left(\frac{P_{sr2totals}}{P_{psl}} \right)^{0.5} \cdot x_{ham} \cdot 2 \cdot k$$

7.2.17 SRM3

7.2.17.1 SR3AR0t

The circulating power in the signal recycling cavity that transmits through the SR3 mirror from the SR2 mirror and is incident on the SR3AR0t beam dump is given by

$$P_{sr30tbd} := P_{sc} \cdot T_{sr3hr} \cdot T_{sr3ar}$$

The light power scattered into the IFO from the SR3AR0t beam dump is given by

$$P_{sr30tbd} := P_{sr30tbd} \cdot BRDF_{platebd} \cdot \Delta_{ifo} (T_{sr3hr} \cdot T_{sr3ar})$$

7.2.17.2 SR3AR3

The power incident on the SR3AR3 beam dump is given by

$$P_{sr3ar3bd} := P_{sc} \cdot T_{sr3hr} \cdot R_{sr3ar} \cdot R_{sr3hr} \cdot T_{sr3ar}$$

The light power scattered into the IFO from the SR3AR3 beam dump is given by

$$P_{sr3ar3bd} := P_{sr3ar3bd} \cdot BRDF_{platebd} \cdot \Delta_{ifo} (T_{sr3hr} \cdot R_{sr3ar} \cdot R_{sr3hr} \cdot T_{sr3ar})$$

7.2.17.3 SR3HR3

The power incident on the SR3HR3 beam dump is given by

$$P_{sr3hr3bd} := P_{sc} \cdot T_{sr3hr}^2 \cdot R_{sr3ar}$$

The light power scattered into the IFO from the SR3HR3 beam dump is given by

$$P_{sr3hr3bd} := P_{sr3hr3bd} \cdot BRDF_{wall} \cdot \Delta_{ifo} (T_{sr3hr}^2 \cdot R_{sr3ar})$$

7.2.17.4 Total Displacement Noise from SR3AR

The total light power scattered into the IFO from the SR3 beam dumps is given by

$$P_{sr3ars} := 2 \cdot (P_{sr30tbd} + P_{sr3ar3bd})$$

The scattered light displacement noise is

$$DN_{sr3arsifo} := TF_{srbs} \cdot \left(\frac{P_{sr3ars}}{P_{psl}} \right)^{0.5} \cdot x_{ham} \cdot 2 \cdot k$$

7.2.18 Cryopump Baffle Scatter

The power incident on the Cryopump Baffle is given by

$$P_{cp} := P_a \cdot \int_{\theta_{cp}}^{\theta_{bt}} 2 \cdot \pi \cdot \theta \cdot BRDF_1(\theta) d\theta$$

The half-angle from the beam tube centerline to the arm beam tube baffle inner edge is

$$\theta_{bt} := \frac{R_{bt}}{L}$$

The light power scattered into the IFO from the Cryopump Baffle is given by

$$P_{cps} := \sqrt{4} \cdot P_{cp} \cdot BRDF_{cp} \cdot \frac{\pi \cdot w_{ifo}^2}{L^2} \cdot BRDF_1(30 \cdot 10^{-6}) \cdot \Delta_{ifc}$$

The scattered light is injected into the arm cavity, and the appropriate scattered light noise transfer function is 'ITM_HR'. The displacement noise (m/rt Hz) is

$$DN_{cpbaf} := TF_{itmhr} \cdot \left(\frac{P_{cps}}{P_{psl}} \right)^{0.5} \cdot x_{beamtube} \cdot 2 \cdot k \cdot cpatter$$

7.2.19 Cryopump Baffle Reflected Scatter

The power reflected by the Cryopump Baffle and incident on the wall is given by

$$P_{cpr} := R_{cpb} \cdot P_{cp}$$

where R_{cpb} is the reflectivity of the Cryopump Baffle.

The light power scattered into the IFO from the wall is given by

$$P_{cprs} := \sqrt{4} \cdot P_{cpr} \cdot BRDF_{wall} R_{cpb} \cdot \frac{\pi \cdot w_{ifo}^2}{L^2} \cdot BRDF_1(30 \cdot 10^{-6}) \cdot \Delta_{ifc}$$

The displacement noise (m/rt Hz) is

$$DN_{\text{cpbafrefl}} := TF_{\text{itmhr}} \left(\frac{P_{\text{cprs}}}{P_{\text{psl}}} \right)^{0.5} \cdot x_{\text{beamtube}}^{2 \cdot k}$$

7.2.20 ETM Telescope Baffle Scatter

The power incident on the ETM Telescope Baffle is given by

$$P_{\text{etmbaf}} := P_a \cdot T_{\text{etm}} \cdot \eta_{\text{etmbaf}}$$

where P_a is the power in the arm cavity, T_{etm} is the transmissivity of the ETM mirror, and η_{etmbaf} is the fractional power that hits the ETM Telescope Baffle.

$$\eta_{\text{etmbaf}} := e^{-\frac{2 \cdot r_{\text{etmbaf}}^2}{w_{\text{etm}}^2}}$$

The light power scattered onto the ETM AR side from the ETM Telescope Baffle is given by

$$P_{\text{etmbafs}} := \sqrt{2} \cdot P_{\text{etmbaf}} \cdot \text{BRDF}_{\text{etmbaf}} \frac{\pi \cdot w_{\text{ifo}}^2}{L^2} \cdot \text{BRDF}_1(30 \cdot 10^{-6}) \cdot \Delta_{\text{ifc}}$$

The displacement noise (m/rt Hz) is

$$DN_{\text{etmbaf}} := TF_{\text{etm}} \left(\frac{P_{\text{etmbafs}}}{P_{\text{psl}}} \right)^{0.5} \cdot x_{\text{hepi}}^{2 \cdot k \cdot \text{etmbafatte}}$$

7.2.21 ETM Telescope Baffle Reflection Scatter

The power reflected by the ETM Telescope Baffle and incident on the chamber wall is given by

$$P_{\text{etmbafrefl}} := P_{\text{etmbaf}} \cdot R_{\text{etmbaf}}$$

where R_{etmbaf} is the reflectivity of the ETM Telescope Baffle.

The light power scattered onto the ETM AR side from the wall is given by

$$P_{\text{etmbafrefls}} := \sqrt{2} \cdot R_{\text{etmbaf}} \cdot P_{\text{etmbafrefl}} \cdot \text{BRDF}_{\text{wall}} \frac{\pi \cdot w_{\text{ifo}}^2}{L^2} \cdot \text{BRDF}_1(30 \cdot 10^{-6}) \cdot \Delta_{\text{ifc}}$$

The displacement noise (m/rt Hz) is

$$DN_{\text{etmbafrefl}} = TF_{\text{etm}} \left(\frac{P_{\text{etmbafrefl}}}{P_{\text{psl}}} \right)^{0.5} \cdot x_{\text{beamtube}}^{2 \cdot k}$$

7.2.22 Fringe-Wrapping

In the small phase-shift approximation the temporal DARM signal (noise) due to light scattered into the IFO mode is

$$S_{\text{SN}}(t) := SN_{\text{XXX}} \cdot E_{\text{SN}} \cdot \frac{4 \cdot \pi}{\lambda} \cdot x_{\text{g}} \cdot A_{\text{SEI}} \cdot \sin(2 \cdot \pi \cdot f_0 \cdot t)$$

The motion of the scattering surface is written as the underlying ground seismic motion, x_{g} , times the motion amplitude transfer function of the scattering surface, A_{SEI} .

The amplitude displacement spectral density is given by the following expression with the transfer coefficient calculated by Hiro (T060073-00 Transfer Functions of Injected Noise)

$$S_{\text{SN}}(f_0) := SN_{\text{XXX}} \cdot E_{\text{SN}} \cdot \frac{4 \cdot \pi}{\lambda} \cdot x_{\text{g}}(f_0) \cdot A_{\text{SEI}}$$

When the horizontal displacement of the scattering surface exceeds approximately $\lambda/8$, the amplitude of the noise no longer increases at the frequency of the scattering surface motion, but becomes non-sinusoidal and is up-converted to noise at odd harmonics of the scattering surface motion frequency. This phenomenon is called fringe-wrapping.

$$S_{\text{SN}}(t) := SN_{\text{XXX}} \cdot E_{\text{SN}} \cdot \sin\left(\frac{4 \cdot \pi}{\lambda} \cdot x_{\text{g}} \cdot A_{\text{SEI}} \cdot \sin(2 \cdot \pi \cdot f_0 \cdot t)\right)$$

We will assume that the transfer functions SN_{XXX} are valid for large phase-shift signals.

This time function is represented exactly by the Bessel series expansion in odd harmonics of the scattering surface frequency, f_0 , with amplitudes given by the Bessel functions of integral order m_n and argument θ .

$$S_{\text{SN}}(t) := S_{\text{B}}(\theta, t)$$

$$S_{\text{B}}(\theta, t) := 2 \cdot \sum_n \left(J_n(m_n, \theta) \cdot \sin(2 \cdot \pi \cdot m_n \cdot f_0 \cdot t) \right)$$

$$\theta := \frac{4 \cdot \pi}{\lambda} \cdot x_{\text{g}} \cdot A_{\text{SEI}}$$

$$m_n := 2 \cdot n - 1$$

At the onset of fringe-wrapping, a significant distortion of the noise temporal waveform has already occurred, as shown in

Figure 59, with the generation of up-converted noise at odd harmonics of the surface motion. The actual time signal and the Bessel function representation of the time signal are both plotted in the figure and agree exactly.

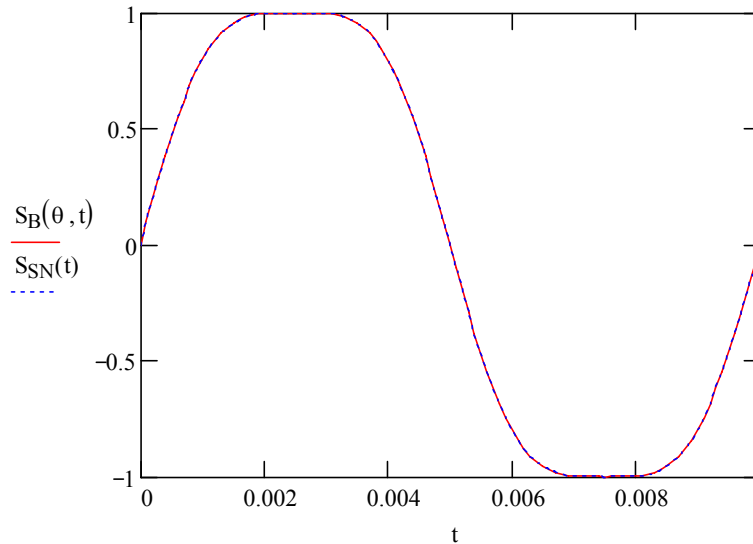


Figure 59: Noise Waveform at the Onset of Fringe-Wrapping, $\lambda/8$

If the displacement of the scattering surface is increased to $\lambda/4$, the fringe-wrapping becomes clearly visible, as shown in Figure 60. The fundamental and the third harmonic contribute most of the noise, as seen by the coefficients of the Bessel functions in the adjacent table.

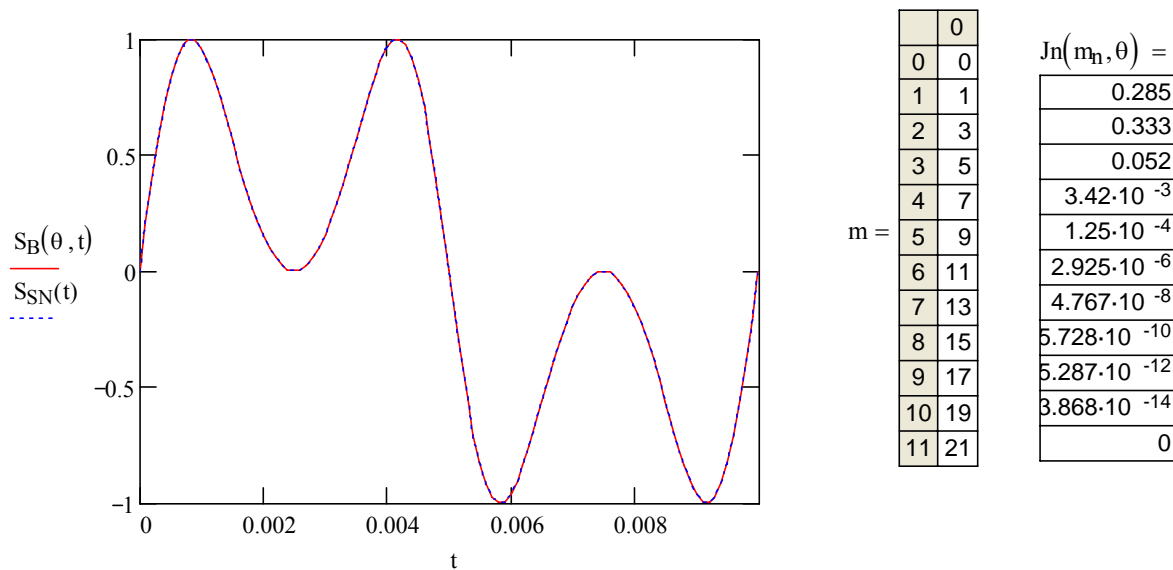


Figure 60: Displacement Noise waveform with Fringe-wrapping, $\lambda/4$

The displacement spectral density, m/rt Hz, of the fringe-wrapped signal (noise) at an up-converted frequency is given by the Bessel function series

$$S_{SNsum}(f) := E_{SN} \cdot SN_{XXX} \cdot 2 \cdot \sum_n \left| J_n \left(m_n, \theta \left(\frac{f}{m_n} \right) \right) \right|$$

Note that the Bessel function phase is evaluated by using the motion of the surface at the lower frequency that corresponds to an odd multiple of the up-converted frequency.

7.2.22.1.1.1 Damped Pendulum Example

Assume that the scattering surface is suspended from a damped, simple pendulum with resonant frequency = 1 Hz, Q = 1000; and the displacement spectral density of the suspension point x_g is $1E-7$ m/ rt Hz.

The amplitude response of the pendulum is given by

$$A_{SEI}(f) := \left| \frac{1}{1 + i \cdot \frac{f}{Q \cdot f_0} - \left(\frac{f}{f_0} \right)^2} \right|$$

The calculated noise displacement spectral density is shown in Figure 61. The total displacement noise, shown in cyan, has peaks at the fringe-wrapped harmonics of the fundamental surface motion. The displacement noise of the fundamental disturbance is shown in red, shifted upwards slightly in the graph for clarity. Additional displacement noise caused by fringe-wrapping is evident at the 3rd and 5th harmonics of the fundamental disturbance.

Even, with such a large motion of the suspension point, the fringe wrap noise of the suspended surface is negligible at frequencies an order of magnitude higher than the fundamental pendulum frequency.

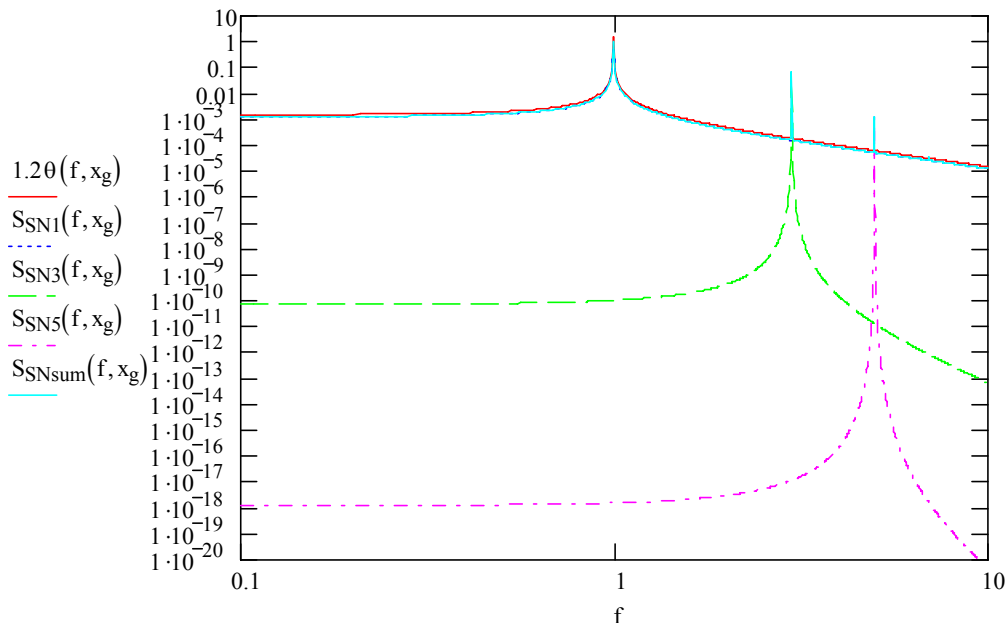


Figure 61: Scattered Light Displacement Noise Caused by Fringe-wrapping**7.3 Scattered Light Parameters**

The IFO parameters that were used for the scattered light calculations are listed in Table 18.

Table 18: IFO parameter values used for scattered light calculation

PARAMETER	VALUE
IFO_length;	4.00E+03
IFO_beamwaist;	1.15E-02
IFO_beam_waist_RC;	2.10E-03
beam_radius_ITM;	5.50E-02
beam_waist_photodetector;	5.00E-03
beam_radius_Faraday;	2.10E-03
lambda;	1.06E-06
IFO_diffraction_angle;	2.95E-05
IFO_solid_angle;	2.72E-09
laser_power;	1.25E+02
recycling_cavity_power_gain;	1.69E+01
reflected_port_power_ratio;	1.00E-03
dark_port_signal_ratio;	1.08E-03
recycling_cavity_power;	2.11E+03
arm_cavity_power;	8.34E+05
ETM_transmitted_power;	1.25E+01
reflected_port_power;	1.25E-01
dark_port_power;	1.35E-01
ITM_transmissivity;	5.00E-03
ITM_HR;	9.95E-01
ETM_transmissivity;	1.50E-05
ETM_Reflectivity;	1.00E+00
PRM_AR_reflectivity;	5.00E-05
PRM_HR_transmissivity;	2.12E-01
SRM_AR_reflectivity;	5.00E-05
SRM_HR_reflectivity;	9.60E-01

PARAMETER	VALUE
SRM_HR_transmissivity;	4.00E-02
diameter_ETM;	3.40E-01
diameter_ITM;	3.40E-01
diameter_PRM;	2.65E-01
diameter_SRM;	2.65E-01
diameter_MMT3;	2.65E-01
Radius_Inner_Cryo;	3.85E-01
Radius_Beam_Tube;	5.31E-01
area_arm_cav_baffle;	6.95E-01
length_armcavbaf_wall;	4.40E+00
manifold_wall_length;	1.40E+01
manifold_wall_angle;	6.64E-02
manifold_wide_angle_scattering_efficiency;	2.24E-20
manifold_baffle_wide_angle_scattering_efficiency;	8.84E-24
BSC_wide_angle_scattering_efficiency;	9.74E-22
AC_Baffle_wide_angle_scattering_efficiency;	5.83E-19
AC_Baf_cyl_wide_angle_scattering_efficiency;	1.14E-20
Area_Arm_Cav_Baf_Hole;	9.08E-02
Length_Arm_Cav_Baf;	1.00E+00
Solid_Angle_COC_Wide_Angle;	1.82E-01
AP2_lens_focal_length;	1.00E-01
lens_AR_reflectivity;	2.50E-03
scatter_loss_Brewster_window;	4.00E-05
incident_angle_Faraday_crystal;	1.70E-02
back_transmission_Faraday_Isolator;	1.00E-03
Faraday_Transmission;	9.00E-01
transmission_ETM_path;	1.00E-02
BRDF_elliptical_baffle_edge;	5.00E-02
BRDF_ETM_Tel_Baffle_Edge;	5.00E-02
BRDF_chamber_walls;	1.00E-01
BRDF_Nozzle;	1.00E-01
BRDF_photodetector;	1.00E-03
BRDF_ITMX_PO_steer_mirror;	1.00E-05
BRDF_COC_30urad;	1.36E+03

PARAMETER	VALUE
BRDF_elliptical_baffle;	5.00E-02
BRDF_arm_cav_baffle;	5.00E-02
BRDF_cryopump_baffle;	5.00E-02
BRDF_Brewster_window;	1.00E-06
BRDF_beam_dump;	5.00E-02
BRDF_ETM_Tel_Baffle;	5.00E-02
BRDF_lens;	1.00E-03
BRDF_Faraday;	4.92E-04
BRDF_manifold_baffle;	5.00E-02
BRDF_OMMT2;	3.00E-03
BRDF_Faraday;	4.92E-04
BRDF_COC_wide_angle;	4.76E-06
a;	1.12E-01
b;	1.30E-01
w;	2.10E-03
h;	1.23E-01
N_Cryopump_Baffles;	4.00E+00
N_Arm_Cavity_Baffle;	4.00E+00
N_Elliptical_Baffle;	0.00E+00
N_ETM_Tel_Baffle;	2.00E+00
N_Manifold;	4.00E+00
N_Surfaces_Faraday;	5.00E+00
N_Surfaces_Brewster;	2.00E+00
Scatter_Efficiency_Cryo_Baffle;	3.32E-06
Scatter_Efficiency_AC_Baffle;	8.79E-06
Scatter_Efficiency_Ellip_Baffle;	3.51E-04
Scatter_Efficiency_ETM_Tel_Baffle;	3.90E-03
Scatter_Efficiency_PRM_Ellip_Baffle;	9.46E-05
Scatter_Efficiency_Wide_Angle;	1.50E-05
cryopump_sus_length;	4.00E-01
cryopump_sus_freq;	7.88E-01
cryopump_sus_Q;	1.00E+03
arm_cavity_baf_sus_length;	8.00E-01
arm_cavity_baf_sus_freq;	2.50E+00

PARAMETER	VALUE
arm_cavity_baf_sus_Q;	1.00E+03
ellip_baf_sus_length;	1.00E+00
ellip_baf_sus_freq;	4.98E-01
ellip_baf_sus_Q;	1.00E+03
cav_bd_sus_length;	1.00E+00
cav_bd_sus_freq;	4.98E-01
cav_bd_sus_Q;	1.00E+02
Faraday_sus_length;	4.00E-01
Faraday_sus_freq;	7.88E-01
Faraday_sus_Q;	1.00E+02
reflectivity_ellip_baffle;	2.40E-05
reflectivity_arm_cav_baffle;	2.40E-05
reflectivity_cryopump_baffle;	2.40E-05
reflectivity_cavity_beam_dump;	2.40E-05
Reflectivity_Brewster;	2.50E-03
reflectivity_ETM_Tel_Baffle;	7.00E-02
reflectivity_manifold_baffle;	7.00E-02
Reflectivity_Faraday_AR;	2.50E-03
PRM_AR_transmissivity;	1.00E+00
PRM_HR_reflectivity;	7.88E-01
SRM_AR_transmissivity;	1.00E+00